Fall 12-2017

Operational Limits of Blade Coating with High Aspect Ratio Pigments

Lisa Weeks
University of Maine, lisa.weeks@maine.edu

OPERATIONAL LIMITS OF BLADE COATING ASSOCIATED WITH HIGH ASPECT RATIO PIGMENTS

By

Lisa Weeks

BS CHE, Montana State University, 2011

MS CHE, Montana State University, 2013

A DISSERTATION

Submitted in Partial Fulfillment of the

Requirements for the Degree of

Doctor of Philosophy

(in Chemical Engineering)

The Graduate School

The University of Maine

December 2017

Advisory Committee:

Dr. Douglas W. Bousfield, Professor of Chemical & Biological Engineering, Advisor

Dr. Albert Co, Associate Professor of Chemical & Biological Engineering

Dr. Michael Mason, Professor of Chemical & Biological Engineering

Dr. Patrick Gane, Vice President of Research and Development, Omya

Dr. Anthony Lyons, Technical Director, Imerys

OPERATIONAL LIMITS OF BLADE COATING ASSOCIATED WITH HIGH ASPECT RATIO PIGMENTS

By Lisa Weeks

Dissertation Advisor: Dr. Douglas W. Bousfield

An Abstract of the Dissertation Presented
in Partial Fulfillment of the Requirements for the
Degree of Doctor of Philosophy
(in Chemical Engineering)
December 2017

During the blade coating of paper, operational issues such as stalagmite formation, scratches or spits can develop at high solids content and high web speeds. For coatings that contain high aspect ratio pigments, these difficulties appear at lower solids concentrations and slower machine speeds than with more spherical shaped pigments. These operational issues are important because plate shaped particles have good properties in publication and barrier grades. A number of possible mechanisms have been described in the literature, but a clear cause has not been established nor have methods to estimate the operational limits been proposed.

The influence of particle characteristics on rheology, dewatering and operational issues was determined with a series of experiments. The effect of particle shape and size distribution on the dewatering and filtercake permeability were analyzed. The porosity and pore size distribution of dried filtercakes were also characterized. Runnability studies were conducted to determine the operational windows based on pigment shape and solids content. A bench top blade coater was developed to measure operational issues; small changes in the roll speed resulted in fluctuations in the speed at which blade deposits begin to appear. A high speed cylindrical laboratory coater (CLC) was used to determine the operational and quality issues for

various solids content for two pigments with different shape factors on two paper surfaces with varying absorption rates; a mobile video camera, mounted to the blade structure, was used to record the coating event.

The rate of dewatering of a coating formulation is influenced but the shape of the particles, where high aspect ratio pigments tend to dewater slower than those with a lower shape factor. High aspect ratio pigments have low filtercake permeabilities compared to the low aspect ratio pigments. The results indicate that the rate of dewatering is controlled by the size of the connections or throats between the pores and not the average pore size. Latex addition, in these systems, did not influence permeability to a large extent.

A method to determine the operational window was developed using the bench top blade coater which provides a measure of the maximum speed attainable at a given solids content before runnability defects appear: operational limits obtained with the bench coater correlate with those obtained with the CLC. With the absence of a base sheet, latex or other additives and binders, typical blade deposits were still generated with the bench coater. Small changes in solids content lead to large changes in coating speed. The influence of a permeable substrate on operational limits was minor. The operating window did not correlate with steady shear viscosity but did seem to relate to complex viscosity. A linear relationship between the operational limits and the difference between the coating solids and the immobilization solids. This relationship may help predict operational limits of other coating formulations. Operating limits seem to be determined by a dynamic flow leading to particle jamming behavior.

A mathematical model was developed to estimate the formation of a filtercake during blade coating. Experimental values for all parameters were based on the conducted runnability studies. The permeabilities of the base sheet and the coating filtercake play a crucial

role in the formation of the filtercake. Using the conditions that are similar to the CLC experiments, it was found that filtercake growth would not have impeded blade coating.

ACKNOWLEDGMENTS

I would like to thank my advisor, Dr. Douglas Bousfield, for his support and guidance over the past four years. Also, need to thank my Paper Surface Science Program mentors, Dr. Pat Gane, Dr. Tony Lyons and Gary Fugitt, for their valuable insight and added industrial practicality to my research project. I also need to thank my committee for their assistance and direction. Without the support of our industrials sponsors of the Paper Surface Science Program, this work would not have been possible. Lastly, I need to thank my family for their love, support and patience throughout my never-ending years in school.

TABLE OF CONTENTS

LIST OF TABLES

LIST OF FIGURES

Chapter 1

INTRODUCTION

Operational issues such as stalagmite formation, scratches or spits develop during blade coating at high solids content and fast web speeds. With coatings consisting of high aspect ratio pigments, these difficulties appear at lower solids concentrations and slower machine speed than with more spherical shaped pigments. There are a number of speculated causes behind this phenomenon. The theories can be divided into three categories: coating formulation characteristics, base stock properties and blade coater conditions.

The shape of the particles in the suspension influences the characteristics of the coating formulations. The rheology, particle packing and water retention are all functions of the pigment shape and size distribution. The base sheet properties of porosity, surface roughness and compressibility interact with coating and the blade coater operating conditions. The possible causes of runnability issues are part of an interrelated and complex system.

Motivation

High aspect ratio pigments, such as delaminated kaolins, have many beneficial properties which make them ideal for paper coating applications. Kaolin improves the printability of the final product with a smooth and excellent surface for ink receptibility (Bundy and Ishley, 1991). The plate-like shape of the kaolin particle is one of the most significant properties responsible for the high print quality (Conceição *et al.,* 2005). Plate-like particles are also used in barrier coatings to improve performance of these coatings. However, there are often process issues during blade coating that are exhibited when coatings contain high aspect ratio pigments. These issues include stalagmite formation, scratches, streaks and spits. This constrains the coatings comprised of these pigments to be applied at lower solids content and

slower machine speeds compared to more spherical shape pigment coatings. This results in higher drying costs and lower quality coatings that decrease the overall efficiency of the process.

A number of theories have been developed to explain the operational issues that are exhibited by coatings that contain plate-like pigments. The dilatant rheological behavior has been suggested as one of the mechanisms behind the formation of defects (Branston *et al.,* 1994). This non-Newtonian behavior of the coating color is one likely cause for runnability issues. Even in simple shear, it is well known that particulate suspensions that have high aspect ratios will have a higher viscosity than those of a low aspect ratio. A high viscosity by itself should not cause operational problems. If the viscosity suddenly increases at a certain shear rate, the blade may deflect in a way that is hard to predict. When a blade runs on its heel or toe, blade bleeding defects are known to be generated (Roper and Attal, 1993). Therefore, dilatant rheology does not explain operational issues, but the control of the blade with a dilatant rheology could be an issue.

The influence of particle orientation on runnability has been discussed in a number of publications (Gane *et al.,* 1992; Gane *et al.,* 1997). The rotation of these plate-like particles during coating is thought to be linked to the formation of whiskers and stalagmites along with altering the packing ability and water retention of the coating layer. The development of stalagmites on blade coaters trigger the runnability issues at high production speeds (Engström and Rigdahl, 1989). While it makes sense that rotation of high aspect ratio pigments in the coating flow would disrupt the smooth flow of particles, a clear demonstration of this mechanism is lacking in the literature as well as established process limitations such as what solids can be applied for certain aspect ratio pigments.

Characteristics of the coating formulation, base stock properties and coater operation conditions have been linked to runnability issues. It is well known that if the solids of the coating increases or the permeability of the base sheet increases, the maximum coating speed decreases. Bousfield (1993) proposed a model of blade coating that predicted the flow field and the buildup of a filter cake on the paper surface during the coating process: if the filter cake thickness approaches the gap between the blade and the paper, the filter cake will be scraped by the blade tip leading to coating defects. This picture seems to explain some results, but it does not directly explain the runnability aspects of high aspect ratio pigments. High aspect ratio pigments may influence the filter cake solids in the model and the viscosity of the coating itself and that could determine the growth rate of the filter cake.

The relationship between these parameters and runnability issues is a complex and interwoven system. The particle shape and size distributions are a critical variable for many of the potential runnability causes. Greater tendency for stalagmite formation has been established for high aspect ratio pigments under certain conditions. However, the properties of the particles that lead to stalagmite formation are still unclear.

Runnability

Runnability is defined as the ease at which a coating is applied to a base sheet. Runnability issues include blade bleeding, stalagmite build up, streaks and spits that limit the solids content and speed at which the coating can be applied. The causes behind the onset of runnability issues are not well understood.

One of the initial indications of potential runnability issues is blade bleeding. This is a buildup of coating on the back side of the blade and is often called a stalagmite. There are three types of blade buildup. Wet bleeding, which is the slow extrusion of coating with the properties

of the coating before shear, or the formation of a dry stalagmite and lastly a combination of both wet and dry stalagmite growth (Gane *et al.,* 1997). Examples of stalagmites from literature are shown in Figure 1.1 and 1.2. The exact conditions that lead to stalagmite formation are currently unknown**,** and so far, only hypothesized (Gane, 1997; Gane *et al.,* 1992). High aspect ratio pigments, narrow particle size distributions, low water retention, high viscosities, high machine speeds and solids contents are some of the conditions which seem to lead to more stalagmite formation (Weigl and Grossmann, 1997).

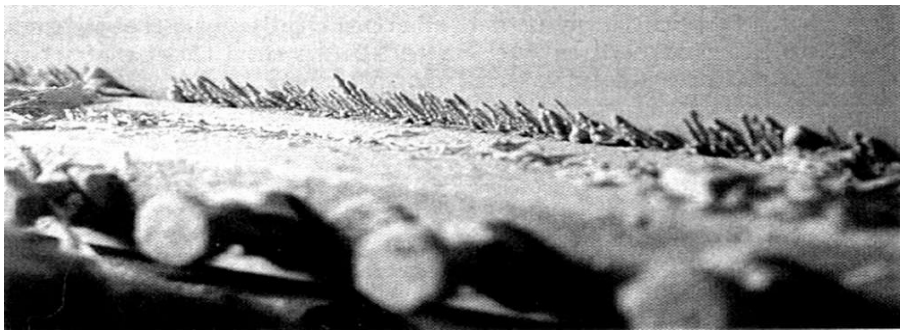

Figure 1.1. Stalagmites on the blade tip taken from Weigl and Grossmann (1997)

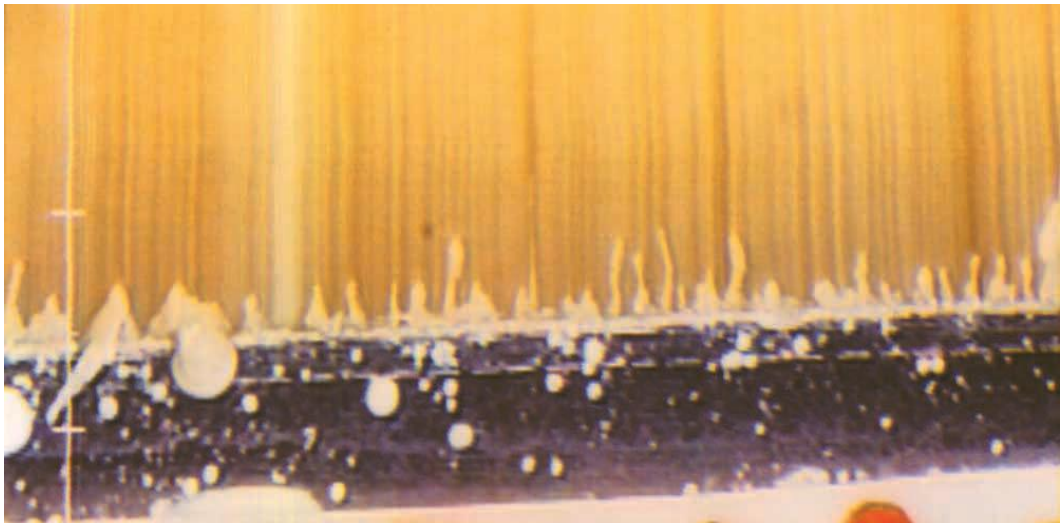

Figure 1.2. Image of blade bleeding and wet stalagmite formation taken from Doi *et al.* (1999)

Stalagmite formation can remain benign during the coating process. The formation of stalagmites does not always result in defects, it does add some uncertianity into the long term runnability of that coating (Ettl *et al.,* 2000). If the stalagmites fall clear of the paper web, they do not cause any damage or defects to the product. When the stalagmite becomes detached from the blade and lands on the surface of the coated paper, deposits result on the surface. Once the stalagmites land on the paper surface, they have the potential to cause damage to equipment downstream from the coater, also (Gane *et al.,* 1992).

Streaks have alternatively been defined as stripes of heavier coating thicknessess that run parallel with the machine direction and can be up to several centrimeters in length (Diass *et al.,* 1998). Spits are created when droplets of the excess coating attach to the coating surface (Gane *et al.,* 1992). An example of streaks is displayed in Figure 1.3 and spits in Figure 1.4. If wet bleeding happens, in extreme circumstances, higher coat weight streaks can wander across the web indicating freedom in the lateral direction, see Figure 1.3. It has been proposed that one of the key mechanisms behind wet bleeding is the transition between relaxation-induced diltancy and plug flow to the establishment of a slip plane on the blade boundary (Gane, 1997).

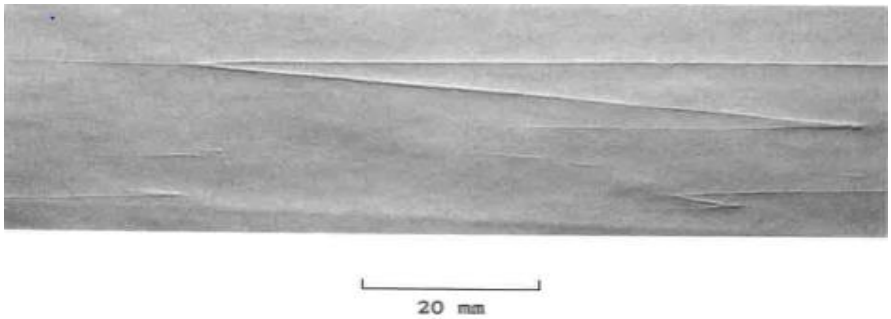

Figure 1.3. Streaks displaying freedom of a lateral boundary on the paper surface taken from Gane *et al.* (1992).

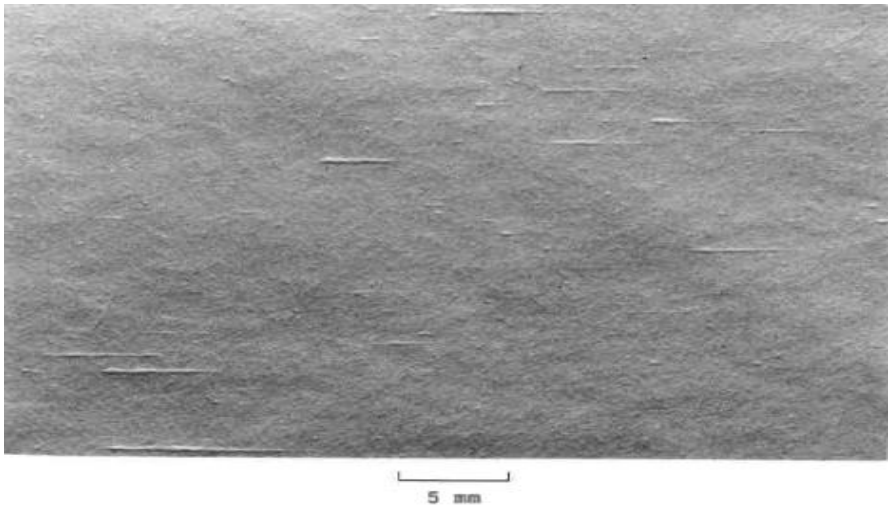

Figure 1.4. Spits on the surface of coated paper taken from Gane *et al.* (1992)

Besides streaks and spits, other effects such as scratches and skips are possible defects that can appear on the final product. Skips on the paper surface are areas barren of coating, which leave the final product with a patterned surface (Ettl *et al.,* 2000). One of the main causes behind skips in the coating layer is entrainment of air or foam bubbles in the coating color (Weigl and Grossmann, 1997). Scratches are indents on the final coating surface aligned with the machine direction (Ettl *et al.,* 2000; Daiss *et al.,* 1998). The precise cause for these defects to occur is still a debated topic. There are many theories based on which interactions between the coating, base stock and blade coater conditions are the main culprit for initiating runnability issues.

Runnability Studies from Literature

Literature is brimming with studies into the possible causes for runnability issues. Many of these investigations were conducted on either bench top or pilot scale blade coaters. Most of these studies focused on how just one or two variables affected the runnability of the coating color. Table 1.1 summarizes each of these past runnability studies. Their experimental methods and conclusions are reviewed.

Table 1.1. Listing of previous runnability studies with their methods and conclusions

Authors	Methods	Conclusions
Branston, R.E. *et al.* (1994)	Experimental – Pilot scale coater	· Development of the bleeding on the blade during coating
Branston, R.E. *et al.* (1994)	Experimental – Pilot scale, SEM, X-ray	· Trunks of the weeps contained more lumps of pigment than the crowns · Possibility of aggregates initiating weeping
Dahlvik, P. *et al.* (2000)	Experimental - Pilot scale blade coater, rheometry, and water retention	· No correlation between stress peaks from dynamic oscillation and runnability · No simple connection between dewatering and runnability · Table of critical coating speeds
Doi, S. *et al.* (1999)	Experimental - Rubber backed bench scale and pilot scale blade coating	· In addition to water retention and high shear viscosity, a third property affects runnability · Table of critical coating speeds
Engström, G. and Rigdahl, M. (1989)	Experimental – Pilot scale coater Theoretical – Equation development	· Shape of the inlet channel between the blade and the base paper plays a role in the runnability
Ettl, R. *et al.* (2000)	Experimental - Ring slit rheometry	· Increased contact time between colliding particles, colloidal suspensions are less stable in converging flow fields · Aggregates were formed resulting in a strong pressure increase and slit was clogged.
Gane, P.A.C. and Watters. P. (1989)	Experimental – Bench coater	· Increased blade angle improves runnability
Gane, P.A.C. *et al.* (1992)	Experimental – Bench coater	· Runnability can be improved in four main areas: pigment characteristics, coating formulation, base sheet properties, and environmental conditions
Gane, P.A.C. *et al.* (1997)	Experimental	· Control the flow geometry, coater speed and solids content to improve particle alignment for better runnability
Ghosh, T. *et al.* (1997)	Experimental – CLC, rheology, water retention	· Critical stress at very small strain correlated well with coating runnability
Hardy, R.E. and Carter, D. (1994)	Experimental – Water retention and CLC	· Raising the immobilization solids level of a coating increases its runnability

Table 1.1 Continued

Authors	Methods	Conclusions
Olsson, F. and Isaksson, P. (1995)	Theoretical – Viscoelasticity	· Backward flow at the blade tip is a result of elastic behavior · Reverse flow could be a cause for stalagmite formation · Adjustment to the blade and flow channel could make the reverse flow disappear
Okomori, K. *et al.* (2002)	Experimental – Water retention, pilot scale blade coater, high shear rheometry, temperature	· Big temperature changes resulted in poor runnability · Temperature changes are dependent on water retention, fluidity and base paper properties
Roper, J. and Attal, J. (1993)	Experimental – Pilot scale, rheology Theoretical – Rheology and flow models	· High shear rheology important in controlling runnability · Shear thickening coaters exhibited runnability issues · Proper set of the coater configuration vital for limiting blade bleeding · Water retention of coating also affects runnability
Suontausta, O.T. (1993)	Experimental – Bench coater, rheology	· Stalagmites formation affected by the shear force of the blade on the coating color. · Increasing the elasticity increases the chances of stalagmite formation
Teirfolk, J-E. and Laaja, V. (1996)	Experimental – Pilot scale blade coater	· Preshearing of clays aids with runnability
Tran, T.H. *et al.* (1993)	Experimental – Bench coater, rheology	· Binders, such as soy polymers or CMC, affect the runnability and stalagmite formation
Vodnick, J.L. *et al.,* (1995)	Experimental – Pilot scale blade coater, high speed video, stop action photography	· Microweeping and microwhiskering appear before blade bleeding occurs · Weeping occurs at site specific locations · Microwhiskers and microweeps appear to form through sudden extrusion coating
Weigl J. and Grossmann, H. (1997)	Experimental – Pilot coater	· Dry whiskers have greater fiber content than dry stalagmites · Base sheet properties affected runnability issues

Table 1.1 Continued

Authors	Methods	Conclusions
		· High aspect ratio clay with a narrow size distribution more predisposed to bleeding · Small doses of starch improve runnability · Increased filler content of base stock increased stalagmite length
Weigl, J. *et al.* (1997)	Experimental – Water retention, capillary viscometry, bench coater	· It is not possible to separate out each coating component's contribution to the rheology or the runnability · Increased filler content of base sheet increased stalagmite length
Willenbacher, N. *et al.* (1997)	Experimental – High shear rheology, wall slip, solid increase due to dewatering	· Not possible to divide out the effect rheological behavior has on runnability from other factors

A comprehensive review of the properties that affect coating runnability will be discussed in the following sections. It has been separated into three main categories: pigment characteristics and coating formulation, base sheet properties, and blade coater operating conditions.

Pigment Characteristics and Coating Formulation

One of the speculated causes for runnability issues is related to the properties of the pigment and the coating formulations. It has been well established that pigments with high aspect ratios may exhibit runnability issues at slower machine speeds and lower solids contents than traditional coatings containing calcium carbonate. The size and shape of a pigment used in a coating play a major role in the properties of that coating. Many past studies state that the rheology of a coating causes the runnability issues. However, others caution that the rheology of importance is not the steady state behavior but that of response to transients (Gane e*t al*. 1992; Gane *et al*., 1997; Gane, 1997). Particle shape has a sizeable effect on the viscosity of the

suspension. A complete understanding of the rheological behavior of a coating is vital to determining its role in the coating application process. Particle shape also affects other properties of the coating. Water retention, packing structure, and orientation are dependent on the morphology of the pigments in the coating. A review of colloidal rheology and the parameters that influence runnability is included below.

The rheology of colloidal suspensions has a long history. It has been studied by many researchers over the years. The volume fraction of the solids, particle size and shape, and the behavior of the suspending medium all add complexity to the rheology of a colloidal suspension. While some coating colors are comprised of monodispersed spherical pigments that follow the general rheology of a colloidal suspension, most coatings consist of non-spherical shaped pigments where the size, shape and the particle size distribution all need to be factored into the behavior of the suspension.

Most suspensions containing colloidal particles follow the general curve as shown in Figure 1.5. The shear rate viscosity curve exhibits four unique regions. Region A is a Newtonian plateau at low shear rate but larger than the yield point shear of the suspension. Region B is a shear thinning region as the shear rate is increased before a second Newtonian plateau appears at a higher shear rate in region C. The last region shows shear thickening characteristics. The motion of the particles in the suspension at each shear rate can predict the viscosity. At the low shear rates, the Brownian motion of the particles allow for them to be randomly disorganized (Bousfield, 1993). This creates the upper Newtonian plateau of region A. As the shear rate is increased, the particles are organized into layers and they are able to flow past one another with relative ease thus creating the intermediate shear thinning region of B. In the Newtonian plateau in region C, the inter-particle interactions dominate over the Brownian motion. The shear thickening region of D is caused by the destruction of the layers of particles. Further shear

thinning is then associated with collective particle motion (Toivakka and Eklund, 1994). The volume fraction of particles, particle size distribution and solvent phase viscosity are some of the factors that determine the appearance and severity of the shear thickening region (Barnes *et al.,* 1989).

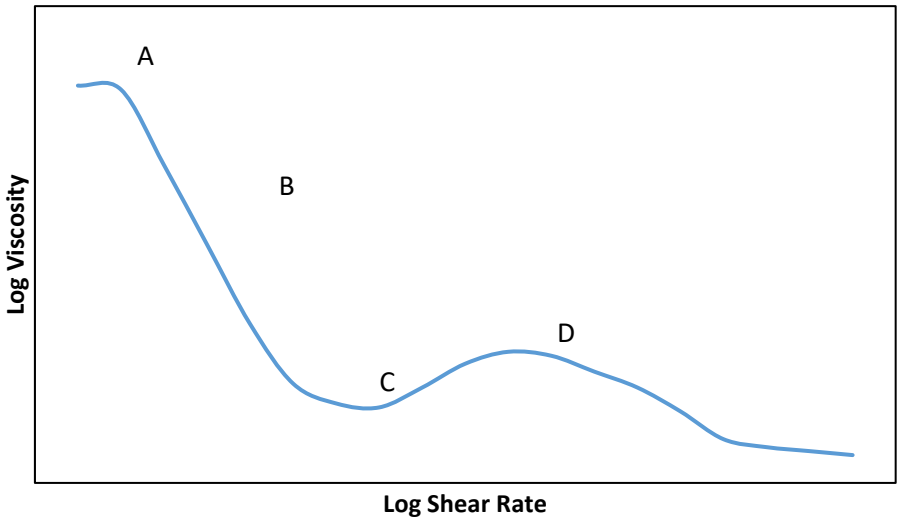

Figure 1.5. General shear rate viscosity curve for a colloidal suspension

Many empirical equations have been developed to describe the shear rate viscosity curve of colloidal suspensions. The Carreau equation has been used in the past to describe the rheology of coatings. This equation quantifies the upper and lower Newtonian plateaus and the shear thinning region in the intermediate zone. It should be noted that this equation does not describe the shear thickening region nor the subsequent shear thinning. The equation is shown in equation 1.1:

$$\frac{\eta - \eta_\infty}{\eta_o - \eta_\infty} = \frac{1}{(1 + (K\dot{\gamma})^2)^{\frac{m_1}{2}}} \qquad \text{Eq. 1.1}$$

where η is the viscosity of the suspension, η_o and η_∞ are the asymptotic viscosity at low and high shear rates, respectively, K is the constant parameter with dimension of time, m_1 is the dimensionless constant and $\dot{\gamma}$ is the shear rate.

The concentration of solids in the suspension has a large effect on the viscosity. The concentration of the particles is often described more realistically in terms of impact on flow by the volume fraction of the pigment contained in the solution. The rheology of a suspension is determined by the hydrodynamic forces exerted on the surface of each of the particles held in the suspension (Barnes *et al.,* 1989). The smaller the distance between the surfaces of the particles the stronger the interparticle forces will be. The ability of a particle to rotate and flow in the suspending liquid without interference from neighboring particles will affect the viscosity (Alince and Lepoutre, 1983). As the maximum flowing fraction is approached, which is the maximum volume fraction that flow is still achievable, there is a sharp rise in the viscosity of the suspension (Hase and Bousfield, 1994). It is desirable to predict the viscosity of a suspension based on the volume fraction of particles since the concentration of particles has such a drastic effect on the rheology of the suspension.

For dilute ($\leq$10%) suspensions of spherical particles, the system behaves more like the idealized volume fraction expression given by the Einstein equation, as shown in equation 1.2. This equation does not account for the size distribution, shape or interparticle interactions in the suspension. Therefore, it is only valid for spherical particles and at dilute concentrations, where the particles are sufficiently separated, and the particle-particle interactions are dominated by the hydrodynamic forces (Barnes *et al.,* 1989).

$$\eta = \eta_s(1 + 2.5\phi) \qquad \text{Eq. 1.2}$$

where η is the viscosity of the suspension, η_s is the viscosity of the suspending liquid and ϕ is the volume fraction.

As the volume fraction of the suspension is increased, the mutual interactions between the particles will cause a steep rise in the viscosity. There are many current equations that describe the relationship between the volume fraction and viscosity. Most of these viscosity relation predictive equations use two parameters to describe the characteristics of these pigments; the maximum packing fraction and the intrinsic viscosity. The maximum packing fraction used in the equations accounts for the crowding effect in the concentrated suspension and the impediment of neighboring particles to rotation and flow (Barnes *et al.,* 1989). This parameter is a function of the particle shape and size along with the particle size distribution. A broader particle size distribution will increase the maximum packing fraction due to the enhanced packing ability of the smaller particles filling the void space between the larger pigments. The intrinsic viscosity is a dimensionless quantity that has been associated with the shape of the particles. The intrinsic viscosity correlates with the amount of resistance to flow for a single particle contained in the suspension (Lindhjem, 1991). Deviations from a perfect spherical particle will cause an increase in the viscosity of the suspension by affecting both the intrinsic viscosity and the maximum packing fraction (Barnes *et al.,* 1989). The shape of the particles in the suspension will alter the intrinsic viscosity more than it will the maximum packing fraction (Lindhjem, 1991).

The Krieger-Dougherty equation is a well-known equation that predicts the viscosity of a suspension based on the volume fraction, maximum packing fraction and the intrinsic viscosity. The equation was derived from the differential form for Einstein's equation for the viscosity of a dilute suspension (Barnes *et al.,* 1989). The maximum packing fraction was added to the equation to account for the crowding effect observed in a concentrated suspension. The

intrinsic viscosity allows the equation to be applied to any particle shape. For a suspension of only perfect spheres, the intrinsic viscosity would be 5/2 (Barnes *et al.,* 1989). The Krieger-Dougherty equation takes the following form to predict viscosity, η as

$$\eta = \eta_s \left(1 - \frac{\phi}{\phi_m}\right)^{-[\eta]\phi_m} \qquad \text{Eq. 1.3}$$

where η_s is the viscosity of the fluid phase, $[\eta]$ is the intrinsic viscosity and ϕ and ϕ_m are the volume fraction and the maximum volume packing fraction of the particulate phase, respectively.

Two other equations have been used to describe the viscosity of concentrated suspensions. Both the Mooney and Eiler equations use the volume fraction, maximum packing fraction and the intrinsic viscosity to describe the viscosity of a concentrated suspension, but the functional forms are different. The Mooney equation is given as

$$\eta = \eta_s \exp\left(\frac{[\eta]\phi}{\left(1 - \frac{\phi}{\phi_m}\right)}\right) \qquad \text{Eq. 1.4}$$

The Eiler equation is given as

$$\eta = \eta_s \left(1 + \frac{[\eta]\phi}{2\left(1 - \frac{\phi}{\phi_m}\right)}\right)^2 \qquad \text{Eq. 1.5}$$

The rheology of a coating has long been a central property for trouble-free application. It has been thought that a coating exhibiting dilatancy during high shear would have a predisposition for stalagmite formation. Dahlvik *et al.* (2000) concluded that a relationship existed between high shear rate and runnability issues. Roper and Attal (1993) discovered that shear thickening coating caused more blade wear even with the blade running parallel to the web. While other researchers have determined that viscosity of the coating has little effect on

the formation of stalagmites (Suontausta, 1993). While there is some debate on how much an effect the rheological behavior has on the coating process, it does seem likely that there is some influence of the viscosity during coating.

The role of viscoelasticity during coating is one of the debated topics. Coating formulations also exhibit viscoelastic properties due the intramolecular forces in the suspension (Barnes *et al.,* 1989). While full coating colors have larger elastic properties due to the interactions between the latex and the particles; small yield stress and storage moduli do exist for pigment slurries (Lohmander and Rigdahl, 2000). The degree of viscoelasticity is a function of the solids content and the amount of latex, with a stronger dependence on the concentration of latex (Dahlvik *et al.,* 2000). Speculation that higher viscoelastic characteristics of the coating can induce difficulties during coating has been examined by multiple researchers. Dahlvik *et al.* (2000) determined that there is no correlation involving runnability and viscoelasticity when measured in the linear viscoelastic regime. High shear rheological measurements at steady state show that viscous forces dominate, and elastic forces are negligible (Ghosh *et al.,* 1997). While the exact role of viscoelasticity has on the initiation of blade bleeding is still open for debate, it is an important characteristic of paper coating suspensions. Further exploration in this area is needed, especially to consider the role of elasticity induced due to rapid changes in shear rate and flow direction, where it is hypothesized that the time for elastic and inertial relaxation is longer than the transient condition of the shear rate regime (Gane, 1997). This reasoning suggests that considering viscoelasticity under classical linear low strain conditions will not resolve the question of the role of viscoelasticity in practice as a cause of normal dilatancy.

While rheology is one of the most cited reasons for runnability issues, other properties such as water retention and the packing ability could also influence the formation of stalagmites. Excess dewatering of the coating is the second most cited source for runnability

problems. As the water penetrates the base sheet paper, the solids content of the coating increases. As this occurs, the solids fraction begins to climb towards the immobilization solids concentration. Once that concentration of particles is reached, flow will cease and the possibilities for defects and runnability issues will amplify. As the blade meters off the excess coating, it will disorder the immobile phase causing defects on the surface of the product (Hardy and Carter, 1994).

How tightly the particles pack together is a function of the shape, size and size distribution. Large aspect ratio pigments have the potential to pack in a dense manner, but any disorientations can result in an enforced loose packing structure. Calcium carbonate, which has blocky particles will form small capillaries when they are tightly packing, while platy pigments can pack tightly together, thus increasing the tortuosity and path length for pressure driven permeating flow (Gane *et al.,* 1992). The effect of particle shape on the packing structure is shown below in Figure 1.6. The packing arrangement will alter the dewatering property of the coating during the application process.

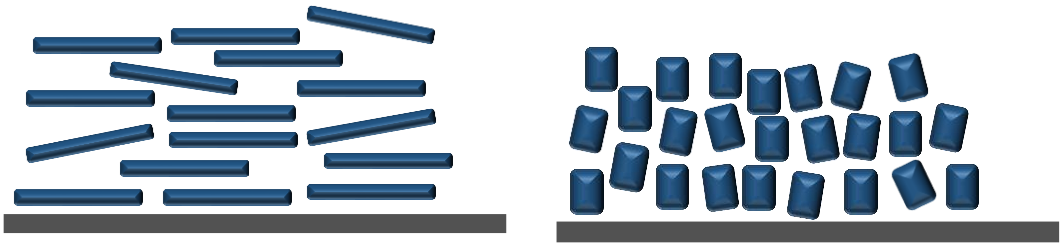

Figure 1.6. Packing of plate shape pigments (left) and blocky particles (right)

The packing structure of the particles in the flow field is a crucial component in determining the runnability of a coating. How the particles are able to pack will affect both the water retention and the ability of the particles to move past each other in a shear field. If the plate like pigments are aligned with the flow field as they pass underneath the blade, then the coating should flow under the blade nip without disruption (Gane and Watters, 1989). However,

if particles are misaligned with the flow field, they will interfere with the packing configuration and could result in the formation of stalagmites (Gane *et al.,* 1997). The exact conditions that lead to a smooth motion of pigments under the blade and the formation of stalagmites is, however, not clear in the literature.

Base Sheet Properties

The properties of the base sheet also influence the ease at which a coating can be applied. The interactions between the web and the coating can alter the coating characteristics. With the porous and absorbing structure of paper, the application of a coating will alter the physical characteristics. These changes include modifications of the surface roughness, debonding of the fibers, and overall weakening of the cellulose network (Ettl *et al., 2000;* Gane *et al.,* 1992). Diminishing fiber bonding on the paper surface can lead to picking, which will contaminate the coating color with paper fibers (Gane *et al.,* 1992). These fibers can build up in the coating due to recirculation of the coating color, and the increased debris concentration has the potential to initiate blade bleeding. The three main aspects of the base sheet that could factor into coating runnability are the porosity, or better defined as permeability, surface smoothness and compressibility.

Dewatering of the coating into the base sheet occurs by a number of mechanisms, including film flow over the fibers and pressure-driven permeation into the network of pores of the base paper. With the large pressure pulse occurring during coating, pressure-driven permeation is the major contributor to the dewatering of the coating color. This dewatering will increase the solids content in the coating layer. With less water in the applied coating color, the coating will have a higher viscosity due to an increase in the solids content or a thinner fluid layer above a filter cake (Okomori *et al.,* 2002). Then the concentration of solids will increase to such a level that stalagmite formation is a more probable occurrence (Weigl *et al.,* 1997).

The distribution of pores in the base paper will influence the penetration rate of water especially in respect to permeability. The quantity of fillers at the surface of the paper will amplify the number of pores and expanding the surface area and the capillary action of dewatering (Weigl *et al.,* 1997), but unless the filler disrupts the packing of the fibers, the permeability will otherwise be reduced. Weigl *et al.* (1997) demonstrated that base stock containing more filler produced longer stalagmites, though it is not understood whether this is due to capillary-driven dewatering or the inevitably smoother sheet resulting from the higher filler content. Gane (1997) proposed that pressure pulse driven dewatering of the coating prior to the blade nip couples with the sudden change of shear rate and flow direction between the metered excess and the coating layer which may lead to an induced bulk slip plane under the blade with the resulting wet bleeding, having the viscosity close to that of un-sheared coating color. The absorptive and permeation properties of the base sheet are major players in the dewatering of the coating and its subsequent runnability.

The surface roughness and compressibility of the base sheet have been speculated to increase a coating's predisposition for stalagmite formation. Suontausta (1993) discovered that increasing the smoothness and compressibility of the base paper escalated stalagmite formation, supporting the comment above as to questioning the role of high filler loading in the base sheet, which generally leads to a smoother surface. At first, this seems counter intuitive, but he demonstrated that a calendered base sheet can swell strongly upon contact with water, leading to more defects during coating. Incompressible base papers have a predetermined dynamic surface void volume, which has been shown to be problematic with respect to coat weight control and constant tip angle blade tensioning mechanisms (Gane *et al.,* 1992). With the characteristics of the base sheet causing additional problems for control of the coater operating

conditions, the runnability issue could increase. Any deviation from the desired blade angle has been demonstrated to increase stalagmite formation (Gane and Hiorns, 1991).

Blade Coater Operating Conditions

The operating conditions of the blade coater can be adjusted to reduce the potential for stalagmite formation. Engström and Rigdahl (1989) determined that increasing the blade angle and thinner blade thickness led to less tendencies to initiate the onset of blade bleeding. Controlling the blade coater settings, such as the blade angle, blade thickness, or the web speed, have been shown to lessen the chance for runnability issues. A balance between these parameters will be necessary for a coating application without any runnability problems.

High solids, fast web speeds and low blade angles have been determined to be one of the worst combinations of variables to aid in the formation of stalagmites (Gane *et al.,* 1992). Lower blade angles have a more drastic rate of change of separation of shear fields leading up to the blade nip than with a higher blade angle. This change in the flow field has been shown to have a greater chance of starting runnability issues. Gane and Coggon (1987) found that by adjusting the blade angle, the packing structure of a clay coating could be controlled. A blade angle of 60^{o} resulted in a smoother finish and higher gloss, which was related to alignment of the particles with the base sheet, than a coating applied with a blade angle of 30^{o} (Gane and Coggon, 1987). Proper alignment of the blade with the base sheet is paramount; running the blade on either heel or tip increases the formation of stalagmites (Suontausta, 1993). Roper and Attal (1993) determined that running on the heel of the blade resulted in weeping and spitting while coating with the toe of the blade developed dry whiskers and more web breaks, findings consistent with the prediction of shear banding as the cause of wet bleeding versus plug flow and relaxation-induced dilatancy as the cause of dry stalagmite formation (Gane, 1997). Coating with the land area parallel to the base sheet resulted in cleaner runs but bleeding did occur with

some coating formulations (Roper and Attal, 1993). The configuration of the blade is a crucial tool for the control of any potential runnability issues.

The flow channel the blade makes with the paper web has an impact on the runnability limits for a coating (Gane *et al.,* 1997). The geometry of a flow channel is controlled by the blade angle and the compressibility of the base paper under the blade (Engström and Rigdahl, 1989). The geometry of this flow channel controls how a particle rotates. When particles are rotating through the shear field, collisions between the particles cause "log jams", and particle structures form, which contribute to skipping and streaking defects (Gane and Watters, 1989). The misalignment of particles with the machine speed has large implications on both the runnability and the final product (Gane *et al*., 1997).

The turbulence in the region before the nip of the blade has both advantages and disadvantages. Rotation of the particles from this flow field can lead to disorganized packing structure, which can contribute to runnability issues. On the other hand, if the shear flow becomes turbulent in this region before the nip it might be expected that it might cause any aggregates of pigments to separate (Daiss *et al.,* 1998). The presence of pigment clumps has been identified as a likely source for the initiation of stalagmite formation and scratches in the coating layer (Daiss *et al.,* 1998; Gane and Watters, 1989), where the latter authors identify the stagnation point at the blade surface prior to the nip entry as a likely source for this structuration and static viscoelasticity. The flow channel created by the blade coater is a dynamic element in controlling the runnability of a coating.

Structure of Thesis

This thesis is written such that each chapter is a standalone paper with background and literature review included. Chapter 2 is a manuscript entitled, "Effect of particle shape and size

distribution on dewatering and filtercake permeability", which was presented at the 2017 TAPPI PaperCon conference. This paper focused on the influence that the shape of the pigment and the particle size distribution had on the water retention and filtercake permeability. The pore size distributions of a range of packed pigments, in the form of a dewatered filtercake, with different shape factors were also analyzed using mercury porosimetry. Chapter 3 contains the results of a runnability study conducted on a bench top blade coater. The critical coating speed was determined for three pigments with different shape factors and varying weight fractions. The influence of the high viscosity and the alignment of the blade was also investigated. The following chapter expands the runnability studies to a larger scale using a cylindrical laboratory coater. The effect of dewatering is included in this trial by testing two base sheets with different permeabilities. The last chapter is a mathematical model of the filtercake buildup on a blade coater during the coating application process. This model estimated the growth of a filtercake during the blade coating process using conditions similar to those in the CLC runnability trials. Included in the appendix is a manuscript titled "The influence of particle shape and blade geometry on particle alignment", which was presented at the 2015 TAPPI PaperCon conference.

CHAPTER 2

EFFECT OF PARTICLE SHAPE AND SIZE DISTRIBUTION ON DEWATERING AND FILTERCAKE PERMEABILITY

Abstract

Excess dewatering of the coating upon contact with paper is one potential source for runnability problems. As the water penetrates the base sheet paper, the solids content of the coating increases. This increase in concentration can lead to operational problems such as scratches or excessive blade wear. The influence of the shape factor of the pigment on the dewatering properties of a coating has not been the subject of a systematic study in the literature.

The effect of the particle shape and particle size distribution on the dewatering and the filtercake permeability were analyzed. The dewatering rates were measured with the common pressure filtration method called the gravimetric water retention (GWR) test, and with a Bristow absorption wheel. The pore size and porosity of the dried filtercakes were characterized with mercury porosimetry. The permeability of the filtercakes was obtained by fitting the data to a filtration equation and predicted by the Carman-Kozeny equation. The particle shape is found to influence the permeability, but the results do not simply follow the theory.

Introduction

The water retention property of a coating is vital for trouble free operation during the application process. Large dewatering rates may cause potential complications during coating because the water loss to the base sheet increases the solids content near the blade nip. As this occurs, the solids fraction begins to climb towards the immobilization solids concentration changing the rheology of the coating. If the solids increase to the immobilization solids, flow will

cease and the possibilities for defects and runnability issues will amplify. As the blade meters off the excess coating, it will disorder the immobile phase causing imperfections on the surface of the final product (Hardy and Carter, 1994). The thickness of the filtercake can become so large that it causes issues during coating including a large pressure pulse which drives more water into the base sheet (Bousfield, 1994).

How tightly the particles pack together is a function of the shape, size and distribution. Large aspect ratio pigments have the potential to pack in a dense manner, but any disorientations can result in an enforced loose packing structure. Calcium carbonate, which has blocky particles will form small capillaries when they are tightly packing, while plate pigments can pack tightly together, thus increasing the tortuosity and path length for pressure driven permeating flow (Gane *et al.,* 1992). The effect on particle shape on the packing structure is depicted in Figure 1.6. The packing arrangement will alter the dewatering property of the coating during the application process, but a clear study of the influence of particle shape on dewatering rates has not been reported in the literature.

Modifying the particle size distribution will alter both the packing structure, the permeability of the filtercake that forms on the paper, and the water holding capacity. Addition of smaller particles, such as a latex, will fill in the pores created from the misalignment of the larger pigment particles. Knappich *et al.* (2000) demonstrated that broadening the particle size distribution using latex improved the water holding capacity of the coating formulation.

When a pigmented coating contacts a porous web, water is absorbed in the pores of the paper. The coating nip, either a blade, roll or rod, generates a pressure pulse that can also force water into the paper pores (Pajari *et al.,* 2003). As water is removed from a coating layer, the solids increase and filtercake layer begins to form on the paper web. The rate of dewatering is

controlled by the permeability of the filtercake that in turn, is determined by the pigment packing, pore size and pore connectivity. Using Darcy's law for flow in porous media and equations that link the filtercake thickness to the volume of water that has moved into the paper, an expression is obtained that predicts the volume of water *V* that is in the paper (Sonn and Bousfield, 2015) as:

$$V = \sqrt{\frac{2K_f \Delta P(\phi_f - \phi)t}{\mu\phi}} \qquad \text{Eq. 2.1}$$

where K_f is the permeability of the filtercake, ΔP is the pressure difference that drives the flow, ϕ_f and ϕ are the volume fraction at immobilization and the coating, respectively, t is the time, and μ is the viscosity of the water phase.

The permeability of the filtercake is a function of the void fraction and the size and shape of the particles in the filtercake. These values can be found by an analysis of the filtercake by porosimetry. The Carman-Kozeny relation estimates the permeability based on the porosity, ε, and the specific surface area, S_o, of the particles as

$$K_{\mathrm{f}} = \frac{\varepsilon^3}{5S_o^2(1-\varepsilon)^2} \qquad \text{Eq. 2.2}$$

In this study, the influence of particle shape and particle size distribution on the water retention property and the permeability of the filtercake is investigated. Multiple methods of examining the dewatering rate are used for a range of pigments with varying shape factors. The packing structure was also explored using porosimetry. The permeability constants calculated from both dewatering tests and the results from Blake-Kozeny equations were compared.

Experimental Method

For this study, a selection of pigments was chosen to provide a range of aspect ratios. Four kaolins and one calcium carbonate were used. Hydrocarb® 60 (Omya), identified as GCC from this point forward, was the selected calcium carbonate pigment. It had the lowest aspect ratio. It was assumed to be about one. The four kaolin clays used for this analysis were Astra-Glaze (Imerys), XP10-6003 (Imerys), XP98-8000 (Imerys) and XP01-6100 (Imerys). These pigments have shape factors that should be similar to aspect ratios of 15, 35, 60 and 90, respectively, as reported by the supplier. These pigments will be identified based on their aspect ratio or shape factor as KXX. For instance, the kaolin pigment with a shape factor of 35 is identified as K35. Slurries of these pigments obtained from their manufacturer were mixed using a high shear mixer to ensure adequate dispersion of the particles. During the slurry only portion of this study, no other dispersants, additives or latexes was added to the suspension other than what is already included by the manufacturer. This was done to limit the complexities of the suspension while focusing in on the affect that particle aspect ratio has on the dewatering of the suspension. The mass fraction was ascertained by a dry weight method.

To address the effect of the addition of a latex on the dewatering of a coating formulation, a plastic polystyrene pigment (DOW 756ANA BK) was used to simulate the inclusion of a binder into the suspension. A single pigment XP1-6003 (Imerys) which has a shape factor of 35 was used. The concentration of the hard sphere latex, with a particle of radius 115 nm, was varied at 5, 10 and 15 pph. A plastic pigment was chosen for this study in order to have the particles retain their shape during testing of the porosity. The coating formulations were mixed using a high shear mixer to ensure adequate dispersion of all components.

The immobilization solids concentration was also determined for each sample. A small volume of sample was placed on the top of a porous ceramic disk. Once the gloss of the surface

of the slurry samples has disappeared, the sample is removed, and the solids content is determined.

The rate of dewatering was measured using two different methods. The first was using the standard gravimetric water retention method (AA-GWR, Kaltec). The amount of water being forced out of a 10 mL sample with one bar of pressure was measured. The dewatering time was varied at intervals of 10, 15, 30, 60 and 90 seconds. This test is a pressure filtration of the suspension and should not be confused with a test performed for pulp fibers called water retention.

The second dewatering test used the Bristow absorption wheel tester (Bristow Laboratory Apparatus). A 10 µL sample of the suspension was placed into the device. The base sheet onto which the suspension was contacted was held constant using HP “brochure” paper; this paper was selected because it has a high absorption capacity with fine pores and a smooth surface. The wheel speed was varied from 0.01 to 10 cm/s to provide different contact times between the sample and the substrate. The Bristow wheel is designed to measure the absorption rate of a pure fluid into the substrate, but here we are using it to measure the dewatering of a suspension at short time. The length of the strip applied to the surface was measured and recorded. The sample was colored with a simple dye to provide better visual assessment and to increase accuracy during measured. All samples were run in triplicate for both dewatering test methods. The weight fraction of all samples was kept constant at 30%. This was required for the Bristow test, any sample with a higher solids concentration did not apply correctly to the substrate

The porosity and pore size distribution of each sample at the immobilization solids content was determined using a mercury porosimeter (Autopore IV, Micrometrics). The sample

used in the device was created following the procedure for the immobilization solids using the porous ceramic disk. The sample was dried in a 105°C oven over night. Once the sample cooled to room temperature, a fragment of the sample was inserted into the porosimeter. A standard procedure was followed, and the cumulative pore volume and the pore size distribution was calculated.

Results and Discussion

Pigment Only Slurries

The results for pigment only slurries are shown in Figure 2.1. GCC dewaters two to five times faster than any of the kaolin samples. As for the kaolin samples, the largest shape factor kaolin has the slowest dewatering rate. The GCC must pack in such a way to leave pores or channels for water to flow through it; this behavior is reasonable as illustrated in Figure 1.6. All the results seem to follow the square root of time dependency expected from Eq. 2.1. The repeatability of the experiments is good, where error bars are less than 5% of the average value. These values are much larger than that which is obtained for normal coatings because the initial solids are 30% for all suspensions.

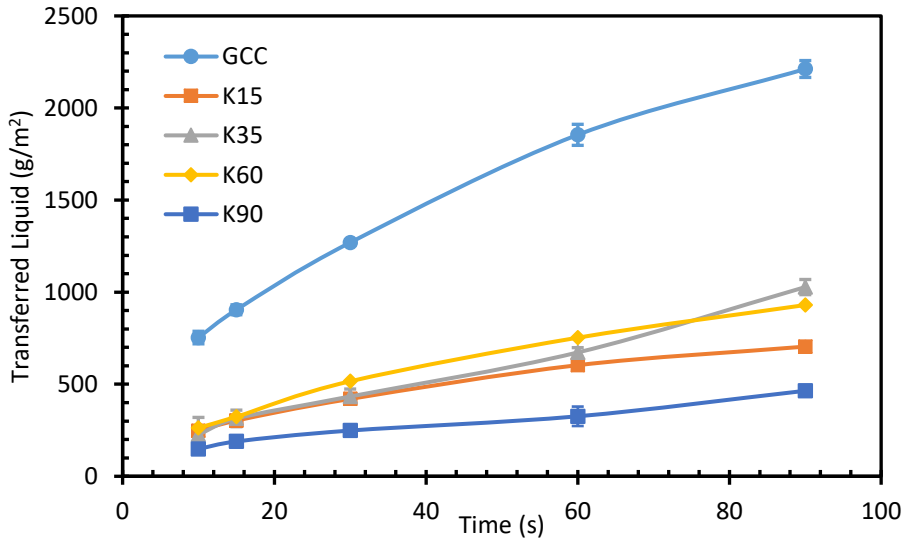

Figure 2.1. GWR results from slurries of the five pigments across a range of dewatering times.

Eq. 2.1 was fitted to the experimental data from the GWR test results to determine the permeability constant of the filtercake. The permeability constant was determined by a least squares regression method. Several parameters were held constant for all samples. The viscosity of the suspending medium was set at 0.002 Pa s. The pressure drop across the sample was set to 1 atm. The immobilizations solids content is different for each of the pigments used in the study. The values used in this study were taken from Weeks *et al.* (2016). The volume fraction of the sample was calculated from the measured weight fraction of the samples used in that test. The solids content of all samples was kept consistent at 30%. Figure 2.2 is an example of how well the fitted equation corresponds to the experimental data collected. Table 2.1 shows the permeability constant for each of the five pigments determined from the GWR results in column 2.

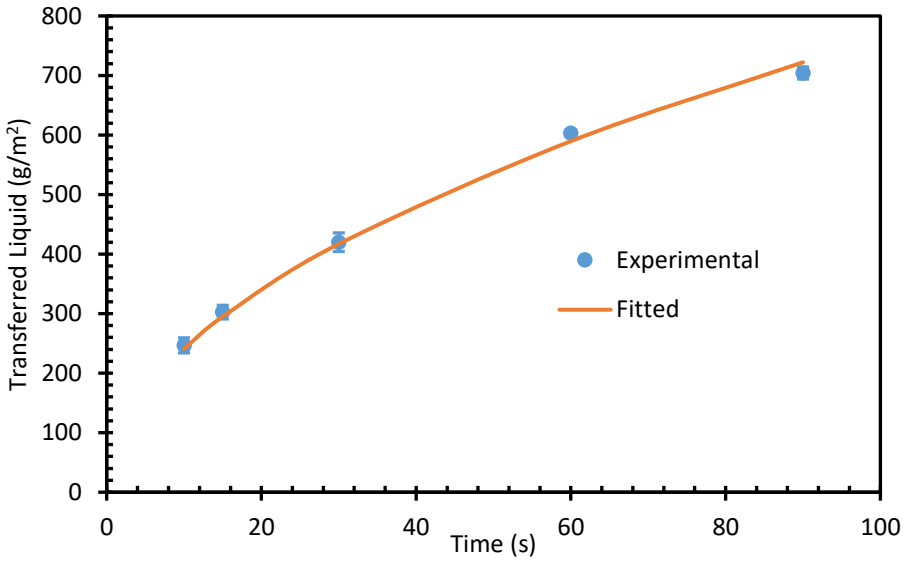

Figure 2.2. The relationship between the experimental values and those predicted for K15 pigment, using Eq. 2.1 for fitting from the GWR test

The pigment only suspensions were tested on the Bristow absorption wheel tester. The results are shown below in Figure 2.3 with the calculated permeability constants in column 3 of Table 2.1. The wheel speed was varied to provide a range of contact times between the

substrate and coating color. To obtain short contact times, the wheel speed was kept high. This was to mimic the very fast contact time observed in the coating application process. The data did show some scatter especially for the short contact time: the high wheel speed of this test may generate some artifacts such as the trough bouncing or the trough riding on a fluid layer.

As in the GWR results, GCC dewaters considerably more than any of the other four kaolin pigments. It is surprising that the K90 sample did not show to be the slowest dewatering case. The shear generated by the test should help to align the particles to generate slow dewatering. It could be theorized at the longer contact times, that the permeability of the substrate is influencing the results. Due to this fact, a definite buildup of a filtercake on the surface of the base sheet could cause the trough to ride or track on the fluid layer. This behavior would give rise to a measured high dewatering rate compared to the actual rate. Another issue may be that the long contact time gives the large plate like particles time to find pores and plug them.

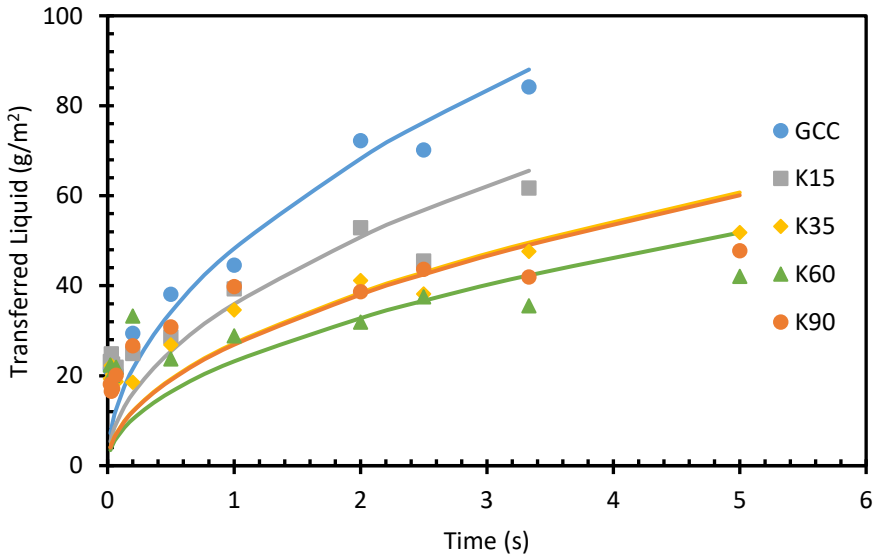

Figure 2.3. Results from the Bristow test for each of the pigments with the fitted equation

After examining the results from the Bristow tests, the question of the effect of the substrate had on the dewatering arose. To account for the permeability of the substrate, a

Bristow test using only dyed water was conducted. The results of this test are shown in Figure 2.4. The permeability constant was calculated using Darcy's law for flow through a porous medium. For this specific substrate, the permeability constant (K_s) was determined to be 2.18 x 10^{-16} m^2 and the roughness coefficient (R_s) that characterizes the surface roughness of the sample was calculated to be 16.148 cm^3/m^2. A mercury porosimetry analysis was also done on this substrate, the porosity was found to be 0.439.

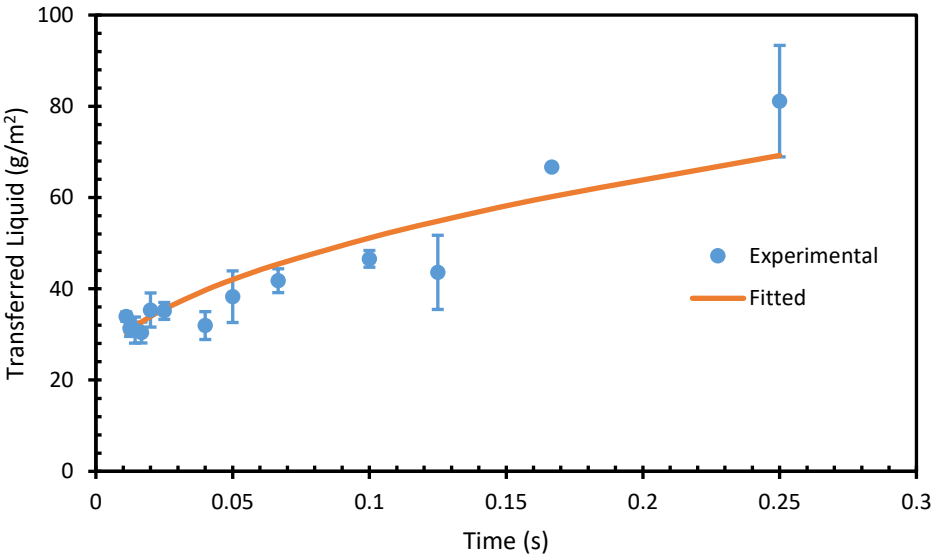

Figure 2.4. Bristow test of the substrate

Armed with this information about the substrate, Darcy's law was modified to account for two layers: filtercake and the substrate. Each layer has its own permeability coefficient. The modified Darcy's law equation used is shown below; where h_f is the height of the filtercake and L_s is the penetration depth of the liquid into the substrate.

$$\frac{dV}{dt} = \frac{\Delta P}{\mu\left(\frac{h_f}{K_f} + \frac{L_s}{K_s}\right)} \qquad \text{Eq. 2.3}$$

Both the height of the filtercake and the penetration depth are functions of the liquid volume transferred from the coating to the substrate. The height of the filtercake is determined by the mass of solids built up from the transferred volume and the amount of water contained

in the filtercake, see equation 2.4. While the penetration depth is determined from the amount of liquid transferred in the substrate and the porosity of the paper, ε, see equation 2.5.

$$h_{\mathrm{f}} = \frac{V\phi}{(\phi_{\mathrm{f}} - \phi)} \quad \text{Eq. 2.4}$$

$$L_{\mathrm{s}} = \frac{V}{\varepsilon} \quad \text{Eq. 2.5}$$

Inserting equations for h_{f} and L_{s} in to equation 2.3, the final equation was to determine the permeability for just the filtercake is shown in equation 2.6. The equation was fitted to the data from the Bristow tests and the permeability constant for the filtercake was determined by a least squares regression method. The results from this equation are displayed in Table 2.1.

$$V = \sqrt{\frac{2\Delta P t}{\mu\left(\frac{\phi}{K_{\mathrm{f}}(\phi_{\mathrm{f}} - \phi)} + \frac{1}{K_{\mathrm{s}}\varepsilon}\right)}} + R_{\mathrm{s}} \quad \text{Eq. 2.6}$$

The packing structure at the immobilization solids was measured using mercury porosimetry. From the immobilization solids data, it is known that as the shape factor increases the immobilization solids decreases. This is due to any disorganization of large plate like particles which will produce sizable disruptions in the packing structure. Figure 2.5 displays the cumulative pore volume for all samples at the immobilization solids level. This plot agrees well with what is observed with the immobilization solids data. K90 has the lowest immobilization solids and the highest cumulative pore volume. GCC has the lowest cumulative pore volume.

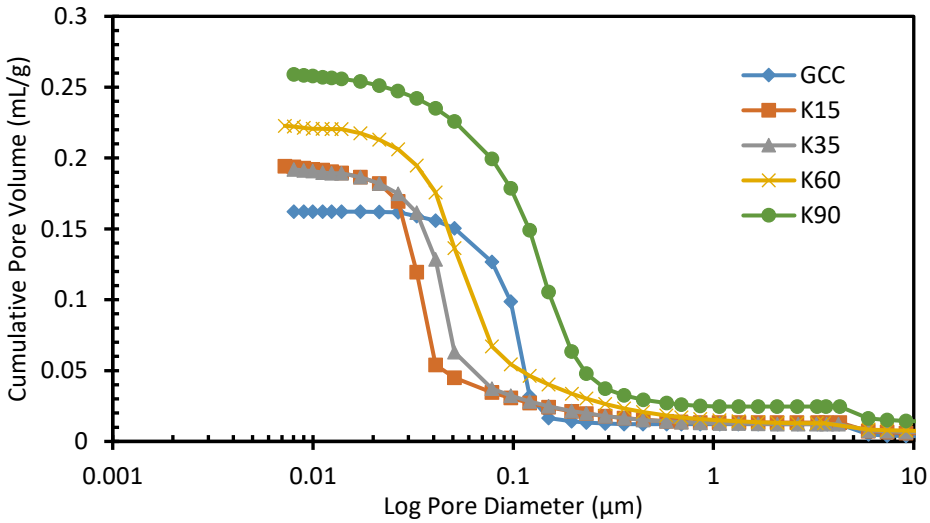

Figure 2.5. The cumulative pore volume for each of the five pigments at their immobilizations solids concentration

The pore size distributions, given in Figure 2.6, show that the large shape factor pigments, K60 and K90, exhibit broader pore size distribution compared to the three other pigments. Also, K90 has larger pores than GCC. K15 had quite fine pores with a peak at around 30 nm. With its large pore size and pore volume, K90 might be considered to have the highest permeability compared to the other pigments, but the dewatering tests display the opposite. The large plate like shape of the pigments may increase the tortuosity and thus the path length the permeating water must take to leave the filtercake.

There could be large pores present in the sample, but the throats connecting these pores could be narrow. As the mercury intrudes into the large pore, it will register as many small pores by the device. These throats connecting the pores are slowing the permeation of water in the system and increasing the tortuosity of the sample. Mercury porosimetry is a simplified model of parallel capillaries to calculate the pore sizes of the sample, it does not account for the actual shape of the pores present (Toivakka and Nyfors, 2001). Gane *et al.,* (1996) were able to overcome the limitation of pore shielding and the compressibility of the coating components to

provide more realistic values using experimental data their software package, which builds a three-dimensional structure of the sample.

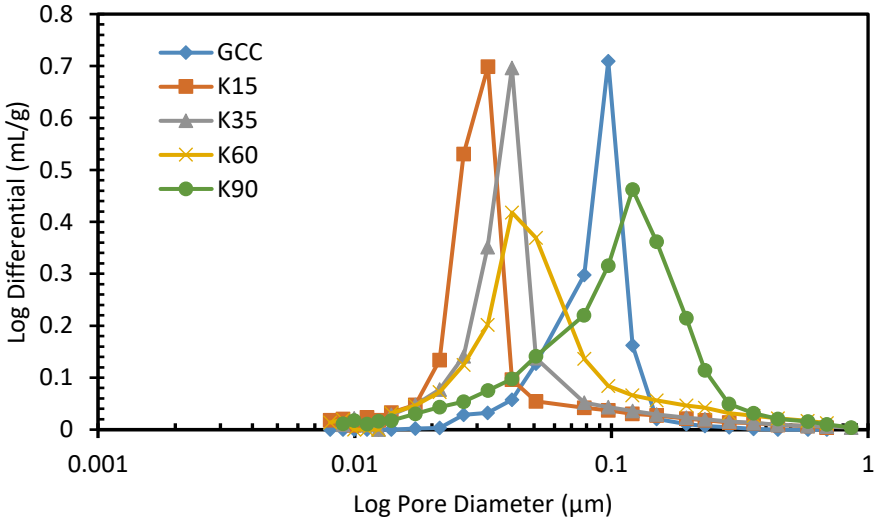

Figure 2.6. The log differential of the pore size distribution for each of the pigments at their immobilization solids concentration

The permeability constant can be estimated from the data provided by the porosimeter using Eq. 2.2. The peak in the pore size, is multiplied by three, to give some effective particle diameter, following the results of Lee (2002), who found that the pore size is around 1/3 of the particle size. Assuming the plate like shape of the particles can be approximated as short cylinders, the estimated particle diameter and the shape factor was used to calculate the specific surface area of the particles. The porosity is from the cumulative volume results in Figure 2.5. Table 2.1 displays the permeability constants calculated from that data. The permeability constants are compared from the other two different testing methods and the Carman-Kozeny Equation. A comparison of these constants in relation to the shape factor is shown below in Figure 2.7. Most of the constants are within a couple of orders of magnitude of each other.

The permeability constants calculated from the Bristow tests only show a minor dependence on the shape factor of the pigment. In contrast, the GWR and Carman-Kozeny relation shows more of the influence of the shape of the pigments on the permeability. The Carman-Kozeny equation predicted a permeability constant for GCC that is in the same order of magnitude predicted from both the GWR and Bristow tests, but with the kaolin pigments it is considerably lower. Since the Carman-Kozeny equation does account for the non-spherical nature of the particles, the decrease in the permeability can be attributed to the inclusion of the shape factor into the calculations. Even with accounting for the substrate contribution in the Bristow test, the permeability constants for the pigments still showed no dependence on the shape factor but it did decrease in value.

Table 2.1. The permeability constants calculated for the pigment only slurries

Pigment	Permeability Constants, $\boldsymbol{K_f}$ (m^2)			
	GWR	Bristow	Carman-Kozeny	Bristow with Substrate
GCC	1.7×10^{-16}	6.5×10^{-18}	2.7×10^{-17}	3.6×10^{-18}
K15	1.8×10^{-17}	4.0×10^{-18}	1.2×10^{-19}	1.7×10^{-18}
K35	3.1×10^{-17}	2.3×10^{-18}	3.8×10^{-20}	8.1×10^{-19}
K60	3.9×10^{-17}	2.5×10^{-18}	4.4×10^{-20}	7.0×10^{-19}
K90	9.0×10^{-18}	4.3×10^{-18}	7.7×10^{-20}	1.5×10^{-18}

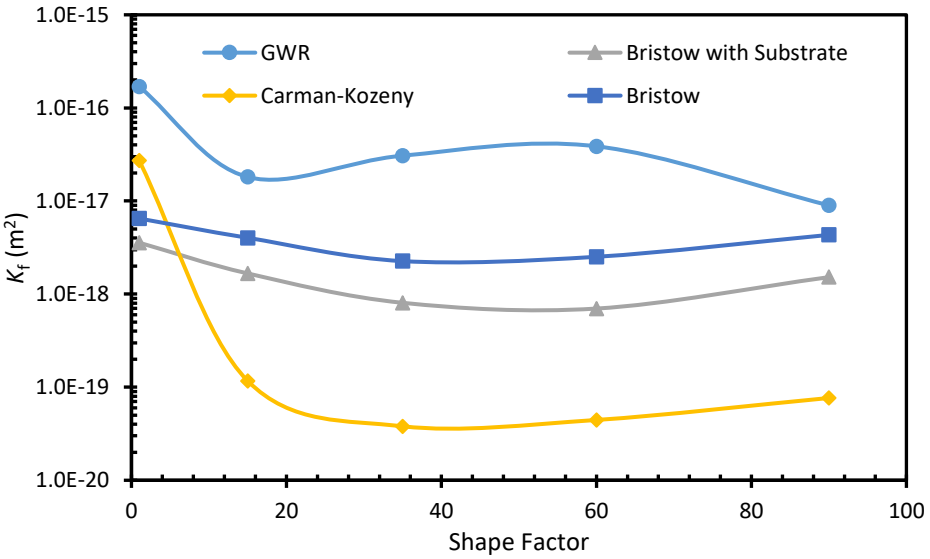

Figure 2.7. A log plot of the permeability constants against the shape factor of the pigments from the GWR, Bristow tests, and the Carman-Kozeny equation.

It is surprising that the permeability constants calculated from the GWR tests are considerably higher than any of the other tests. One of the possible causes for these results could be that the shear during the Bristow test is aiding in the alignment of the particles. With the particles positioned parallel with the substrate, the packing structure will be tighter and less permeable for water. Another possible reason to explain the differences between the permeability constants is the size of the pores in the membranes used in the GWR test method. The standard procedure calls for a 5 µm membrane. Each of the pigments contain a portion of fines that will be able to pass through the membrane. This will create a thinner filtercake on the surface of the membrane. At this point, the exact cause cannot be firmly concluded.

Effect of Particle Size Distribution on Dewatering

Altering the particle size distribution will modify the water holding capacity of a suspension. In coating formulations, the main component are pigments and latex, which is small spherical particles. The latex particulates will fill in the voids created by the disorganization of the high shape factor pigments. This will alter the packing structure and the tortuosity of the filtercake. To investigate this impact on the water retention, a single pigment (K35) was selected and the concentration of a monosize hard plastic pigment, used to simulate a latex, was varied at 5, 10, and 15 pph. The coating formulations were tested on the GWR, Bristow and the porosimeter.

The outcome of the GWR dewatering results are shown in Figure 2.8. At short dewatering times, the addition of plastic pigment had no effect on the water holding capacity of the suspension. As the dewatering time increased, the water retention improved for the samples containing the plastic pigment. With the increased time spent in the device, the small plastic particles could have acted as plugs, filling the pore space and slowing down the movement of water. But, the presence of the plastic pigment had only minor influence on the

dewatering rate. This trend is observed in the calculated permeability constants displayed in Table 2.2. The constants are very similar for each of the plastic pigment concentrations.

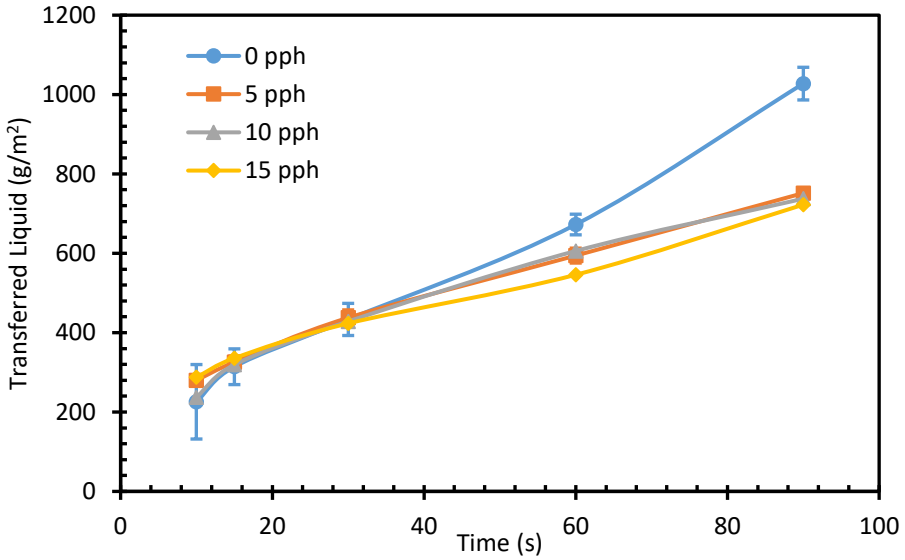

Figure 2.8. GWR results for coating formulations containing varying concentrations of plastic pigment

The results from the Bristow tests are shown in Figure 2.9. Examining these data determined that the addition of the plastic pigment and altering the particle size distribution decreased the water retention property of the coating formulation when the latex concentration is small. As the plastic pigment concentration increases, the rate of dewatering decreases and is lower than the pigment only suspension for the highest latex concentration. The permeability constants for this test were calculated from Eq. 2.1, shown in Table 2.2, and are of reasonably similar values.

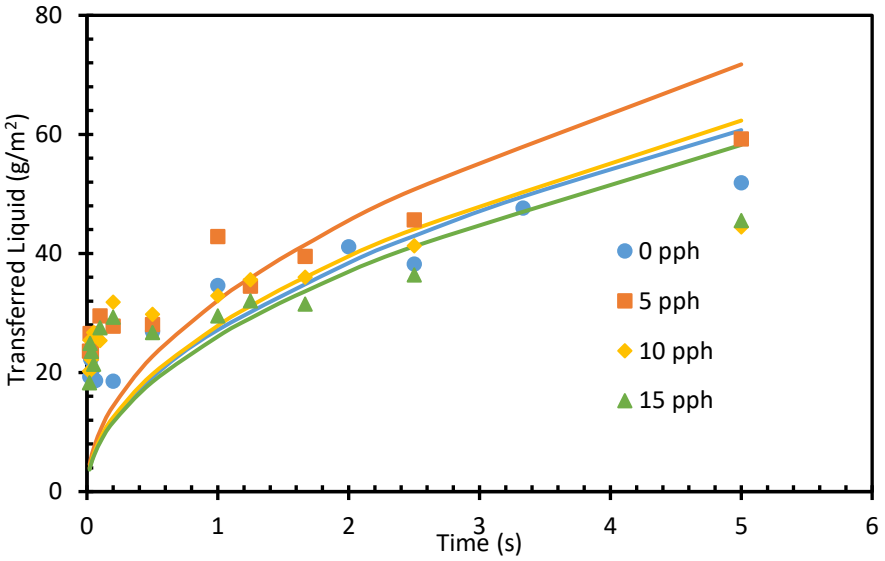

Figure 2.9. The results from the Bristow test from the four plastic pigment concentrations with the fitted equations

The results from both the GWR and Bristow tests are contradicting. In the static dewatering scenario of the GWR tests, the addition of presence of the small plastic pigment aided in water retention property. While in the transient dewatering test on the Bristow wheel, the addition of plastic pigment in the slurry increased the dewatering. It could be theorized that this phenomenon could be attributed to the movement of the particles during the test. In the case of static dewatering the particles are collecting on the membrane and the latex particles move through the building filtercake and fill in the pore space. While during the Bristow tests, the pigment particles are flowing and rotating, the latex particles hinder the movement of the platelet particles as they rotate. This movement is allowing for the system to dewater at a greater rate than in the absence of the plastic pigment particles.

Altering the particle size distribution will cause disruptions in the packing structure of the pigments. The immobilization solids and the pore sizes were measured. The addition of the plastic pigment decreases the immobilization solids, as observed in Figure 2.10. The fine plastic pigment must fill many of the voids and does not disrupt the packing of the kaolins. Although the differences between the immobilization solids is quite small at 0.02%. The slight differences

between the immobilization solids is seen in the cumulative pore volume plot shown Figure 2.11. The total pore volume for all latex concentrations is remarkably similar.

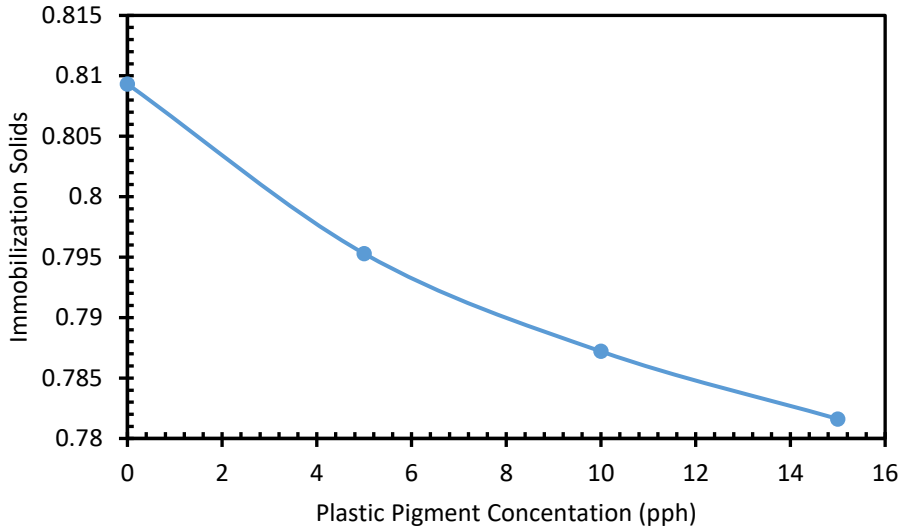

Figure 2.10. The effect of increasing the plastic pigment in a coating formulation on the immobilization solids

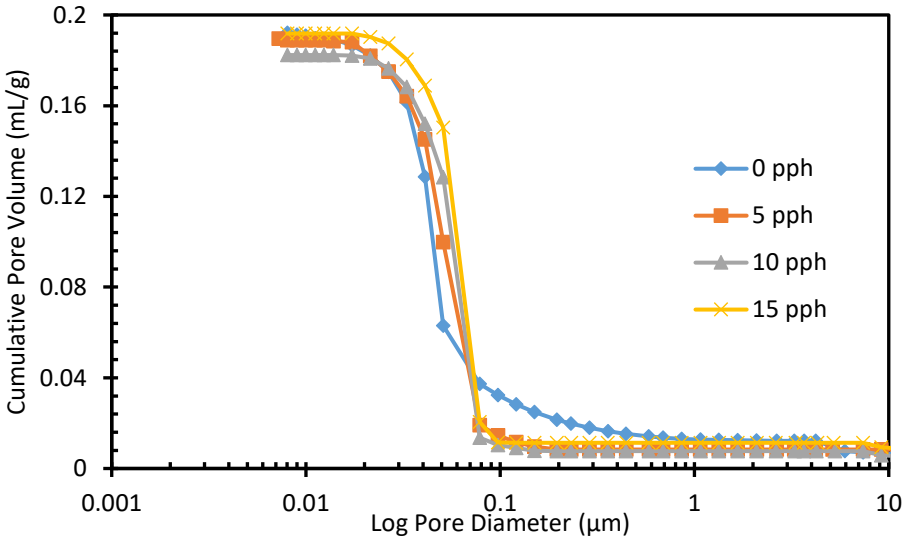

Figure 2.11. Cumulative pore volume for each of the four plastic pigment concentrations

The inclusion of plastic pigment in the suspension does influence the pore size distribution shown in Figure 2.12. The presence of these particles must act to disrupt the packing and causes the average pore size to increase from 40 nm to 50 nm. Permeability constants were calculated using data obtained from the mercury porosimeter and the Carman-

Kozeny equation. These coefficients are displayed in Table 2.2. The computed values are similar which would be easily predicted after examination of the data.

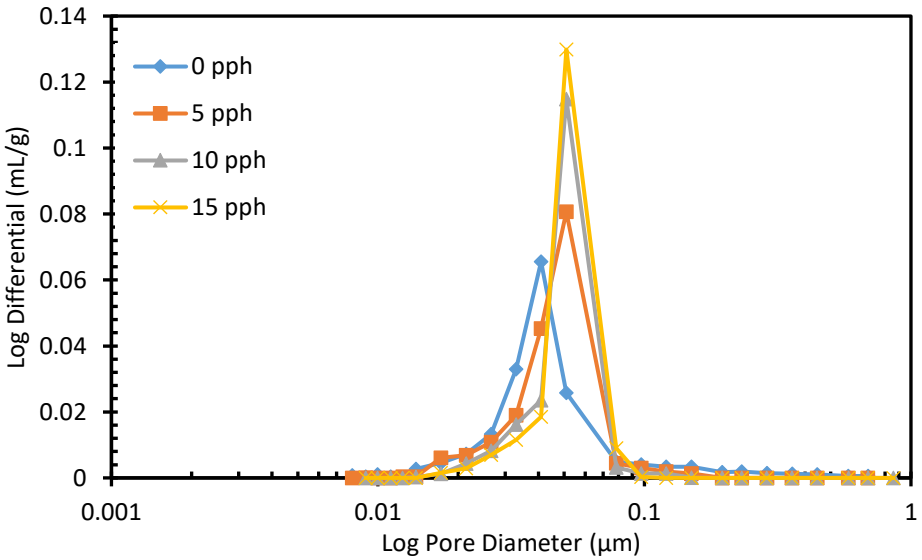

Figure 2.12. The log differential of pore size distribution for the four plastic pigment concentrations

Table 2.2. Permeability constants calculated by GWR, Bristow and Carman-Kozeny equation

Plastic Pigment Concentration (pph)	Permeability Constants, K_f (m²)			
	GWR	Bristow	Carman-Kozeny	Bristow with Substrate
0	3.0×10^{-17}	2.3×10^{-18}	4.6×10^{-20}	7.0×10^{-19}
5	2.0×10^{-17}	3.3×10^{-18}	3.0×10^{-20}	1.3×10^{-18}
10	1.9×10^{-17}	2.6×10^{-18}	4.8×10^{-20}	8.0×10^{-19}
15	1.9×10^{-17}	2.2×10^{-18}	4.4×10^{-20}	6.3×10^{-19}

With the permeability constants calculated using the two testing methods and the Carman-Kozeny relation, a comparison of these values is interesting. Figure 2.13 shows the results of this comparison. The constants are up to three orders of magnitude different. One point is clear; the permeability constant is not a function of the plastic pigment concentration in the coating formulation. Both the GWR and Bristow predict values that are higher than the Carman-Kozeny equation. These similar trends seen in this data set were also observed in the

pigment only slurries. The same theories behind the cause can be applied to this particular scenario.

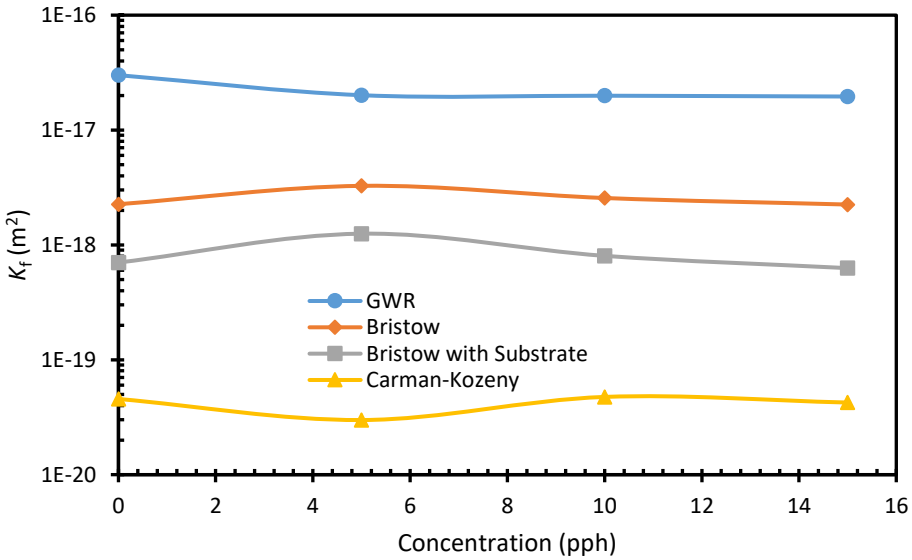

Figure 2.13. A log plot of the permeability constants as the plastic pigment concentration is increased

Conclusions

The rate of dewatering of a coating formulation is influenced by the shape of the particles, where high aspect ratio pigments tend to dewater slower than those with a lower shape factor. The pore size and pore volume, however, of the high aspect ratio kaolin were larger than other pigments. This result indicates that the rate of dewatering is controlled by the size of the connections or throats between pores and not the average pore size. While, the Carman-Kozeny equation does predict the permeability constant, it is lower than predicted from the dewatering tests.

The addition of a hard sphere latex to modify the particle size distribution decreased the permeability of the filtercake a small amount. The inclusion of the plastic pigment did not majorly alter the immobilization solids nor the pore volume to any larger extent. Therefore, the plastic pigment may be acting to block some of the fine channels that influence the rate of dewatering.

CHAPTER 3

IMPACT OF PIGMENT SHAPE ON RUNNABILITY USING A BENCH TOP BLADE COATER

Abstract

Operational issues such as stalagmite formations, scratches, or spits develop during blade coating of high solids coatings at high web speeds. Coatings that contain high aspect ratio pigments exhibit these difficulties at lower solids concentrations and slower machine speeds than coatings comprised of more spherical shaped pigments. There are a number of potential reasons behind this phenomenon, but a clear mechanism is not well established.

Using a bench top blade coater without a base sheet, the goal of this study is to understand the operational limits that occur due to the coating suspension interacting with the blade. Pigment suspensions are applied in excess in front of the blade. A camera, mounted near the blade exit is used to detect defects and buildup on the backside of the blade. The machine speed at which deposits on the blade first appear was determined for three pigments having different shape factors and at varying weight fractions. Investigations into the effect of tip angle and the possibility of blade deflection was also conducted. A Newtonian fluid was also used in the coating device. A runnability window based on shape factor and solids content was developed. Small changes in the solids concentration displayed changes in the speed at which blade deposits begin to appear. No operational issues could be produced using the Newtonian fluid. Presence of the particles at solids concentration nearing their immobilization solids must be contributing to the development of runnability issues.

Introduction

High aspect ratio pigments, such as delaminated kaolins, have many beneficial properties which make them ideal for paper coating applications. Traditionally, kaolin is used to

improve the printability of the final product with a smooth and excellent surface for ink receptibility (Bundy and Ishley, 1991). The plate like shape of kaolin particles is one of the most significant properties for achieving good base stock coverage in light weight coating to enable the high print quality to be reached (Conceição *et al.,* 2005). However, there are often process issues during blade coating that are exhibited when coatings contain high aspect ratio pigments. These issues include stalagmite formation usually accompanied with wet bleeding, scratches, streaks, and spits. This constrains the applicability of coatings comprising these pigments to lower solids content coating colors and slower machine speeds compared to those based on a more spherical shape pigment coating. This results in higher drying costs and lower quality coatings that decrease the overall efficiency of the process. This will also reduce the expected benefits of using high shape factor pigments in the coating.

Runnability is defined as the ease at which a coating is applied to a base sheet. Operational issues include blade bleeding, stalagmite build up, streaks and spits that limit the solids content and speed at which the coating can be applied. Many researchers have theorized on the factors that contribute to these problems, but the real mechanism behind the onset of these issues are not fully understood.

One of the initial indications of potential runnability issues is blade bleeding. This issue is related to the buildup of coating on the back side of the blade that has a wet viscosity consistency. Continued bleeding can lead to the formation of wet structures adhering to the blade tip, termed stalagmites. Alternatively, a drier structure can be observed directly forming a stalagmite without the wet bleeding appearance. Following this observation, there are three types of blade buildup: wet bleeding, which is the slow extrusion of coating with the properties of the coating before shear, or the formation of a dry stalagmite and lastly a combination of

both wet and dry stalagmite growth (Gane, 1997). Examples of stalagmites from literature are shown in Figures 1.1 and 1.2.

Stalagmite formation can be benign during the coating process. The formation of stalagmites does not always result in defects; it does add some uncertainty into the long term operation of that particular coating (Ettl *et al.,* 2000). If stalagmites fall clear of the paper web, they do not cause any damage or defects to the product. When the stalagmites become detached from the blade and land on the surface of the coated paper. These deposits also have the potential to cause damage to equipment downstream from the coater (Gane *et al.,* 1992).

Streaks have been defined as stripes of heavier coating thicknesses that run parallel with the machine direction and can be up to several centimeters to meters in length (Daiss *et al.,* 1998). Spits are created when droplets of excess coating attach to the coating surface (Gane *et al.,* 1992). Besides streaks and spits, other defects such as scratches and skips are possible flaws that can appear on the final product. Skips on the paper surface are areas barren of coating, which leave the final product with a patterned surface (Ettl *et al.,* 2000). Scratches are indents on the final coating surface aligned with the machine direction (Ettl *et al.,* 2000; Daiss *et al.,* 1998). The precise cause for these defects to occur is still a debated topic. Several theories have been developed to explain the operational issues that are exhibited by coatings that consist of plate shaped pigments. High aspect ratio pigments, narrow particle size distributions, low water retention, high viscosity, fast web speeds and high solids are some the properties that haven been cited that seem to lead to more runnability issues (Weigl and Grossmann, 1997; Gane *et al.,* 1997; Gane, 1997). There are many theories in which interactions between the coating, base stock and blade coating conditions are considered the main culprit in initiating runnability issues.

Many past studies have pointed to the rheology being the cause of the operational trouble. The particle shape has a sizable effect on the viscosity of the suspension. High aspect ratio pigments tend to have a higher viscosity at lower solids content than spherical pigments. Dahlvik *et al.* (2000) concluded that a relationship exists between high shear rate rheology and runnability issues. In contrast, Suontausta (1993) determined that viscosity of the coating had little effect on stalagmite formation. Others caution that the steady state rheology is not important but the response to the transient shear is the controlling mechanism (Gane *et al.,* 1992; Gane *et al.,* 1997; Gane, 1997). The role of viscoelasticity during coating is one of the debated topics. It has been proposed that coatings, a multiphase dispersion, will have viscoelastic deformation when subjected to sudden changes in strain and thus leading to relaxation-induced dilatancy (Gane, 1997). The combination of the pressure pulse underneath the blade and the elastic component in the z-direction of the coating will generate relaxation-induced dilatancy, where the suspending liquid is forced from the particle structure. As the web speed is increased, the velocity profile under the blade changes to plug flow with a slip plane against the blade (Gane, 1997). When the slip plane moves away from the surface of the blade into the bulk, wet bleeding and extrusion of un-sheared coating will appear on the blade (Gane, 1997).

A high viscosity in itself should not be the only cause behind operational problems. If the viscosity increases at a certain shear rate, the blade may deflect in a way that is hard to predict. The alignment of the blade during coating has a large effect on a coating's runnability and the quality of the final product (Roper and Attal, 1993). Also, the flow channel between the blade and the base sheet controls the rate of particle rotation. When particles are rotating through the shear field, collisions between the particles cause "log jams", and particle structures form, which contributes to skipping and streaking defects (Gane and Watters, 1989). Although,

dilatant rheology alone does not explain operational issues, deflection of the blade and alterations in the flow channel could be a contributing factor.

The influence of particle orientation on runnability has been discussed in a number of publications (Gane *et al.,* 1997; Gane *et al.,* 1992). The rotation of these plate like particles during coating is thought to be linked to the formation of whiskers and stalagmites along with altering the packing ability and water retention of the coating layer. The development of stalagmites on blade coaters trigger the runnability issues at high production speeds (Engström and Rigdahl, 1989). While it makes sense that rotation of high aspect ratio pigments in the coating flow would disrupt the smooth flow of particles, a clear demonstration of this mechanism is lacking in the literature as well as established process limitations as what solids can be applied for certain aspect ratios.

Characteristics of the coating formulation, base stock properties and coater operation conditions have been linked to runnability issues. It is well known that if the solids of the coating increase or the permeability of the base sheet increases, the maximum coating speed decreases. Bousfield (1993) proposed a model of blade coating that predicted the flow field and the buildup of a filter cake on the paper surface during coating process: if the filter cake thickness approaches the gap between the blade and the paper, the filter cake will be scraped by the blade tip leading to coating defects. This picture seems to explain some results, but it does not directly explain the runnability issues of high aspect ratio pigments. These plate shaped pigments may influence the filtercake solids in the model and the viscosity of the coating, and that could determine the growth of the filtercake.

Doi *et al.* (1999) mapped out the critical coating speed as a function of clay and calcium carbonate composition as well as latex type; a laboratory coater with a base sheet was used to

find the critical coating speed before defects were observed. They found that the speed which defects first appear was always lower for coatings containing clay compared to ground calcium carbonate. The latex size also can have an influence on the critical coating speed. The authors did not find a correlation between high shear viscosity and the critical coating speed but could explain some pilot scale results with the laboratory device if they considered dewatering. An unknown "third" factor is needed to explain, but the mechanism behind this third factor was not clear.

In this study, an examination of the critical coating speed is undertaken for three pigments each with different shape factors. The experiments are similar to those described by Doi *et al.* (1999) except here the influence of just the pigment aspect ratio is isolated. An operating window based on the shape factor and the solids content was developed. Also examined is the effect that high viscosity and blade alignment has on the runnability of pigment slurries.

Experimental Method

This study focused on three kaolin pigments: Astra-Glaze (Imerys), XP10-6003 (Imerys) and XP01-6100 (Imerys). These pigments have on average shape factors of 15, 35 and 90, respectively, as reported by the supplier. Shape factor is defined in a specific manner by the supplier but can be taken as an average aspect ratio of the plate-like particles. These pigments will be identified based on their aspect ratio or shape factor as KXX. For instance, the kaolin pigment with a shape factor of 35 is identified as K35. Slurries of these pigments were prepared using a high shear mixer to ensure adequate dispersion of the particles. The mass fraction of the slurries was ascertained by a dry weight method. In this work, no other dispersants, additives or latex was added to the suspension other than what is already included by the manufacturer.

This was done to limit the complexities of the suspension while focusing in on the affect that particle aspect ratio has on the interaction with the blade coater.

A bench top blade coater was used in this study. A schematic of the device is shown below in Figure 3.1. It consists of a rubber covered roll with a diameter of 10.16 cm and length of 24.13 cm. The turning speed is computer controlled and variable up to a roll surface speed of 1,200 m/min, but is usually operated at speeds less than 600 m/min. The runnability study was conducted with a stiff steel blade with a bevel angle of 45^{o}. The loading force for the blade was applied by two low static friction air pistons using compressed air. The blade angle was determined from the tangent of the point of contact between the roll and the blade. Proper alignment of the blade is crucial, since running on the heel has is known to induce runnability issues. The loading force on the blade was applied using two compressed air pistons. The pressure of the compressed air entering the piston was kept constant at 8 psi for all runnability trials. This corresponds to a blade loading force of 11.2 N/m. This blade coater does not include any base sheet. The absence of the base sheet will remove the effect of permeation dewatering of the coating layer into the substrate, and thus eliminated one of the possible causes of runnability issues.

Using this coating device, the critical coating speed was obtained by determining at what speed runnability issues first appear at varying weight fractions. Since there was no dewatering of the coating and no additives in the slurry, the solids content of the sample was higher than a traditional coating formulation in order to generate any runnability issues. A small camera (GoPro Hero 3+) was positioned near the exit of the blade to record any defects that may occur during the trial.

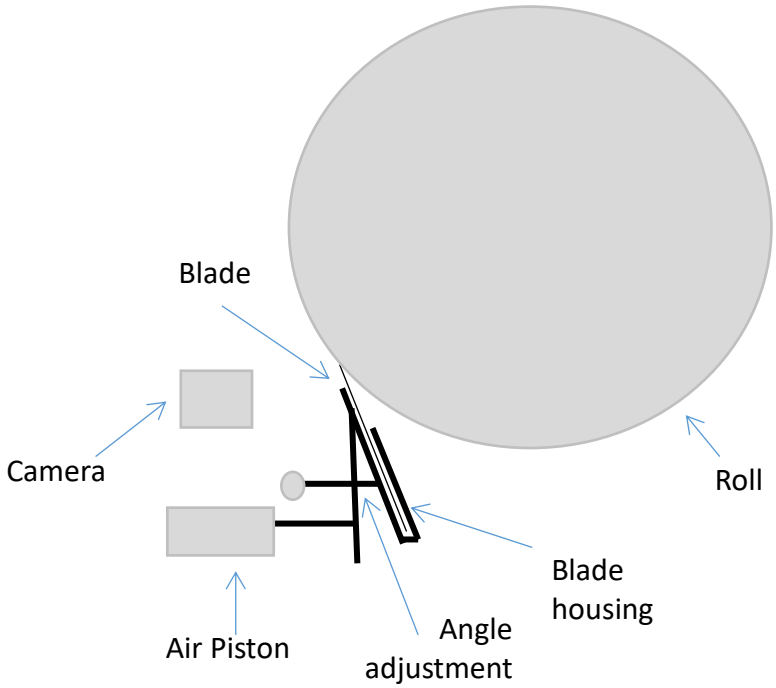

Figure 3.1. Schematic of the bench top blade coater

Proper blade alignment is crucial for high quality product. The runnability studies were completed with a 45° bevel blade held at a blade angle of 45°. At this set up, the land area of the blade was running parallel to the rubber roll. If the high viscosity of the pigment was pushing the blade to run on the heel of the blade, the observed stalagmite formation could be attributed to the blade position. To ensure that the blade is running on the toe or at least parallel to the backing roll, a still steel blade with a 30° bevel was also inserted into the blade holder device. This blade angle was held constant at 45° but now the tip angle was altered to 15°. The goal of this test is to be certain that the blade is running on toe and that even if the blade deforms some amount due to high viscous forces, that the blade does not start operating on the heel. Running on the heel of the blade has been shown the encourage blade weeping and spitting (Roper and Attal, 1993). While running on the toe of the blade removes the chances of sub-atmospheric pressure under the blade and cavitation, it could also induce dry whiskers and web breaks (Roper and Attal, 1993). Figure 3.2 shows the differences between blade and tip angle.

The same procedure for determining the critical coating speed was repeated using K90. The results between the two tip angles were compared.

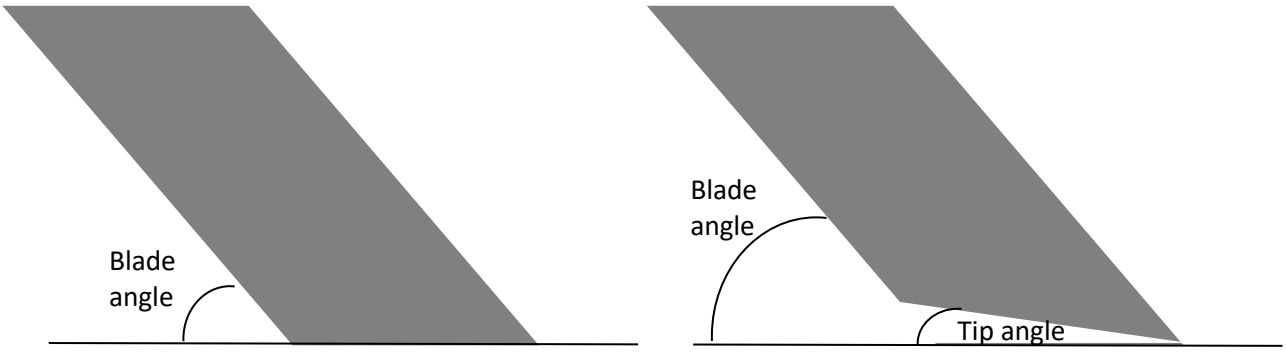

Figure 3.2. Schematic displaying the difference between blade and tip angles.

One of the hypotheses behind the onset of runnability problems is the high viscosity of the high aspect ratio pigments. To examine if high viscosity of the pigment slurries per se is potentially one of the factors behind the observed stalagmite formations, high fructose corn syrup, a Newtonian fluid with a comparable viscosity of 1.5 Pa s at 226 s^{-1}, was coated using the bench top blade coater. The critical coating speed was determined for this fluid using the same conditions as the pigment slurries.

The viscosity of the slurries at a shear rate of 10,000 s^{-1} and varying weight fractions was found using a cup and bob rheometer (Kaltec Hercules Hi-Shear Viscometer) using bob E and a ramp time of 20 s. The data were fitted to the Krieger-Dougherty equation which relates the viscosity to the volume fraction using two parameters to describe the sample, following a similar method as outlined in Weeks *et al.* (2016). The low shear viscosity of each of the slurries used in the runnability study was determined using a Bohlin Gemini II rheometer using a 25 mm diameter parallel plate geometry with a gap of 1 mm. All samples were at room temperature and completed in triplicate. The immobilization solids were determined for each of the pigments

by placing a small volume of the slurry onto a porous ceramic disk. Once the wet gloss forms the surface of the slurries disappeared, the sample was removed and the solids content determined.

Results and Discussion

In preparation for the runnability test, pre-trials were completed on the bench top blade coater to confirm the device's ability to apply a clean and uniform layer of coating. Figure 3.3 is a still image taken from a video of a K90 slurry trial showing no runnability issues or defects.

Figure 3.3. A frame taken from video of K90 at a solids content of 58% and roll speed of 480 m/min showing no deposits or stalagmites on the blade. Red arrows show the roll surface motion. Red dotted oval shows the key area of interest where the blade is touching the roll.

Depending on the solids of the slurry and the speed of the roll, the defects observed were varied. They ranged from small stalagmite beginning to form at specific locations on the blade to large extrusions or stalagmites building up across the entire backside of the blade. Figure 3.4 shows the varying number of defects observed during the trials. Spitting was observed during the cases when considerable stalagmites were present.

Figure 3.4. Left: Small stalagmites on the backside of the blade with K90 at 59.43% solids and a roll speed of 360 m/min. Right: Large stalagmites across length of blade with K90 at 58.7% solids and a roll speed of 480 m/min.

The results of the runnability tests are displayed below in Figure 3.5, where the solids content is given as mass fraction. For solids content less than that recorded in the plot, no runnability issues were seen at the maximum speed of the tests (480 m/min). Minute changes in the solids concentration altered the critical coating speed. On average, only 1.4% difference in the solids concentration between the critical coating speed at 240 m/min versus at 480 m/min. Both K15 and K35 displayed the onset of stalagmite formation at weight fractions of 73.6% and 71.7%, respectively. K90 displayed runnability issues at a solids concentration of only 59.2%. These weight fractions are higher than what would be used in an industrial setting, but these suspensions did not have latex or additives. These experiments show that similar defects occur for all pigments and that these defects did not require absorption or roughness from a paper surface to occur.

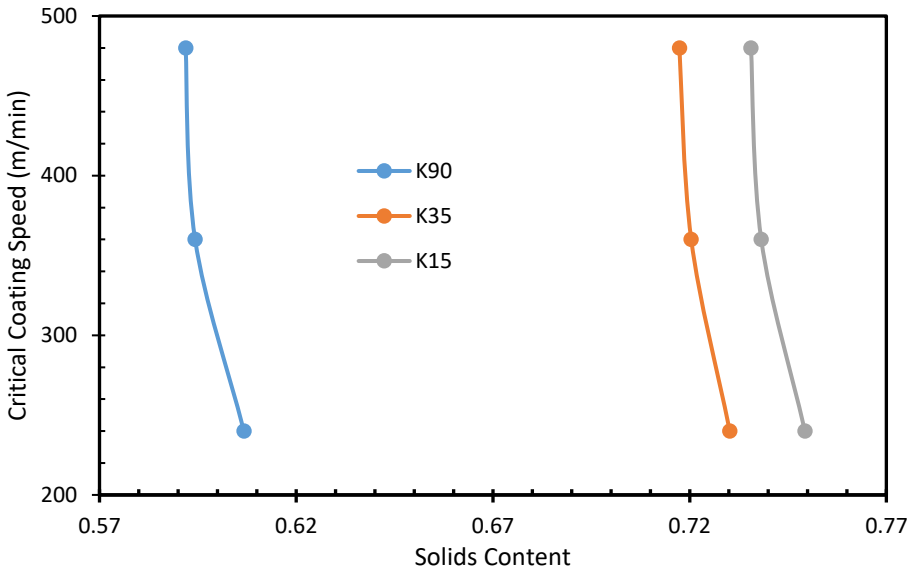

Figure 3.5. Critical coating speed based on the solids content for each of the three tested pigments

While examining the videos taken during the runnability study, there was evidence of wet bleeding in some cases. Figure 3.6 is taken from one video that displays an occurrence of wet bleeding. All coating was being removed from the rubber roll and extruding out and collecting on the backside of the blade. This observation supports the theory of the relaxation-induced dilatancy with a slip plane. The slip plane moved from the surface of the coating against the blade to the interface between the roll and the coating. The interactions between the coating, the backing roll and the blade material would be a contributing factor to potential operational issues.

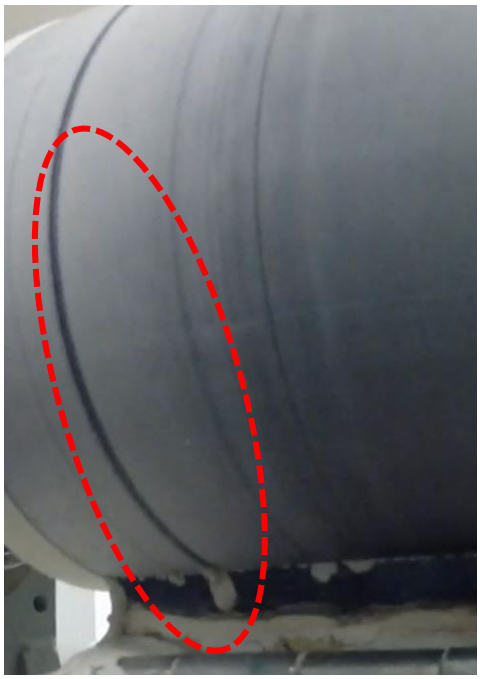

Figure 3.6. Wet bleeding with possible slip plane failure at the roll surface with K90 at a solids concentration of 59.43% and a roll speed of 360 m/min

The solids concentrations used for the bench scale lab coater were actually higher than the maximum flowing solids obtained from fitting the viscosity-solids behavior to the Krieger-Dougherty equation. Figure 3.7 displays the viscosity-weight fraction relationship between the three pigments; the viscosity was recorded at 10,000 s^{-1} shear rate. All slurries had a higher solids content than what was testable on the Hercules Hi-Shear viscometer. The slurries quickly over torqued the limits of the device. This equipment uses a cup and bob geometry that applies steady shear while ramping to a high shear rate and back down again. While during the coating process, a large and sudden shear force is exerted on the suspension. This would suggest that the dynamic response of the pigment slurry to the instantaneous force is important for coating runnability.

The red oval highlights the range of weight fractions that was used. K15 and K35 showed a similar viscosity to weight fraction relationship. The viscosity begins to increase at similar solids concentrations. This grouping resembles the trends observed in the runnability window.

The Krieger-Dougherty equation, shown below in Eq. 3.1, was fitted to the experimental data. This equation calculated the viscosity based on the volume fraction and two parameters characterizing the suspension. One of the parameters is the maximum flowing fraction. It has been shown that this value is on average 10% lower than the immobilization solids content and likely linked to the volume fraction at which unhindered particle movement in the suspension has become restricted (Weeks *et al.,* 2016),

$$\mu = \mu_s \left(1 - \frac{\phi}{\phi_m}\right)^{[\mu]\phi_m} \qquad \text{Eq. 3.1}$$

where μ_s is the viscosity of the fluid phase, $[\mu]$ is the intrinsic viscosity, and ϕ and ϕ_m are the volume fraction and maximum packing fraction of the particle phase, respectively.

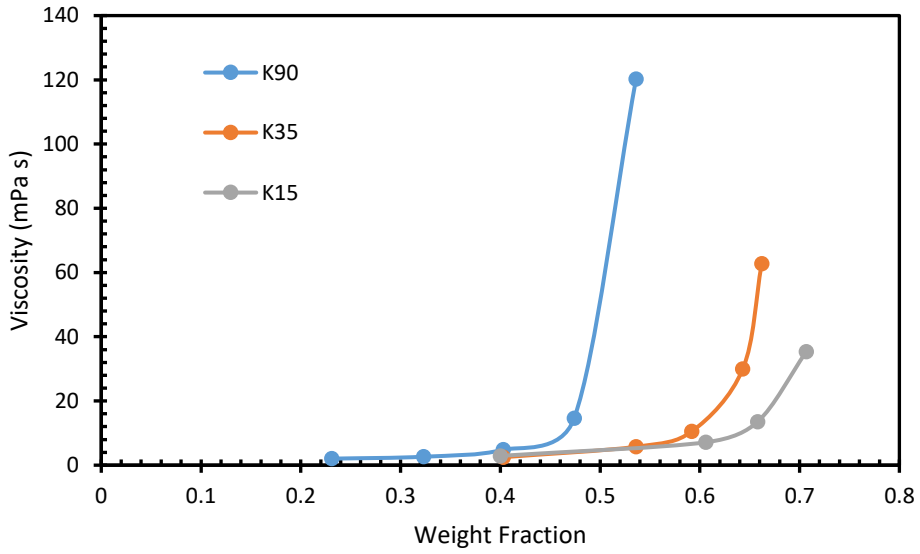

Figure 3.7. Viscosity at varying weight fractions for three pigments at a shear rate of 10,000 s^{-1} with highlighted range of slurries tested

A comparison between the maximum flowing fraction, immobilization solids and the maximum coating solids, which is weight fraction of the slurry with a critical coating speed of 480 m/min, is shown in Figure 3.8. All three parameters are functions of the shape factor of the pigment. For K90 and K35, there is a large difference between the maximum flowing fraction and the immobilization solids. There is a much smaller difference, however, between those

values for K15. The maximum coating speed falls between the maximum flowing fraction and the immobilization solids. This result does not hold true for the lowest shape factor pigment. All weight fractions used in the runnability study for K35 and K90 were above the maximum flowing fraction, while K15 are below. It could be tentatively concluded that the rotational freedom of high aspect ratio pigments is indeed a critical factor in respect to high shear rheology and the instantaneous response under a coating blade.

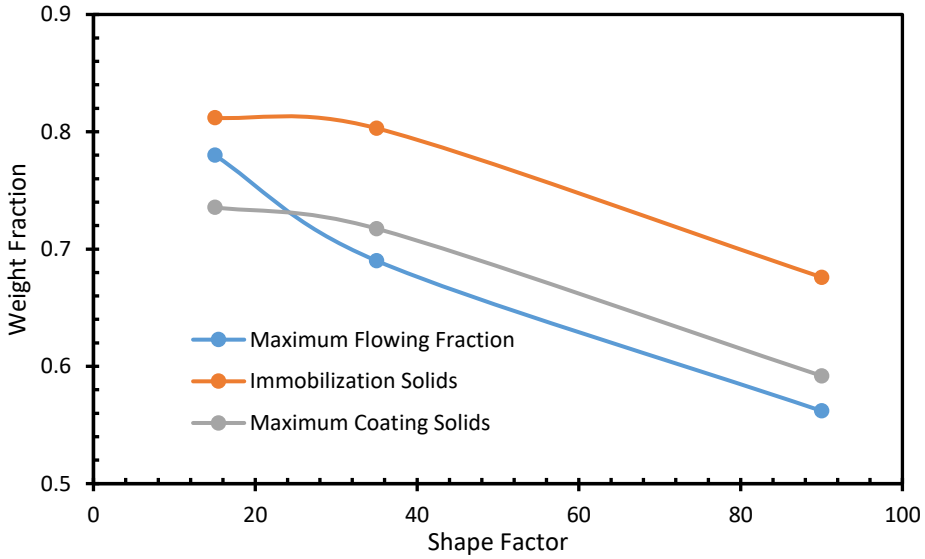

Figure 3.8. Weight fraction for the maximum flowing fraction, immobilization solids and the maximum coating solids based on the shape factor of the pigment

This anomaly with K15 was noticed during the completion of the runnability tests. Following the trends set by the other two pigments, it was hypothesized that the solid content of the K15 slurries would be between the maximum flowing fraction and the immobilization solids. When slurries of K15 were tested in that expected solids range, the rubber roll could not turn at the set speed. These slurries were of the same consistency as the K90 and K35 slurries as determined by simple hand mixing. The slurries were viscous, difficult to stir and pour. The solids content of K15 was diluted by 5% before it able to be run in the blade coater. At this lower solids concentration, the slurry was very easy to stir and pour. It was surprising that defects were still possible to generate on the coating device at this solids concentration because it was

below the maximum flowing solids. While K15 could be coated at the high solids the concentration was lower than the maximum flowing solids, while the other two pigments were able to be applied at solids above the maximum flowing solids. The reason for this behavior is not clear but it must relate to a dynamic response of the suspension.

Blade deposits appeared when the solids content of the slurry was close to the immobilization solids for the pigment. The difference between the immobilization solids and the solids content of the tested slurry, which will be called ΔS, was calculated for the all trials. There does seem to be a trend developing. Figure 3.9 displays this relationship. As the solids concentration of the slurries decreases thus ΔS increasing, higher machine speeds were possible before any operational issues developed. This relationship appears to be linear, with a slope of 12,000 m/min. This result is quite interesting and valuable in that for a wide range of particle aspect ratios, the maximum coating speed follows this simple relationship. While other rheological parameters to predict this maximum speed may be possible and based on physics, this simple relationship is only based on the solids content of the coating and the immobilization solids of the system.

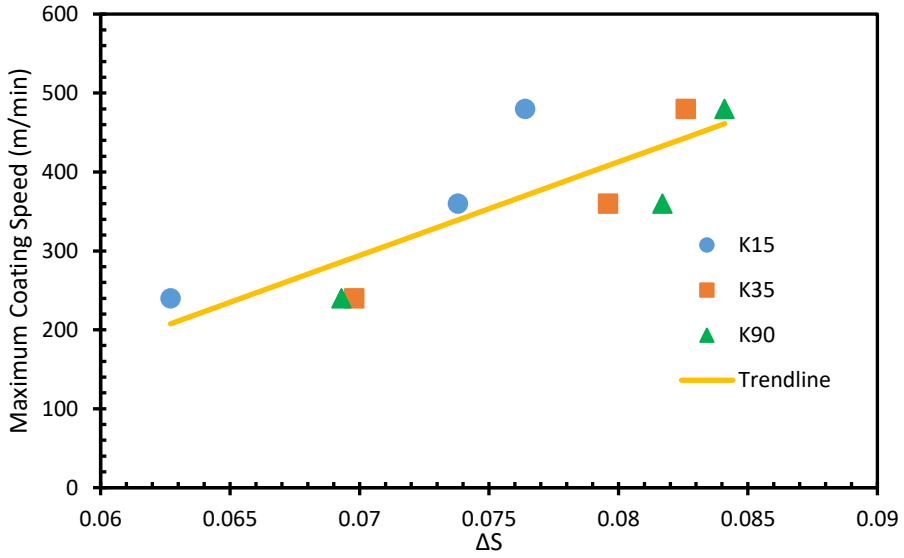

Figure 3.9. Linear relationship between Δ*S* and the critical coating speed for K15, K35 and K90

One issue that is a concern is that as coating viscosity increases, the blade will tend to deflect changing the blade angle to run on the heel as discussed. Deflection of the blade to run on the heel has the potential to induce the onset of runnability. Past work has proven that running on the heel of the blade stimulated weeping and spitting (Roper and Attal, 1993). Using the bench top blade coater with a blade with a 15^{o} tip angle, the runnability tests for K90 were repeated; this tip angle should make sure that the blade is not running on heel but on the tip. The critical coating speed was determined for slurries at the same weight fraction in the previous test using a 0^{o} tip angle, which is the blade aligned parallel to the base sheet. Figure 3.10 displays the stalagmites built up on the backside of the blade during the first runnability tests with the blade running parallel to the rubber roll with a 0^{o} tip angle. While, Figure 3.11 shows the stalagmites when the blade is running on the toe of the blade with a 15^{o} tip angle. For both tip angles, the critical coating speeds was seen at the same weight fractions. The amount of stalagmite formation for either tip angle was equivalent.

This result is strong evidence that the mechanism for operational issues is not related to cavitation under the blade caused by the tip deflection and running on the heel of the blade. With the viscosity of the slurries being high and a tip angle of 0^{o}, there was the possibility that the force exerted on the blade by the slurry could be the cause behind the observed runnability problems. Simulations of a blade coater show that only a small defection of the blade is necessary to change the pressure profile underneath the blade. Coating with a tip angle of 15^{o} ensures that the blade was running on the toe and not being pushed to run on the heel. Considering the results from the comparison between coating with a 0^{o} tip angle and one with a 15^{o} tip angle, it can be concluded that operational issues in this case are not caused by the blade being deflected and running on the heel.

Figure 3.10. Stalagmite formation on the blade with a 0° tip angle for K90 at 60.62% solids and a roll speed of 240 m/min

Figure 3.11. Stalagmite formation on the blade with a 15° tip angle for K90 at 60.85% solids and a roll speed of 240 m/min

A Newtonian fluid, high fructose corn syrup, with a viscosity that is comparable to the test pigment suspensions was used in the bench top blade coater. The viscosities of the three pigment samples and the corn syrup are shown below in Figure 3.12 determined using a controlled stress rheometer with a cone and plate geometry. Only the viscosity profiles for the solids content with a critical coating speed of 360 m/min are shown. The viscosity profiles for each of the three weight fractions are very similar. As the shear rate increases, the viscosity all fluids become similar. During the runnability test using the corn syrup, no runnability issues could be produced and a uniform layer of syrup was applied to roll at the highest testable speeds. This observation leads to the theory that the presence of the particles in the coating is key to cause of runnability issues. The packing interactions between the particles are affecting

the way the pigment slurry behaves and potential induced interparticle interactions, therefore a full understanding of this area is paramount to discovering the causes behind runnability issues.

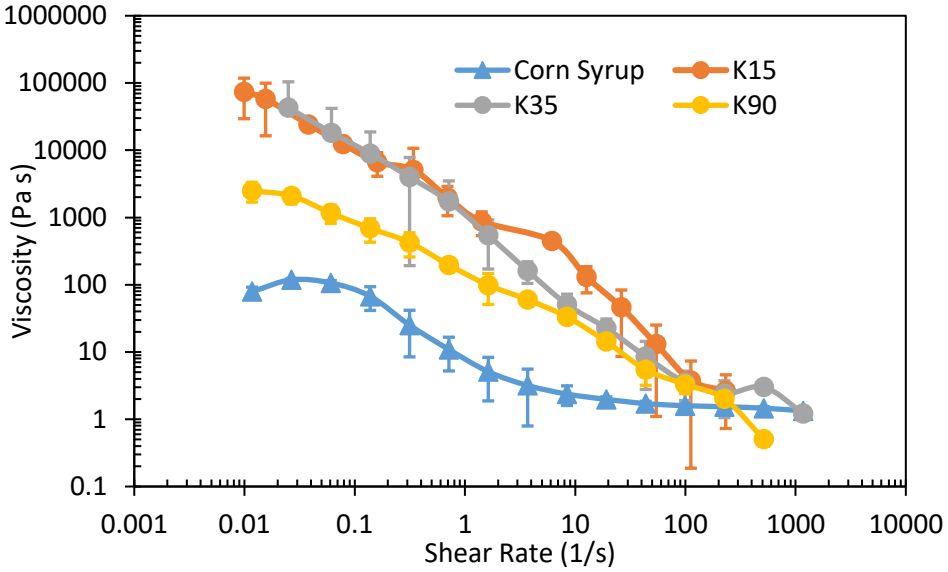

Figure 3.12. Low shear viscosity profiles for corn syrup, K15 (73.82%), K35 (72.04%) and K90 (59.43%)

Blade deposits began to appear when the solids concentration of the slurry neared the immobilization solids of that pigment. At these high solids, interactions between the rotating particles could be causing disruptions in the flow field and the packing structure. The collision of particles could arise from disrupting the arrangement of particles, which contributes to the formation of skipping and streaking on the final product (Gane and Watters, 1989). Higher aspect ratio pigments required more available space for rotation than spherical pigments. They are capable of causing larger instabilities in the packing structure with little movement.

Conclusions

The coating window was characterized for pigment suspensions as a function of solids and pigment shape factor. As expected, the higher shape factor of the pigment had a lower maximum coating solids compared to the low shape factor pigments. The onset of coating operation issues occurs within a solids range of around 1.5%. With the absence of a base sheet, formulation latex or other additives and binders, blade deposits were still generated. Tests using

the different tip angles of the blade, demonstrated that observed blade deposits are not generated from the blade deflecting to the heel position; cavitation events therefore do not explain the operational limits. The inability to produce any runnability issues when coating with either a Newtonian fluid or a low solids concentration establishes that coating near the immobilization solids is required to create blade deposits with a non-absorbent base sheet and at the tested machine speeds. At high solids, the interactions between rotating particles could be disrupting the structure and causing jams in the coating layer during shear. These disruptions could be contributing to the onset of runnability issues.

CHAPTER 4

INFLUENCE OF PIGMENT PARTICLE SHAPE ON RUNNABILITY USING A CYLINDRICAL LABORATORY COATER

Abstract

Process issues such as blade deposits, scratches, spits and defects on the coating surface develop during blade coating of paper at high solids content and fast machine speeds. Coatings that contain high aspect ratio pigments display these issues at lower solids concentrations and slower web speeds than spherical or block shaped pigments. The shape of the pigment particles influences the characteristics of the coating formulation after drying, high aspect ratio pigments can lead to high gloss surfaces that have good printing properties ad are interest in barrier coatings. The rheology, particle packing, and water retention are all functions of the pigment shape and size distribution. The base sheet properties of porosity, surface roughness and permeability interact with the coating and the blade coater operating conditions. The possible causes of poor runnability are part of an interrelated and complex system.

A cylindrical laboratory coater (CLC) was utilized to determine the speed at which operational and quality issues begin at varying solids concentration for two pigments with different shape factors on two different paper surfaces with varying absorption rates. An operational window was developed for both pigments. Characteristics of the pigment suspensions were explored to find a relationship with the onset of operational problems. The high shear rate viscosity of these suspensions did not explain the operational windows. The difference between the solids concentration and the immobilization solids, which is a function of the shape factor, has a linear relationship to the runnability limits. This could be ascribed to

the tight packing structure of the particles as the solids content approaches the immobilization solids.

Introduction

Problems during coating application develop during blade coating at high solids concentrations and fast web speeds. These problems included quality issues, which affect the properties of the final product. These comprise scratches, streaks and the non-uniformity of the coating layer. Also, operational issues can arise during the coating process. Deposits of coating on the backside of the blade and spits are common problems. Coatings consisting of high aspect ratio pigments exhibit these difficulties at lower solids contents and slower machine speeds than low aspect ratio pigments. Many theories on the causes behind this phenomenon have been suggested, as reviewed in Chapter 1. The characteristics of the coating formulation, base sheet properties and blade coater conditions all seem to play a role in the operational limits. While there has been much work on the topic of high speed blade coating at high solids, there is still a lack of understanding of the basic mechanisms that limit the speed or solids of various formulations.

The shape of the pigment particles affects a wide array of the properties of the coatings. Water retention, packing structure, rheology and particle orientation are all functions of the particle shape factor. Even in simple shear, it is well known that particulate suspensions that contain high aspect ratio particles will have higher viscosity than those with a more spherical shape at the same solids level. However, this behavior alone does not explain operational issues, because a high viscosity fluid should be able to be coated with blade coaters. Gane has discussed in a number of publications the influence of particle orientation for a smooth coating application; the rotation of these high aspect ratio pigments during the coating process is thought to be linked to the formation of stalagmites and whiskers (Gane *et al.,* 1997). If the

large particles flow parallel to the base sheet, no runnability issues occur. When the particles become misaligned to the paper surface, collisions between neighboring particles cause jams in the flow field to form, thus causing issues. As the shape factor of the particles increases, the more available space for rotation is required. While these mechanisms make sense, it is hard to study the actual high speed operation and verify these mechanisms.

The orientation of the particles will also influence the packing ability and water holding capacity of the coating. How tightly the particles pack together is a function of the shape, size and size distribution. Large aspect ratio pigments have the ability to pack in a very dense manner, but any disorientations could result in a loose packing structure. The rate of dewatering is affected by the shape and packing ability of the pigment. Tightly packed platy pigments will have an increased tortuosity and path length for pressure driven permeating flow (Gane *et al.,* 1992). As the solids concentration of the coating increases due to dewatering into the base sheet, the chances for defects in the coating layer are increased. The blade scraping across an immobile layer of particles could cause quality problems in the final product or operation issues (Okomori *et al.,* 2002). When particles rotate in a shear field, collisions between the particle cause jams and particle structures form, which contribute to skipping and streaking defects (Gane and Watters, 1989).

The properties of the base sheet and the blade coater operating parameters can affect the occurrence of runnability issues. The porosity and permeability of the substrate will alter the dewatering of the coating color as the coating contacts the substrate before the blade removes the excess coating. The surface roughness and compressibility of the base sheet have been speculated to increase a predisposition for stalagmite formation (Suontausta, 1993). Controlling the blade coater setting can reduce the potential for runnability issues. Increasing the blade angle and using thinner blade thicknesses had diminished chances to promote the onset of

blade build up (Engström and Rigdahl, 1989). Gane and Coggon (1987) found that by adjusting the blade angle, the packing structure of the clay could be controlled. The flow channel the blade makes with the base sheet has an impact on the runnability limits for a coating. The compressibility of the base sheet and the backing roll and the blade angle will determine the flow channel (Engström and Rigdahl, 1989). The parameters that affect a coating's runnability are complex and interwoven.

Researchers have been using pilot scale coating equipment to study runnability limits for some time. Ghosh *et al.* (1997) determined that runnability on a CLC correlated with the critical stress of a coating at very small strains. Adding fine clay particles and altering the particle size distribution had a positive impact on increasing the immobilization solids and the water holding capacity of a coating and thus improving its runnability (Hardy and Carter, 1994). Dahlvik *et al.* (2000) studied the influence of the rheological properties of clay based coatings on their runnability using a pilot scale coater: high viscosity corresponded to more operational difficulties and defects in the coating surface, but no clear relationship between the viscoelasticity and runnability could be defined. A slower rate of dewatering of a coating improved runnability (Dahlvik *et al.,* 2000).

In this study, the effect of pigment particle shape on runnability using the CLC was examined. The roll speed effect on operational issues both during coating and quality problems in the final product was examined for two pigments with high and low shape factors over a range of solids. An exploration into the relationship between runnability and the characteristics of the pigment as a function of shape factor was conducted.

Experimental Method

Two pigments were used in this runnability study; Astra-Glaze (Imerys) and XP01-6100 (Imerys). These pigments have average shape factors of 15 and 90, respectively, as reported by the supplier. Shape factor is defined in a specific manner by the supplier but can be taken as an average aspect ratio of plate shaped particles. These pigments will be identified based on their aspect ratio or shape factor as either K15 or K90. Slurries of these pigments were prepared using a high shear mixer to ensure sufficient dispersion of the particles. The mass fraction of the slurries was determined by an infrared moisture analyzer (IR-35, Denver Instruments). In this runnability study, no other dispersants, additives or latexes were included in the suspension other than what is already added by the manufacturer except for a small amount of a dye (<1% by weight). This dye helped color the white pigment to aid in the detection of quality issues in the final coating layer. This was done to limit the complexities of the suspension while focusing on the effect that particle aspect ratio has on the interaction with the coating equipment. The viscosity of the pigment suspensions at a shear rate of 10,000 s^{-1} and varying weight fractions was measured using a cup and bob rheometer (Kaltec Hercules Hi-Shear Viscometer) using bob E ad a ramp time of 20 s. The data were fitted to the Mooney equation which relates the viscosity to the volume fraction using two parameters to describe the sample, following a similar method as that outlined in Weeks *et al.* (2016). The viscoelasticity data of the slurries were determined using a Bohlin Gemini II rheometer with a 25 mm parallel plate geometry. An oscillatory test with a frequency sweep between 0.1 and 30 Hz at a constant strain of 0.01 was used. The immobilization solids were determined for each of the pigments by placing a small volume of the slurry onto a porous ceramic disk. Once the wet gloss from the surface of the slurries disappeared, the sample was removed and the solids content determined.

The base sheet used in these tests was a paperboard coated on one side with a basis weight 222 g/m^2. The coated side of the substrate was less permeable and had a smoother surface than the uncoated side. The base paper pore size distribution was characterized by mercury intrusion porosimetry. The porosity of the base sheet was found to be 0.25. The absorption rate of water was determined for each side of the paper by the Bristow wheel tester (Bristow Laboratory Apparatus). The results are shown below in Figure 4.1.

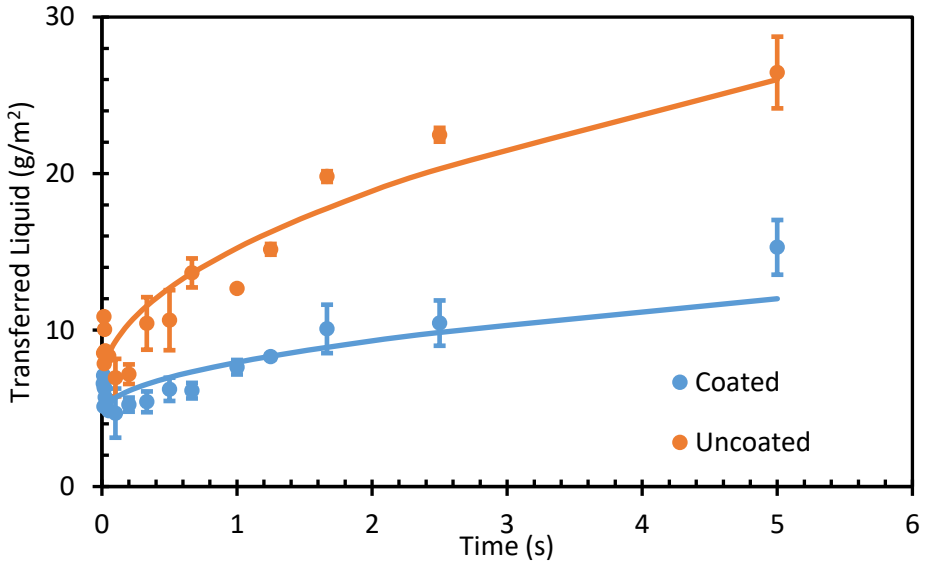

Figure 4.1. Results from the Bristow wheel tests for the coated and uncoated sides of the substrate

The runnability tests were conducted on the CLC (CLC 6000, Sensor and Simulation Products). The pre-dry and the post-dry settings were kept constant for all trials at 5 and 15 seconds at 50% power, respectively. The coat weight was also held steady at an average of 25 g/m^2 by adjusting the gap setting on the CLC. A small wireless camera (GoPro Hero 3+) was attached to the bottom of the moving carriage. It was used to record any potential operational issues that occurred at the blade exit. A photo displaying the location of the camera to the blade and pond is shown below in Figure 4.2. The solids concentration of each of the two pigments was varied and the speed at which operational and quality issues begin to appear was determined.

Figure 4.2. Photo showing the blade and pond (top arrow) and the location of the camera (bottom arrow)

Results and Discussion

The runnability issues that arose during this study were classified into two categories: operational and quality. The most common observed quality issues were skip coating and scratches; these were determined by examination of the coated region. Operational issues included blade deposits or spits. These problems were observed during the coating application process. Determination of any operational issues was completed after analysis of the recorded video of the trial. Two operational defects were seen on the video. Blade deposits, shown in Figure 4.3, are small amounts of coating that is extruded onto the backside of the blade. The second observed was spitting. Figure 4.4 displays a large episode of spitting of coating from the blade nip.

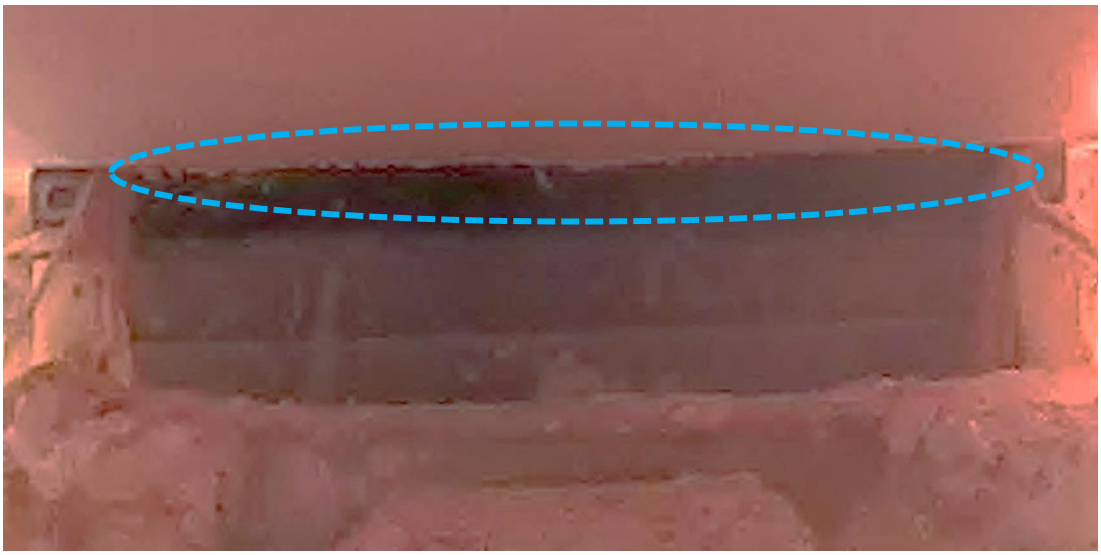

Figure 4.3. A frame taken from a video of K15 at a solids content of 72.9% and roll speed of 609.6 m/min showing blade deposits on the backside of the blade. The blue dotted oval shows the key area of interest where the blade is touching the roll.

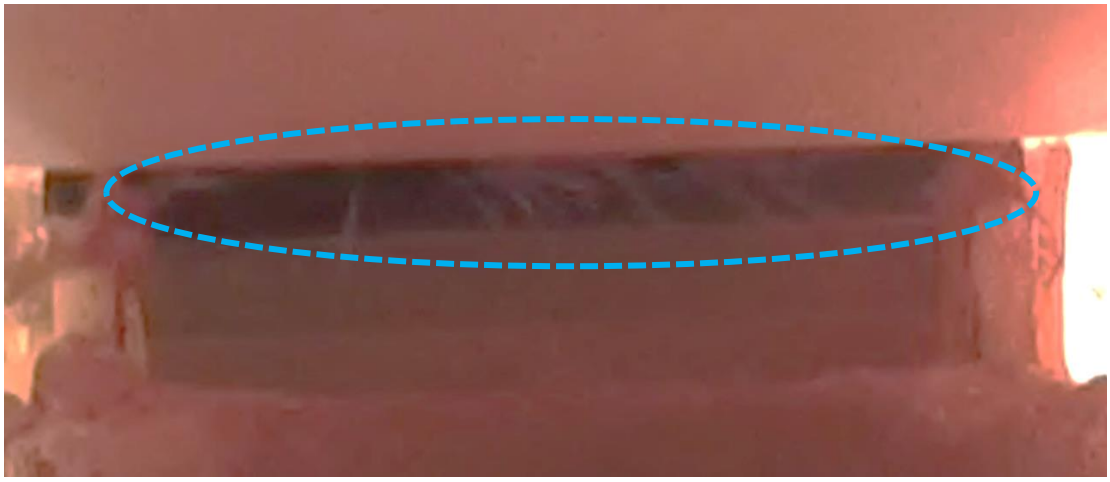

Figure 4.4. A frame taken from a video of K15 at a solids content of 73.7% and roll speed of 457.2 m/min showing spitting from the blade. The blue dotted oval shows the spits.

The second runnability issue that was observed was quality problems with the coating layer on the substrate. Figure 4.5 displays deep scratches in the coating layer that run with the machine direction. One of the most common quality issues was a non-uniform layer of coating on the surface of the substrate. This skip coating phenomenon is presented in Figure 4.6. There are sections of substrate that are void of coating.

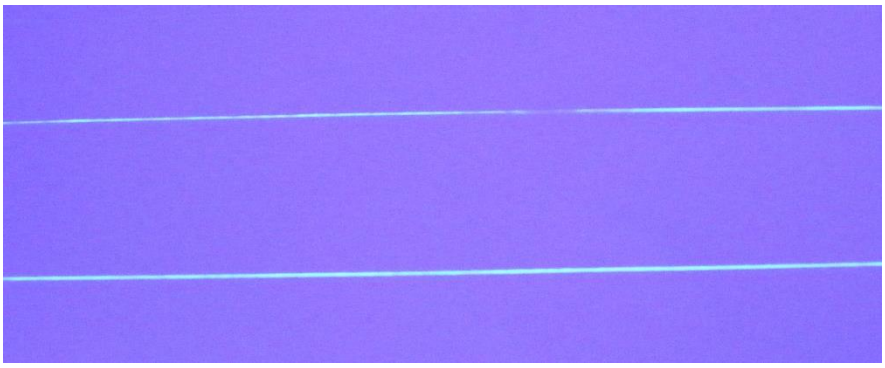

Figure 4.5. Two scratches running parallel with the machine direction in the coating sample from a trial using K90 at 55.8% solids concentration and a roll speed of 914.4 m/min on the uncoated substrate illuminated with a black light

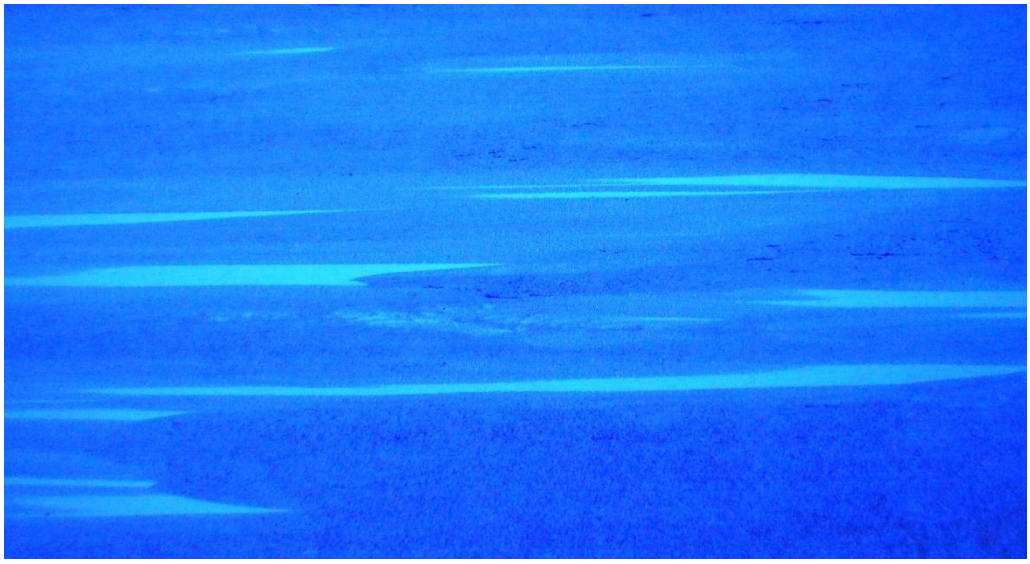

Figure 4.6. Skips in the coating from a trial using K15 at a 71.3% solids content at a roll speed of 914.4 m/min on the uncoated substrate illuminated with a black light

The results from the runnability study for K15 are shown below in Figure 4.7, where the solids content is given as mass fraction. There were only minor differences between the data with the uncoated and coated sides of the paper. Quality problems on the coating layer appeared at the same solids concentrations and roll speeds. The differences between the two sides of the paper are when blade deposits begin to materialize on the back side of the blade. On the uncoated substrate, operational issues begin to appear at slower machine speeds than problems with the quality of the coated product at the highest solids content. For the coated

substrate, both operational and quality problems appear together for the highest two solids concentrations.

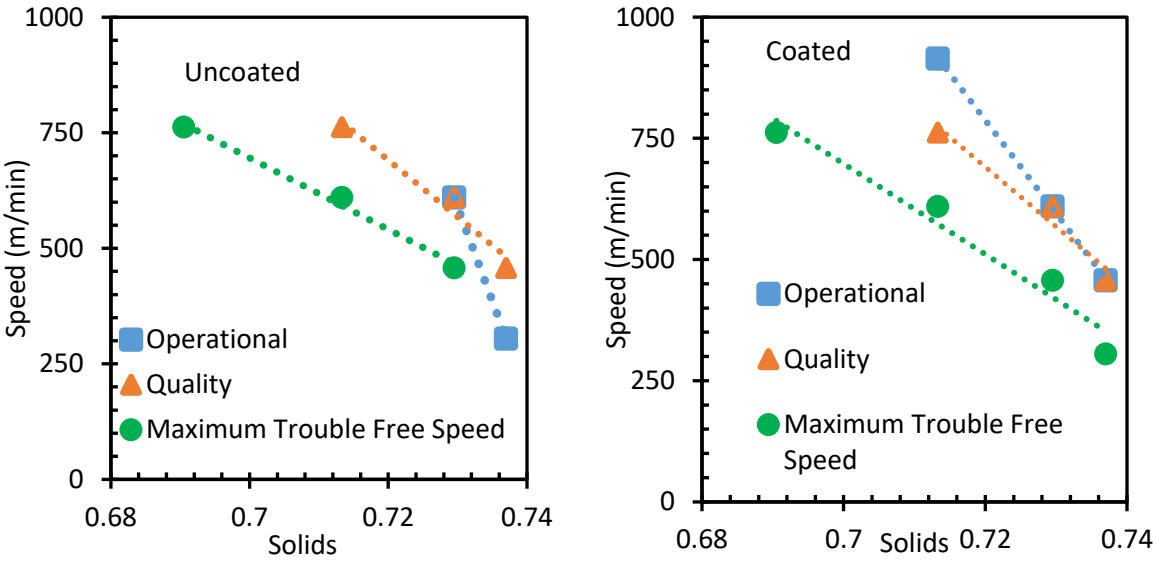

Figure 4.7. Runnability window developed for K15 on both the uncoated and coated substrates

The results from the runnability study with K90 are shown below in Figure 4.8 for both the uncoated and coated substrate. During the trials with the coated substrate, operational issues only developed once at reaching the highest solids tested. But during the tests with the uncoated base sheet, blade deposits were much more prevalent. The difference between these runnability windows could be attributed to the affect that the base sheet has on the coating process. The uncoated substrate has a higher permeability and could cause more dewatering of the coating than the less permeable coated substrate.

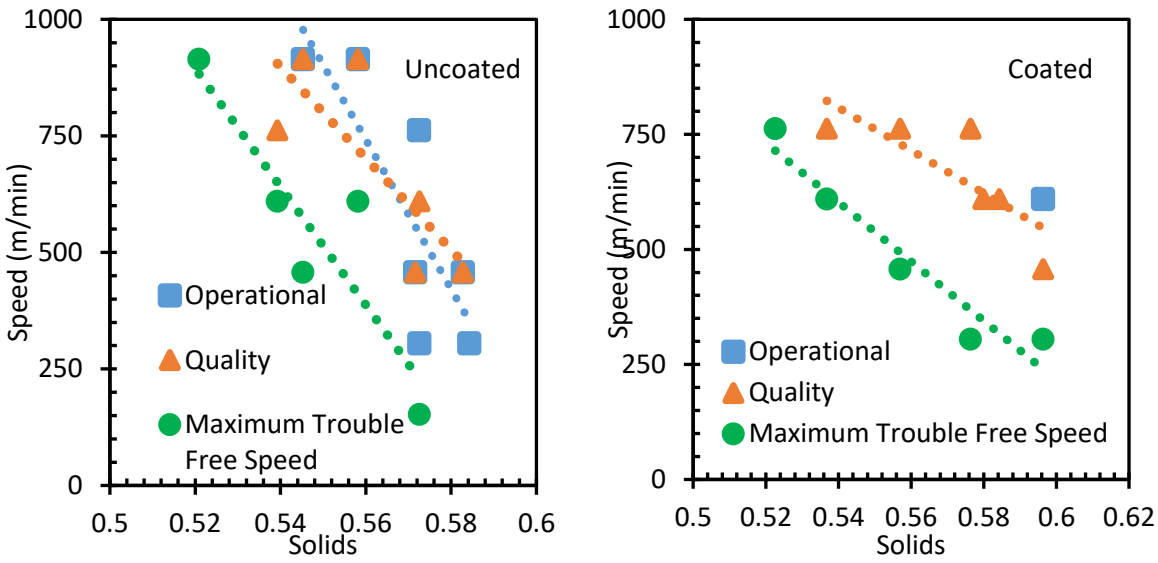

Figure 4.8. Runnability window developed for K90 on both the uncoated and coated substrates

The results from the runnability trials on the CLC were compared to the findings of the bench top blade coater discussed in Chapter 3. Since the bench top blade coater did not employ a base sheet, only the onset of operational defects could be detected. The results of this comparison are shown below in Figure 4.9. The maximum speed of the bench top coater was similar to the lowest speed conducted on the CLC, and for K15 the onset of operational defects overlaps for the two devices. With the rubber roll covering of the bench top blade coater being smooth and non-absorbent and the coated side of the substrate sharing parallel qualities, the speed and solids concentration when blade deposits appear begin to line up. The results in Fig. 4.9 are important in that they show that the bench coater results do match well with the higher speed CLC results. The bench scale results likely could be used to predict the occurrence of operational issues at a high speed.

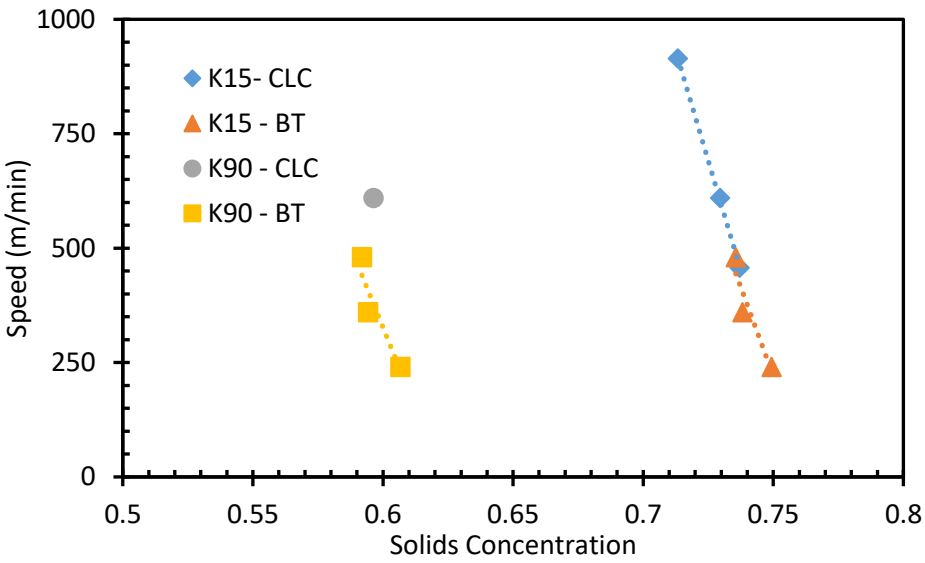

Figure 4.9. Comparison of the results for the onset of operational problems for both K15 and K90 on the CLC with the coated substrate (CLC) and the bench top blade coater (BT)

When the results from the bench top blade coater are compared to the onset of operational issues on the CLC using the uncoated substrate, a small reaction to the absorption of water into the base sheet is seen. This phenomenon can be seen in Figure 4.10. For K90, at the same machine speed defects begin to appear at lower solids concentrations on the CLC than with the non-absorbent bench top blade coater. With K15, the comparable solids concentrations displayed blade deposits at differing machine speeds. Blade deposits were seen at slower roll speeds on the CLC with the uncoated substrate than with the bench top. There is, therefore, a minor effect of dewatering and absorption occurring during the coating application process.

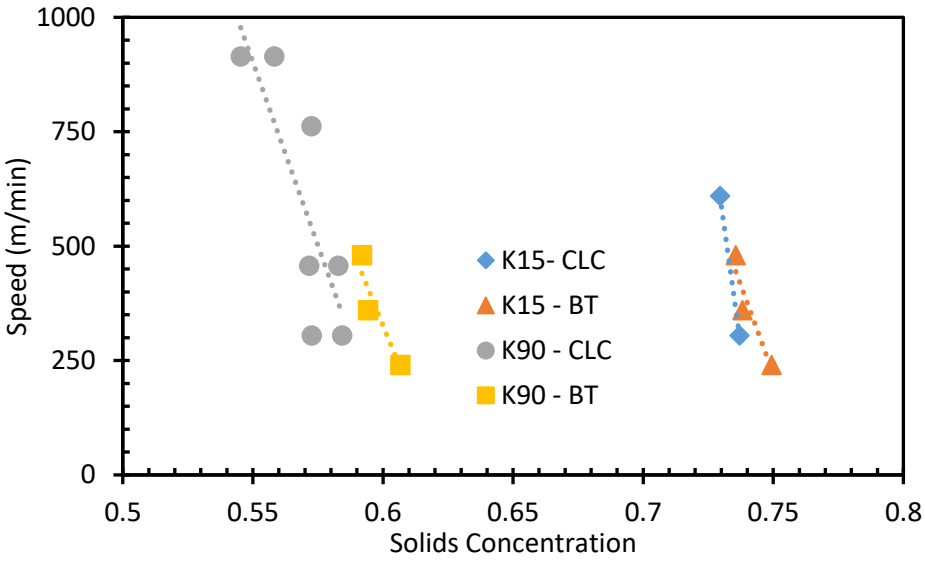

Figure 4.10. Comparison of the results for the onset of operational problems for both K15 and K90 on the CLC with the uncoated substrate (CLC) and the bench top blade coater (BT)

During the examination of the recorded video taken throughout the runnability trials, evidence of slip plane breakage during coating became evident. Figures 4.11 and 4.12 are still images taken from the video. Coating is being extruded from the blade nip. Also, a non-uniformity in the coating layer on the substrate is visible. This phenomenon could be related to a similar event seen on the bench top blade coater, see Figure 3.6. A slip plane forms between the blade and the coating layer due to relaxation-induced dilatancy. Something causes that slip plane to move from the surface of the blade to the interface between the coating and the substrate, and thus allowing the coating to be extruded from the nip and a defect on the surface of the final product. Further investigation into the potential causes to the movement of the slip plane will be required.

Figure 4.11. Still image taken from a video of K15 at a solids content of 73.7% and a roll speed of 457.2 m/min showing spitting from the blade and corresponding defect on the roll surface

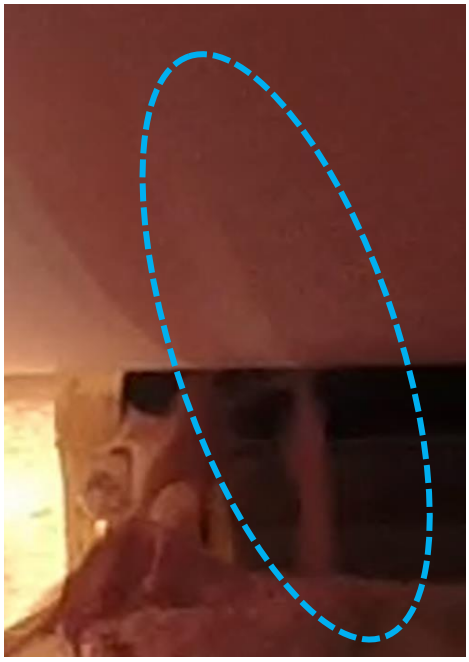

Figure 4.12. Image taken from a video of K15 at 73.7% solids content and a roll speed of 457.2 m/min displaying a spit from the blade and defect on the substrate surface

In the quest to determine the causes behind the onset of runnability issues, an analysis of the characteristics of the coating at the solid concentration which developed operational issues using both the results from the bench top blade coater, discussed in chapter 3, and the CLC using only the coated substrate was undertaken. Only the coated substrate data were used due to the effect of the dewatering on the more porous and permeable uncoated substrate has on the runnability limits. Many past studies indicated a relationship between runnability and the viscosity. The viscosity of each slurry at high solids level was estimated after fitting Mooney's equation, shown below, to the experimental data given in Figure 3.7. The more common Krieger-Dougherty equation could not be used because the solids content of some of the tested slurries was above the maximum flowing fraction found by fitting the data at various solids. Fitting the data to the Mooney equation results in larger maximum flowing fractions than the Krieger-Dougherty equation. The calculated viscosities for all the tested slurries are displayed below in Figure 4.13. The viscosity of the slurries calculated are not comparable. The viscosity for the highest solids concentration for K15 is the about the same viscosity for lowest solids content of K90,

$$\mu = \mu_s \exp\left(\frac{[\mu]\phi}{\left(1 - \frac{\phi}{\phi_m}\right)}\right) \qquad \text{Eq. 4.1}$$

where μ is the viscosity of the coating suspension, μ_s is the viscosity of the fluid phase, $[\mu]$ is the intrinsic viscosity and ϕ and ϕ_m is the volume fraction and the maximum flowing fraction of the particulate phase, respectively.

Many of the clean operating conditions on the bench coater and the CLC are at larger solids levels than what can be measured in the concentric cylinder rheometer. This result indicates that a dynamic effect is at play in the blade coaters, where the suspension experiences the shear

field for a short amount of time. The short duration shear event under the blade may not give time for some type of jam structure to develop compared to the concentric cylinder situation. This short duration allows the suspension to be applied with the blade at solids larger than what would be expected from the steady shear behavior.

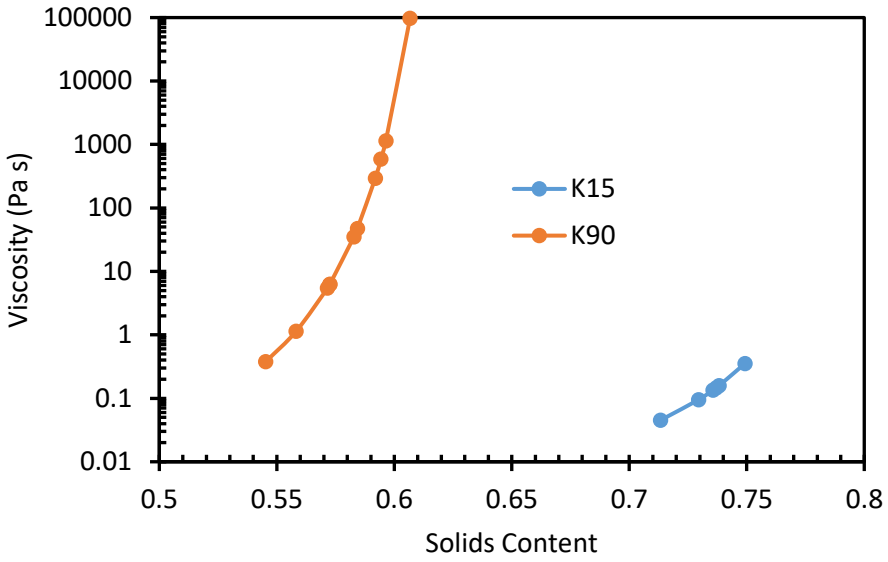

Figure 4.13. Calculated viscosity (Pa s) from the Mooney equation for K15 and K90 at the solids content used in the runnability studies

With the steady shear viscosity unable to determine a correlation with the onset of operational problems, exploration into the complex viscosity was conducted; the complex viscosity is not the same as a dynamic viscosity but may give a sense of the effective viscosity at short times. Figure 4.14 displays the complex viscosity at the solids content that was used in the runnability studies. The value shown in the figure is the average complex viscosity over the frequency range of 10 to 30 Hz. There was a substantial amount of noise in the data. The complex viscosities at different solids concentrations are of similar values while in steady shear there are orders of magnitude difference in viscosity. As the solids concentration increases, there is only a small change in the complex viscosity.

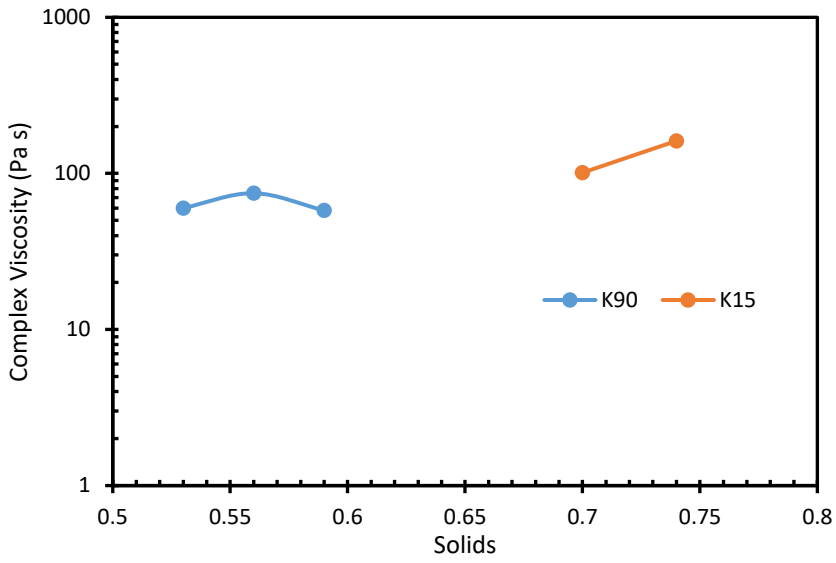

Figure 4.14. A plot of the relationship between the complex viscosity and the solids content for K15 and K90.

Because the complex viscosities are of the same magnitude for the two pigments, there might be a relationship with the runnability of the suspension. Figure 4.15 displays the relationship between the complex viscosity and the machine speed where operational issues developed during the runnability studies. There may be a trend that could be used to predict when a coating might begin to exhibit operational issues. Currently, it is not able to predict when a pigment will exhibit runnability issues. This suggests, however, there might be potential to provide information on the dynamic response of the particles during blade coating. Additional research into the area will be needed to determine this potential relationship.

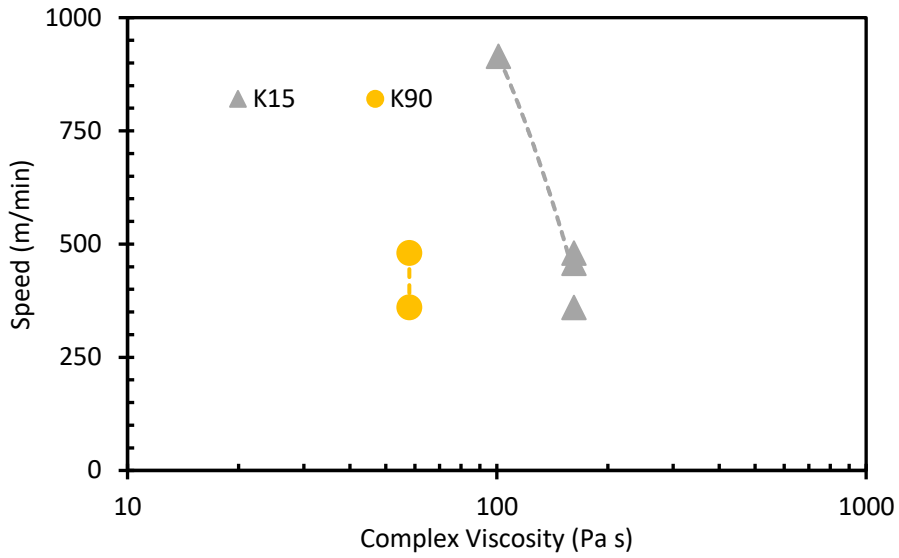

Figure 4.15. Plot showing the relationship between the complex viscosity and the maximum coating speed for K15 and K90

Operational difficulties began to appear at high solids concentrations approaching the immobilization solids for the pigment. Recall that the immobilization solids concentration is a function of the shape, size and size distribution of the pigment. The difference between the immobilization solids and the solids content of the tested slurry, which will be called ΔS, was calculated for all tests. There seems to be a connection between ΔS and the runnability window. Figure 4.16 displays the relationship between these two parameters. As the ΔS increases, the slurry was able to run at higher speeds before blade deposits were visible. As the solids concentration approaches the immobilization solids, hence ΔS heads towards zero, operational problems start at very low speeds. The relationship appears to be linear, with a slope of 18,684 m/min. K15 data points are closer to the predicted trend. There does seem to be a bit more scatter with the K90 data points.

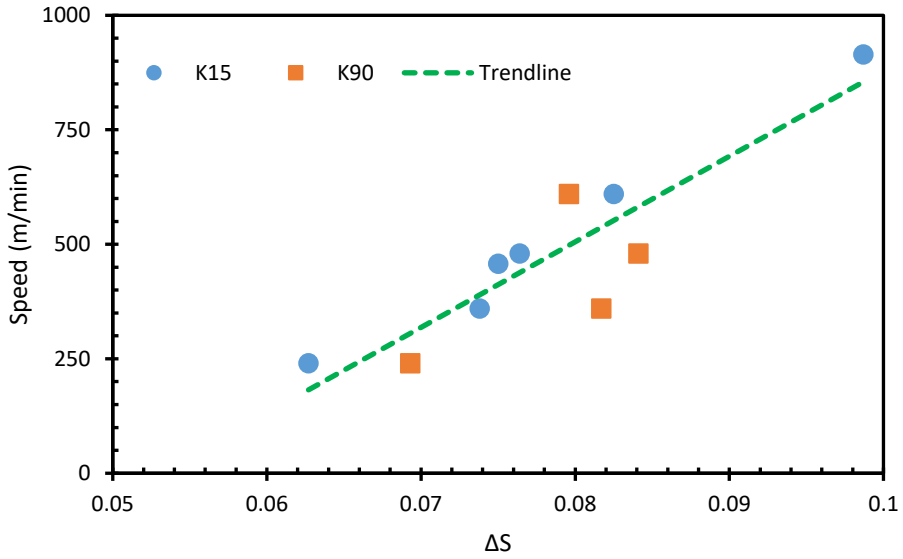

Figure 4.16. Linear relationship between ΔS and the roll speed at which operational issues appear for both K15 and K90

While the results are for only the two pigments used in this study, the data do seem to collapse onto a single line. If this relationship holds true for other pigments of varying shape factors, the maximum operational speed could be quickly calculated. A simple test to determine the immobilization solids would be necessary to estimate the maximum coating speed for the desired solids concentration. The immobilization solids will take into account the particle shape and size distribution. This relation would prove to be very useful for many applications.

Conclusions

The runnability limits using the CLC was determined for two pigments of varying shape factors using two substrates. Operational and quality issues were observed, and the onset of problems occurred around the same operating conditions. The effect of the permeability differences between the two base sheets was minor. The results obtained from the bench top blade coater and the CLC did show correlation. The solids content of the all slurries was high and approaching the immobilization solids.

These suspensions could be applied at solids higher than the maximum flowing solids value obtained by fitting the Krieger-Dougherty equation. The operational limits did not correlate with the viscosities predicted from the Mooney equation. Operational limits occurred at steady shear viscosities which were orders of magnitude different, but for the complex viscosities they were similar; this result indicated that the operational issues must relate to a dynamic response of the suspension. The runnability limits did correlate with ΔS, the difference in solids between the immobilization solids and the coating solids. This parameter seems to have a linear relationship with the operation limits. This relationship could be attribute to the lack of available space for particle motion in the high shear field underneath the blade and may be of some value in predicting operational limits of other systems.

CHAPTER 5

ESTIMATING FILTERCAKE GROWTH DURING BLADE COATING

Abstract

The formation of a filtercake on the surface of the paper during blade coating was been theorized as one of the potential sources of operational difficulties during the coating process. As the water penetrates the base sheet, the solids content increases. This increase in concentration can lead to operational problems such as scratches or excessive blade wear. Characteristics of the coating formulation, properties of the base sheet and blade coater operating conditions were all accounted for in development of a mathematical model that calculated the formation of a filtercake during blade coating.

Experimental values for all parameters were based on data taken from the previously conducted runnability studies. The filtercake model was able to correctly estimate the pressure pulse exhibited underneath the blade. As the speed of the web is increased, both the pressure in the coater and the growth of the filtercake rises. The permeability of the base sheet and the coating plays a crucial role in the formation of the filtercake. Using the conditions that parallel the previous runnability studies, it was found that filtercake growth would not have impeded blade coating. Further refinement of the model will be necessary to predict the solids content and web speed at which the filtercake closes the blade gap.

Introduction

A clear mechanism that explains the root causes behind runnability is not clear in literature. There are many mechanisms that seem to explain the behavior, but a quantitative prediction based on these mechanisms is lacking. These operational issues are a complex and interwoven system where it is some combination of coating characteristics, base sheet

properties and blade coater operating conditions which impact the results. Work is needed to link mathematical models with fundamental mechanisms to predict runnability.

Particle motion simulations are a powerful tool that allows researchers to examine how the particles influence measurable properties of the coatings and the motion of pigments during coating application. Bousfield in 1990 was one of the first to apply these simulations for the paper industry using Stokesian dynamics. Estimating the viscosity from particle motion simulations, and comparing to experimental data, was one of the first tasks completed using this technique. The viscosity of colloidal suspensions is dependent on the interactions between the particles. Bilodeau and Bousfield (1998) were able to predict the shear thinning behavior of a suspension of spherical particles. The decreasing viscosity is a result of particle structures disintegrating and slipping (Bilodeau and Bousfield, 1998). Barbesta *et al.* (2001) built upon that work and added CMC to the model. The CMC supplemented into the simulation was treated like a salt addition (Barbesta *et al.,* 2001). The model was able to accurately determine the slope of the shear thinning region but was under estimating the upper Newtonian plateau of the viscosity shear rate curve (Barbesta *et al.,* 2001). A simple shift was needed to adjust the data to coincide with experimental data.

Toivakka and Eklund (1996) examined the effect of particle size distribution using particle motion simulations in a simple shear field. The shear thickening behavior was only observed for monodispersed suspensions; the small particles will disturb the links between large particles (Toivakka and Eklund, 1996). During this work, it was observed that small particles move towards the boundaries and force the larger particles to the bulk of the suspension. There is a size segregation of particles during flow (Toivakka and Eklund, 1996). Lyons *et al.* (2003) also investigated the effect of particle size distributions. The simulations were improved to included thousands of particles and the geometry was altered to the complex system of a blade coater.

Similar results of size segregation were found. Smaller particles tended to accumulate against the boundaries of the flow field caused by the larger particles pushing them to those locations (Lyons *et al.,* 2003). The separation of particle sizes during flow predicted by the particle motion simulations may explain why coating with a broad size distribution can be applied at higher machine speeds with the small particles acting as a lubricating layer under the blade.

The boundary conditions of the particle motion simulation can be altered to incorporate realistic conditions observed during coating. Absorption of water into the base sheet is one of the modifiable boundary conditions. The effect of the absorbing boundary was first investigated by Bousfield in 1990. An increase in the concentration of particles near the paper surface was seen but no significantly different magnitude of forces was calculated on the blade or the paper web (Bousfield, 1990). Expanding this effect of absorbing boundary condition was developed to calculate the formation of a filtercake during coating. As the coating is dewatered, a filtercake is formed. The thickness of the filter cake can become so large that causes issues during coating including a large pressure pulse which drives more water into the base sheet (Bousfield, 1994). As the filtercake begins to completely fill the gap between the paper web and the blade surface, the blade could disrupt the immobile phase and induce quality issues in the coating layer (Hardy and Carter, 1994). Using this model, the maximum coating speed before the filter cake becomes an issue was determined. The results from the model correlate with the finding published in literature (Bousfield, 1994). The outcome of this model shows the potential for simulation models to predict issues during coating or to develop operational windows for coating formulations.

The simulation used in this model was built off the platform used in the Bousfield (1994). One of the main differences in the construction of the equations, was that the penetration of suspending liquid was included in this updated version. The goal is to understand

the magnitude of the influence of filtercake buildup on the runnability results in the previous chapter. Experimental values from the runnability study discussed in Chapter 4 were used as input values. Results are compared to the experiments.

Model Development

The first step of model development was to determine the boundaries of the system. Using a commercial finite element analysis program (COMSOL Multiphysics) a basic blade coater geometry was built. Figure 5.1 displays this set up. The blade is assumed to be always running parallel to the paper web. Each of the major operating condition variables could be altered to assess the effect on the velocity, pressure and shear rate profiles. The four key parameters controlling the blade coater operations are the blade angle (θ), the blade thickness (δ), the distance between the blade and the substrate (h), and the speed of the paper web (U). The edges of the blade were given the value of the web speed. Zero-gauge pressure boundary conditions were set at the entrance and the exit of the flow direction. This model provides the location of the stagnation point at the blade nip, and verification of the pressure pulse profile generated in the filtercake simulations.

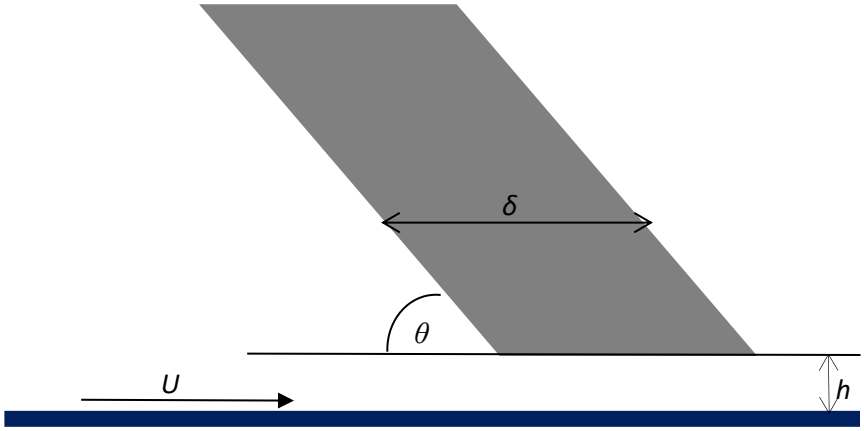

Figure 5.1. Schematic of the blade coater geometry that was used in the fluid dynamics analysis

The stagnation point was determined to be 4.5 mm from the nip of the blade based on the results from the finite element model. The blade angle and blade thickness of 45° and 0.38

mm, respectively, were used in the filtercake analysis. The top boundary of the system was determined by the distance from the surface of the substrate and the blade, h_{B}. The height of the filtercake (h_{F}) and the penetration depth of into the substrate (L_{P}) are functions in the *x*-direction. Figure 5.2 defines the geometry of the filtercake model.

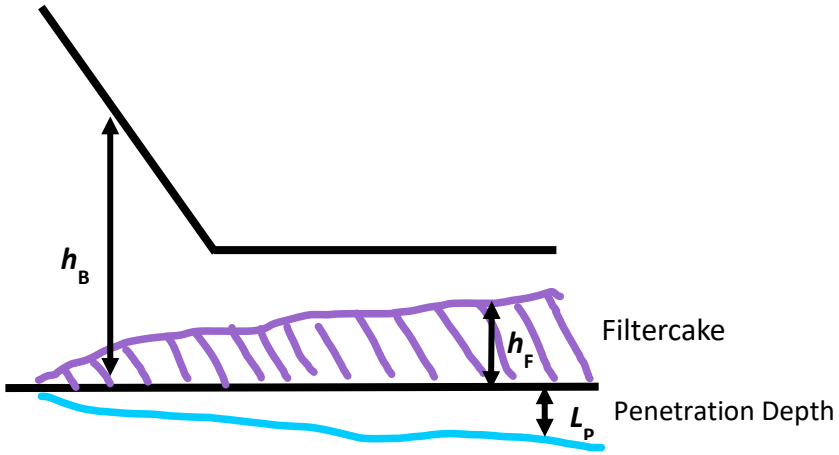

Figure 5.2. Diagram of the blade coater used in the filtercake model

The velocity of the coating at any location between the filtercake and the blade surface in the system can be determined using the equation of momentum that can be simplified from the Navier-Stokes equation by assuming an incompressible fluid and a constant viscosity. When the distance between the blade and the coating filtercake is small, the Navier-Stokes equation reduces to the lubrication approximation as:

$$\frac{\partial P}{\partial x} = \mu \frac{\partial^2 V_x}{\partial y^2} \qquad \text{Eq. 5.1}$$

where P is the pressure, μ is the viscosity of the suspension, and V_x is the velocity in the *x*-direction.

Two boundary conditions are required to solve for the velocity profile. A no slip condition was applied to the blade surface and the top of the filtercake. The velocity was set to

zero and the speed of the web, respectively. Using those boundary conditions, Eq. 5.1 is integrated to obtain the velocity profile for coating between the filtercake and the blade surface as:

$$V_x = \frac{U(h_\mathrm{B} - y)}{(h_\mathrm{B} - h_\mathrm{F})} + \frac{\partial P}{\partial x}\left[\frac{y^2 - yh_\mathrm{B} - yh_\mathrm{F} + h_\mathrm{B}h_\mathrm{F}}{2\mu}\right] \qquad \text{Eq. 5.2}$$

At any vertical slice in Figure 5.2, the total volumetric flow rate, Q, has to be the same to conserve mass. The net flow of the fluid between the filtercake and the blade surface is an integration of the velocity. Combined with the volume of the filtercake and the fluid in the paper, the expressions is obtained as:

$$Q = \int_{h_\mathrm{F}}^{h_\mathrm{B}} V_x \,\mathrm{d}y + Uh_\mathrm{F} + UL_\mathrm{P}\varepsilon \qquad \text{Eq. 5.3}$$

The first term accounts for the flow rate between the blade and the filtercake. The second term is the volumetric flow rate per unit width of the filtercake per slice. The last term accounts for the amount of liquid transferred into the base sheet of porosity ε. When the velocity profile in Eq. 5.2 is inserted into this continuity equation and integrated we obtain:

$$\frac{\mathrm{d}P}{\mathrm{d}x} = \left[Q - \frac{U(h_\mathrm{B} - h_\mathrm{F})}{2} - Uh_\mathrm{F} - UL_\mathrm{P}\varepsilon\right]\left(\frac{12\mu}{(h_\mathrm{B} - h_\mathrm{F})^3}\right) \qquad \text{Eq. 5.4}$$

This is the standard lubrication expression for flow between the surfaces, but it takes into account the flow carried with the filtercake and the fluid contained in the substrate. This is a modified version of the expression in Bousfield (1994) because it now takes into account the volume of the fluid in the substrate.

To estimate the dewatering of the coating into the base sheet, Darcy's Law was employed. It was modified to account for two layers: filtercake and the substrate. Each layer has its own permeability coefficient. The permeability constant for the filtercake, K_F, is dependent

on the particle size, shape and size distribution. For this study, the filtercake permeabilities used were from gravimetric dewatering tests discussed in Chapter 2 and reported in Table 2.1. The permeability constant for the substrate, K_{s}, was determined from the base sheet used in the runnability studies discussed in Chapter 4.

$$\frac{\mathrm{d}V_p}{\mathrm{d}t} = \frac{\Delta P}{\mu\left(\frac{h_{\mathrm{F}}}{K_{\mathrm{F}}} + \frac{L_{\mathrm{P}}}{K_{\mathrm{s}}}\right)} \qquad \text{Eq. 5.5}$$

Both the height of the filtercake and the penetration depth are functions of the liquid volume transferred from the coating into the substrate, V_{p}. The height of the filtercake is determined by the mass of solids built up from the transferred volume and the amount of water contained in the filtercake. While the penetration depth is determined from the amount of liquid transferred and the porosity of the paper.

$$h_{\mathrm{F}} = \frac{V_{\mathrm{p}}\phi}{\phi_{\mathrm{p}}} \qquad \text{Eq. 5.6}$$

$$L_{\mathrm{P}} = \frac{V_{\mathrm{P}}}{\varepsilon} \qquad \text{Eq. 5.7}$$

The spatial derivative is needed to calculate the growth of the filtercake and the penetration depth. Each of the variables is dependent on the amount of liquid transferred from the coating into the base sheet. To predict the height and depth at each time step, Euler's method and the spatial derivative were utilized.

$$\frac{\mathrm{d}h_{\mathrm{F}}}{\mathrm{d}x} = \frac{\mathrm{d}V_{\mathrm{P}}}{\mathrm{d}t}\frac{\phi}{\phi_{\mathrm{P}}U} \qquad \text{Eq. 5.7}$$

$$\frac{\mathrm{d}L_{\mathrm{P}}}{\mathrm{d}x} = \frac{\mathrm{d}V_{\mathrm{P}}}{\mathrm{d}t}\frac{\varepsilon}{U} \qquad \text{Eq. 5.8}$$

Parameters needed to characterize the pigment were taken from laboratory measurements, and ϕ and ϕ_{P} represent the volume fraction of the coating and the

immobilization solids, respectively. The immobilization solids were 0.62 and 0.44 for K15 and K90, respectively. The viscosity was held constant at 2 Pa s for both pigments. This viscosity corresponds to the value determined from the parallel plate rheometer, see Figure 3.11. The density was set to 1,450 kg/m^3. The viscosity of the suspending liquid was 0.894 mPa s. Along with these measured parameters of the pigment slurries, the initial condition for the filtercake height, penetration depth and the pressure at the entrance will need to be entered into the simulation. The initial filtercake thickness was estimated to be 0.001 µm; this value is needed to do a numerical integration and is adjusted to be large enough to keep the calculation stable, but small enough to not influence the results. The penetration depth was calculated based off the initial filtercake height. The inlet pressure at the stagnation point is calculated from the mechanical energy balance, as shown in the equation below,

$$P_{\text{inlet}} = \frac{\rho U^2}{2} \qquad \text{Eq. 5.9}$$

where P_{inlet} is the pressure at the stagnation point and ρ is the density of the coating.

The final filtercake height, penetration depth and coat weight are calculated using a simple numerical analysis method. A reasonable initial guess for *Q* is inserted in the model. Using the built-in solver function in Microsoft Excel™, the value of *Q* is adjusted until the outlet pressure is atmospheric.

Results and Discussion

The pressure profile results from the filtercake build up were compared to the pressure field generated from the finite element model. The same conditions were inserted into both models. The web speed was 457 m/min. The parameters were set to K15 at a solids mass fraction concentration of 0.78. One large difference between the two models is the inclusion of an absorbing boundary conditions. The filtercake model uses the less permeable substrate,

while the finite method does not account for any dewatering. This dissimilarity would account for the difference between the height of the peaks of the pressure pulse. As the permeability of the base sheet is decreased, the pressure pulse for the model is closer to the finite element results. The very similar profile does validate the hydrodynamics of the model.

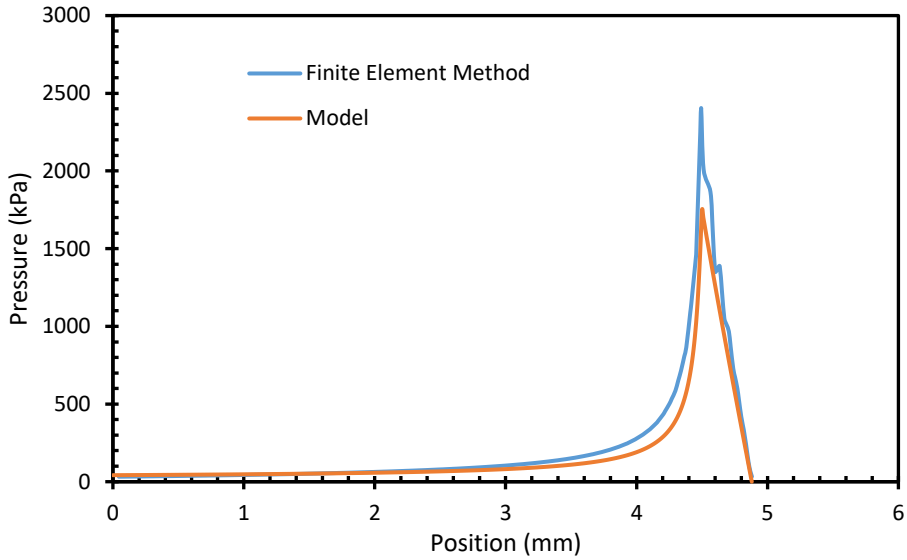

Figure 5.3. Pressure profile developed under the blade from the finite element method and filtercake models

The height of the filtercake increases as the machine speed is increase. Figure 5.4 displays the growth of the filtercake for K15 at a solids concentration of 0.78 along with the corresponding pressure profile. As expected, the pressure underneath the blade is large at high machine speeds. The pressure is the driving force of the dewatering into the base sheet as described by Darcy's law, see Eq. 5.5. Thus, the filtercake is larger when the speed of the coater is increased. There is an uptick in the rate of filtercake growth as the coating is approaching the blade nip and just underneath the blade. This position corresponds to the large pressure pulse that is exhibited in the pressure profile. The increase in the filtercake thickness at small positions comes from the rapid increase due to the stagnation pressure that scales with velocity squared.

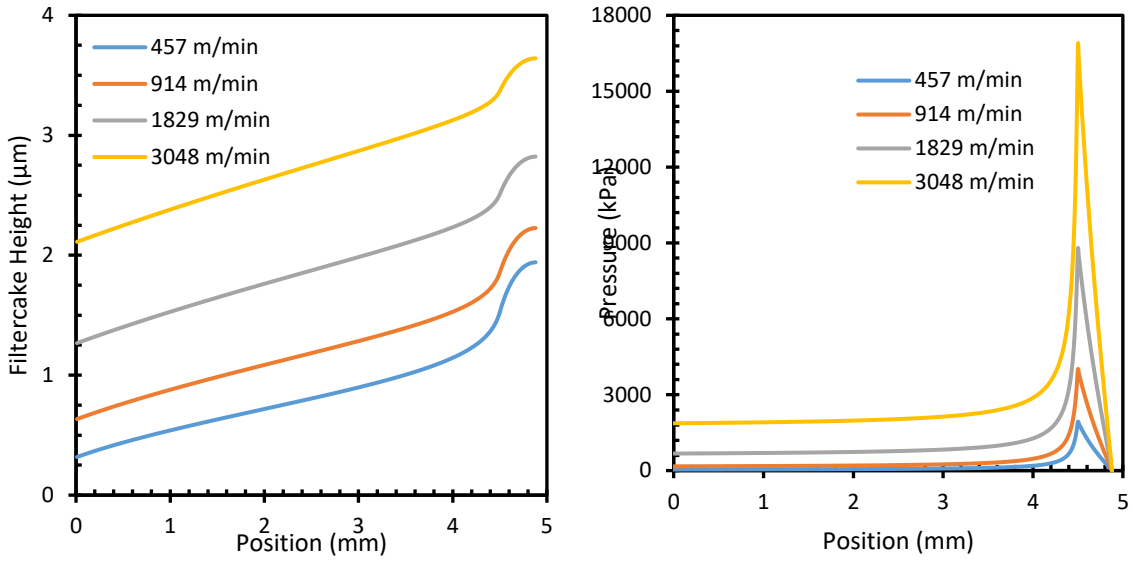

Figure 5.4. Height of the filtercake at varying machine speeds for K15 at a solids concentration of 0.78 and the corresponding pressure pulse profile

Figure 5.5 displays the growth of the filtercake at the exit of the blade during varying ratios of the solids concentration to the immobilization solids for the two substrates. As the ratio of the solids increases, the height of the filtercake is also larger. It requires less water to be removed from the sample to form a filtercake when the solids concentration of the coating is approaching the immobilization solids. The permeability of the base sheet additionally affected the formation of the filtercake. The filtercake formed on the surface of the uncoated base sheet was three times larger than on the less permeable coated substrate. The rate of the filtercake build up is also larger for the uncoated substrate as the web speed is ramped up.

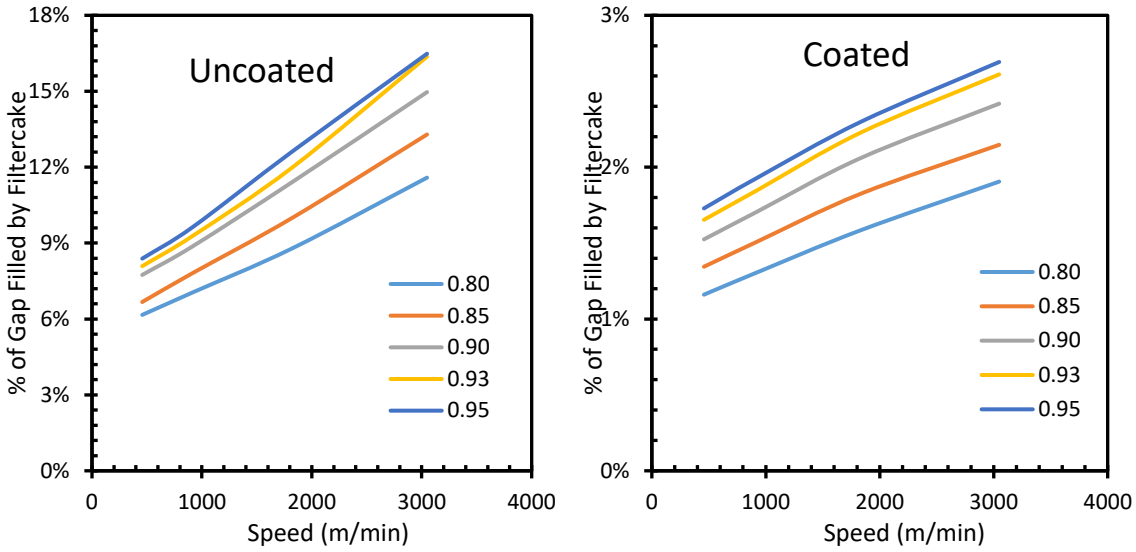

Figure 5.5. Plots of the filtercake growth at the exit of the blade for K15 at varying ratios of solids content to immobilization solids for two substrates.

The growth of the filtercake was calculated for K90 at the same machine speed and solids ratios. Similar trends were observed as with K15. The results are displayed below in Figure 5.6. Filtercake formation on the uncoated substrate was three times larger than what was predicted on the coated substrate. The effect of the permeability of the substrate was also observed with a larger filtercake forming on the uncoated substrate.

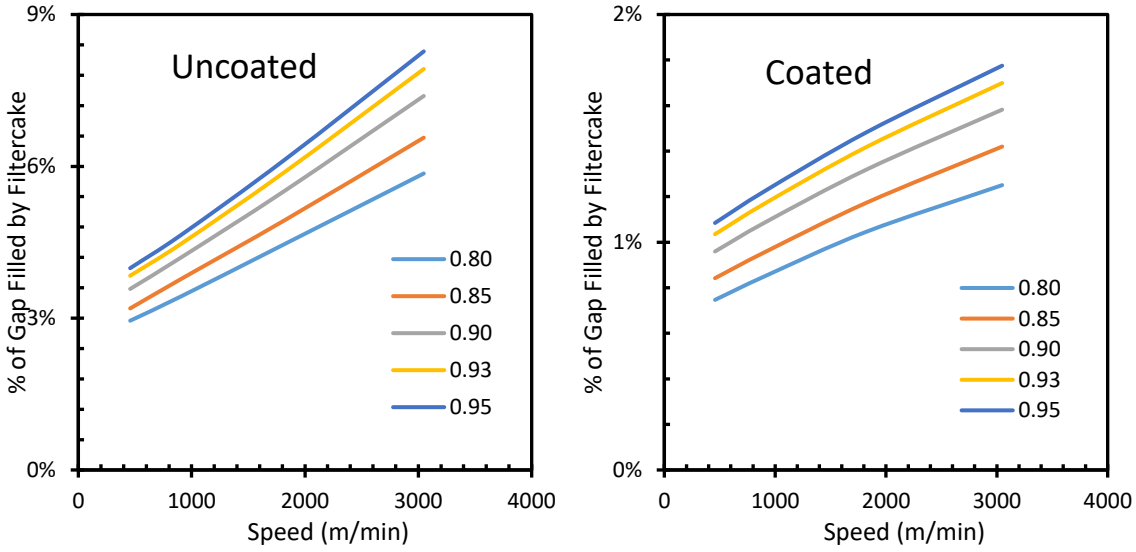

Figure 5.6. Plots of the filtercake growth at the exit of the blade for K90 at varying ratios of the solids content to the immobilization solids for two substrates

The permeability of the coating is a function of the shape of the pigment. K90 has a lower permeability and a greater water holding capacity than K15. This is evident when a comparison is made on the amount of filtercake growth formed between the two pigments, as displayed in Figure 5.7. Using the uncoated substrate, K15 has double the amount of filtercake growth in the blade gap than does K90. When the substrate is less absorbent, the effect of the decreased water loss is also seen in the filtercake thickness, though K15 does still has more filtercake growth in the blade gap but the thickness is closer to that of K90.

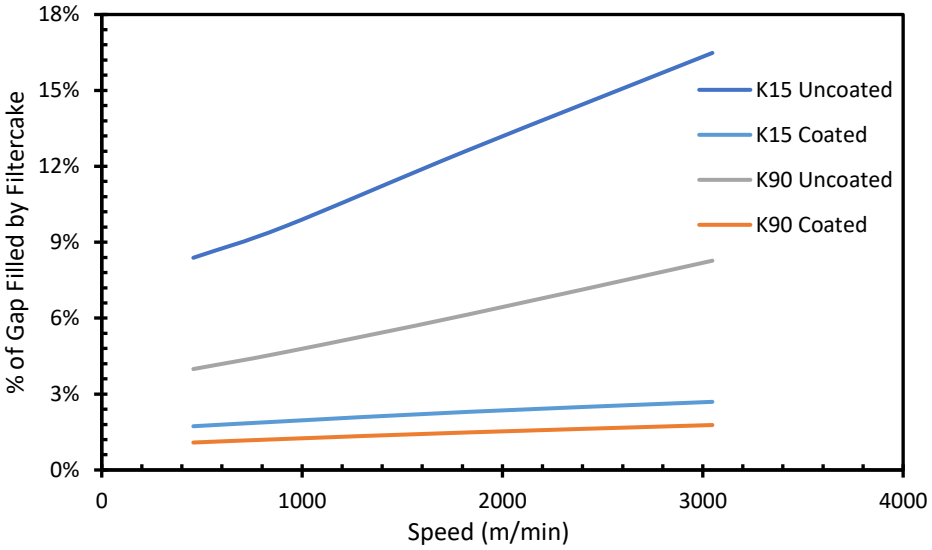

Figure 5.7. Filtercake growth for K15 and K90 at a solids ratio of 0.93 for both the coated and uncoated substrate

The results from this filtercake simulation model do not explain the results from the runnability study discussed in Chapter 4. Table 5.1 displays the calculated filtercake height at the exit of the blade and the percentage of the blade gap closed by the formation of the filtercake for several cases where operational difficulties were present in the runnability study. The filtercake filled only 6.15% of the gap in the worst case scenario. The filtercake does not grow to such a degree that it will close the blade gap for the parameters used here.

Table 5.1. Calculated filtercake using conditions which operational problems were observed during previous runnability studies

Pigment	Solids (mass fraction)	Substrate	Speed (m/min)	Filtercake height (μm)	Percentage of gap filled by filtercake
K15	0.737	Uncoated	305	1.69	6.15
	0.737	Coated	457	0.36	1.27
K90	0.5843	Uncoated	305	1.11	2.77
	0.5964	Coated	610	0.32	0.78

The model was unable to predict the solids concentration and the speed at which the filtercake will close the gap between the substrate and the blade surface. The current version of the model solved in Excel had trouble predicting filtercake thickness that was close to that of the gap. It was possible to obtain a filtercake that filled 30% of the gap, but any increase in either the web speed or the solids concentration caused the model to fail to converge or to converge to a non-physical result. Decreasing the step size in the *x*-direction along the length of the model will aid in discovering the maximum speed before the filtercake begins to close the gap. Pigment slurries are known to exhibit shear thinning behavior. In this model, low shear viscosity was used. Rheological data at shear rates comparable to those experienced during blade coating will increase the validity of the model.

Conclusions

A model was developed that estimates the growth of the filtercake during blade coating. The filtercake simulation model was able to predict the pressure pulse underneath the blade which was comparable to the pressure profile generated using a finite element analysis. Properties of the base sheet and the coating formulation affect the growth of the filtercake during blade coating. Decreasing the permeability of either the coating or the substrate resulted in less filtercake growth in the gap between the blade and the paper surface. On an absorbent base sheet, the water retention of the suspension plays a larger role in the formation of a

filtercake. This effect is diminished as the permeability of the base sheet is decreased. The model predicted that filtercake formation was small for the experimental conditions in Chapter 4.

The model was unable to converge to realistic solutions for speeds or solids concentrations at which the filtercake would fill the gap between the paper surface and the blade. Refinement of the model will be necessary to determine this point. Decreasing the step size down the length of the blade coater will aid in delicacy required to calculate the filtercake height as it closes the distance between the blade.

CHAPTER 6

CONCLUSIONS AND SUGGESTIONS FOR FUTURE PLANS

The effect of particle shape and characteristics on dewatering, rheology and coating application limits was examined with a series of experiments. The rate of dewatering and filtercake permeability were analyzed. Pore size distribution and porosity were determined for a dried filtercake. Runnability studies were completed to determine the operational limits based on the solids content of the coating and the shape of the pigment particles. A bench top blade coater without the absence of a base sheet displayed that small changes in solids concentration resulted in fluctuations in the speed which coating issues begin. The effect of the permeability of the substrate was investigated using the CLC for two pigments with varying shape factors. A mobile video camera, mounted to the coating device, was used to record the process. Finally, a mathematical model was developed to calculate the filtercake formation during the blade coating application process using experimental conditions.

Many properties of the coating and the substrate can affect the operational limits of a coating. The dewatering of the suspensions by the substrate displayed a minor effect on both the maximum coating speed and the formation of a filtercake layer for conditions studied here. It was possible to generate blade deposits in the absence of a base sheet. The model calculated small filtercakes that would not have impeded the coating process. The rate of dewatering for a pigment also had only a slight impact on the runnability limits. High aspect ratio pigments tend to have slower dewatering rates than more spherical shaped pigments. Analysis of the porosity and pore size distribution of a dried filtercake demonstrated that high shape factor pigments have larger pores and broader distributions. These results indicated that size of the connections between the pores is controlling the rate of dewatering.

The rheology of the suspension is one of the most cited causes behind the onset of operational issues. There was no correlation between the steady shear viscosity and the maximum coating speed. Analyzing the dynamic viscosity of the pigment slurries, there could be some form of relationship between the complex viscosity and the maximum coating speed. The complex viscosity was fairly constant across the range of solids that was associated with operational problems. This does not explain how small changes in the solids concentration resulted in large fluctuations in the maximum coating speed. Problems during coating began when the solids concentration approaches the immobilization solids of the coating. The immobilization solids are dependent on the shape of the pigment and how tightly the particles will pack together. For two pigments with different shape factors studied at high shear rates, a linear relationship between the maximum coating speed and the difference between the coating solids and the immobilization solids was found.

In the high solids suspension, the interactions between rotating particles could be disrupting the packing structure and causing jams in the coating layer. These disruptions could be promoting the onset of the operational issues. The higher aspect ratio pigments require more available space for rotation than a spherical or blocky pigment. This concept of particle jamming should be observed in the rheological characteristics. The issues observed during blade coating are related to the particles' response to the intense and instantaneous shear and the large pressure pulse that occurs at the blade nip.

Based on the results and the discussion in this dissertation, here are some suggestions for future research:

- To gain further insight into the effect of latex addition and adjustments to the particle size distribution has on the porosity, packing structure, and immobilization solids,

expansion of the work completed in chapter 2. Determining the immobilization solids and the pore size distribution for suspensions containing pigments of varying shape factors and latex concentrations. The runnability studies demonstrated the importance of the packing structure on the operational limits.

- The runnability studies on both the bench top blade coater and the CLC were only conducted using pigment-only slurries. Continuing the work to determine the operational limits using full coating formulations is obviously needed. The coatings will need to be fully characterized to assess which parameters form a relationship with the operational limits. The inclusion of binders, latexes and additives can influence the particle-particle interactions, thus modifying the basic properties of the colloidal suspension.
- Refinement of the filtercake model will be necessary to determine under which conditions the filtercake will close the gap between the surface of the substrate and the blade. Decreasing the size of the steps taken along the length of the blade coater will enhance the model ability to locate the runnability limits caused by filtercake build up. Usage of rheological data at conditions similar to blade coating will increase the strength of the model.
- Further study of the complex viscosity of the coating suspensions. As shown in Chapter 4, there may be a relationship between the complex viscosity and the maximum coating speed. This will also provide additional insight on how the particles react under strain, providing more information on the concept of particle jamming.
- The conclusions from this research project begin to show that the movement of the particle during coating is one of the critical causes behind runnability issues. Particle motion simulations can predict both particle trajectory and rotation during blade

coating and would provide valuable insight. High aspect ratio pigments require more volume for rotation, but their rate of rotation is lower than spherical particles. Any movement during coating can cause large disruptions in the packing structure.

WORKS CITED

Alince, B., & Lepoutre, P. (1983). Viscosity, packing density and optical properties of pigment blends. *Colloids and Surfaces*, *6*(2), 155-165.

Barbesta, F., Bousfield, D. W., & Rigdahl, M. (2001). Modeling of rheological properties of coating colors. *Journal of Rheology (1978-present)*, *45*(1), 139-160.

Barnes, H.A., Hutton, J.F., and Walters, K. (1989). *An Introduction to Rheology.* New York, NY: Elsevier Science Publishing Company

Bilodeau, R. R., & Bousfield, D. W. (1998). Shear-thinning predictions from particle motion modeling. *Journal of Rheology (1978-present)*, *42*(4), 743-764.

Boersma, W.H., Laven, J., and Stein, H.N. (1995) Computer simulations of shear thickening of concentrated dispersions, *Journal of Rheology,* 39, 841-860.

Bousfield, D. W. (1990, May). The simulation of pigment motion during blade coating. In *Proceedings of TAPPI Coating Conference* (pp. 325-334). Tappi Press Atlanta, GA.

Bousfield, D. W. (1993). Particle Motion During Shear. The influence of particle shape and roughness on rheology. *Nordic Pulp and Paper Research Journal (Sweden)*.

Bousfield, D.W. (1994). Prediction of velocity and coat-weight limits based on filter-cake formation. *TAPPI Journal. 77(7),* 161-171.

Bousfield, D.W., Isaksson, P., and Rigdahl, M. (1997) Modeling of particle motion at the exit of a blade coater, *Journal of Pulp and Paper Science,* 23, 6, J293-297.

Brady, J.F. and Bossis, G. (1985) The rheology of concentrated suspensions of spheres in simple shear flow by numerical simulations, *Journal of Fluid Mechanics,* 155, 105-129.

Brady, J.F. and Bossis, G. (1988) Stokesian dynamics, *Annual Review of Fluid Mechanics,* 20, 111-157.

Branston, R.E., Clark, P.C., Errico, M. Scriven, L.E., Sheehan, J.G., Suszynski, W.J., Takamura, K., and Vodnick, J.L. (1994). Weeping in blade coating Part 1: High-speed video and still macrophotography. *TAPPI Journal, 77(1),* 131- 138.

Branston, R.E., Clark, P.C., Errico, M. Scriven, L.E., Sheehan, J.G., Suszynski, W.J., Takamura, K., and Vodnick, J.L. (1994). Weeping in blade coating Part 2: SEM and X-ray analysis of microtome-sectioned weeps. *TAPPI Journal, 77(4),* 117-124.

Bundy, W. M., & Ishley, J. N. (1991). Kaolin in paper filling and coating. *Applied Clay Science*, *5*(5), 397-420.

Conceição, S., Santos, N. F., Velho, J., & Ferreira, J. M. F. (2005). Properties of paper coated with kaolin: the influence of the rheological modifier. *Applied clay science*, *30*(3), 165-173.

Dahlvik, P., Lohmander, S., Larson, L., & Rigdahl, M. (2000). Relations between the rheological properties of coating colors and their performance in pilot-scale coating. *NORDIC PULP & PAPER RESEARCH JOURNAL*, *15*(2), 106-113.

Daiss, A., Wagner, H. G., & Wirth, T. (1998). Flow structures within the distribution chamber of a high speed short dwell coater-Numerical investigation and comparison with experimental data. In *COATING PAPERMAKERS CONFERENCE* (pp. 565-582). TAPPI PRESS.

Doi, S., Shiratori, N. & Yasukawa, A. (1999). Laboratory measurement of bleeding potential during blade coating. *Tappi Journal,* 82(5), 101-110.

Durlofsky, L, Brady, J.F., and Bossis, G. (1987) Dynamic simulation of hydrodynamically interacting particles. *Journal of Fluid Mechanics,* 180, 21-49.

Engström, G., & Rigdahl, M. (1989). Stalagmite formation during blade coating. The effects of process conditions. *Tappi journal*, *72*(8), 135-138.

Ettl, R., Schadler, V., & Willenbacher, N. (2000). Runnability and flow-induced aggregation of paper coating suspensions. *NORDIC PULP & PAPER RESEARCH JOURNAL*, *15*(5), 509-514.

Ferguson, J. (1991). *Applied fluid rheology.* New York, NY: Elsevier.

Gane, P. A. C. (1997). Relaxation-induced dilatancy in separable visco-elastic suspensions: proposing a novel rheological phenomenon. In *1997 Tappi Advanced Coating Fundamentals Symposium*.

Gane, P. A. C., & Coggon, L. (1987). Coating blade geometry: its effect on coating color dynamics and coated sheet properties. *Tappi journal*, *70*(12), 87-96.

Gane, P. A. C., & Watters, P. (1989). Pigment particle orientation: an analysis of the opportunities for optimizing blade coater runnability and coated sheet properties by controlled flow geometry. *Paperi ja puu, 5,* 517-533.

Gane, P. A., Hooper, J. J., & Grunwald, A. (1997). Coating pigment orientation: a comparative analysis of the application mechanisms and properties of blade and roll coatings. *Tappi journal*, *80*(2), 109-115.

Gane, P. A., Kettle, J. P., Matthews, G. P., & Ridgway, C. J. (1996). Void space structure of compressible polymer spheres and consolidated calcium carbonate paper-coating formulations. *Industrial & engineering chemistry research*, *35*(5), 1753-1764.

Gane, P. A., McGenity, P. M., & Watters, P. (1992). Factors influencing the runnability of coating colors at high speed. *Tappi journal*, *75*(5), 61-73.

Gane, P.A.C. and Hiorns, A.G. (1991). Modelling of blade shape brings pilot coating closer to mill practice. Paper Technology, 32(4). 26-32.

Ghosh, T., Lavoie, P. A., & Carreau, P. J. (1997). Rheology of coating colors and their runnability on a cylindrical laboratory coater. *Tappi journal*, *80*(11), 186-192.

Hardy, R. E., & Carter, D. (1994). Fine particle clay modifications solve coater runnability problems. *Pulp and paper (USA)*.

Hase, K. R., & Bousfield, D. W. (1994). Kaolin pigment-latex interactions during coating. In *COATING CONFERENCE-TAPPI* (pp. 49-49). TAPPI PRESS.

Hsu, R. and Ganatos, P. (1989) The motion of a rigid body in viscous fluid bounded by a plane wall. *Journal of Fluid Mechanics,* 207, 29-72.

Jeffery, G.B. (1922) The motion of ellipsoidal particles immersed in a viscous fluid. *Proceedings of Royal Society,* London, Ser. A, 102, 161-179.

Jeffrey, D.J., and Acrivos, A. (1976) The rheological properties of suspensions of rigid particles, AICHE Journal, 23, 3, 417-432.

Knappich, R., Burri, P., Lohmuller, G., & Hugener, P. (2000). Wet and dry coating structure of calcium carbonate pigments with narrow particle size distribution. *Tappi journal*, *83*(2).

Lee, D. I. (2002). The critical pigment volume concentration concept for paper coatings: I. Model coating systems using plastic pigments and latex binders for paper coating applications. *Journal of Korea Technical Association of the Pulp and Paper Industry*, *34*(5), 1-17.

Lindhjem, C. (1991). Particle packing and shape effects on the rheological characteristics of paper coating pigments. In *COATING CONFERENCE – TAPPI* (pp. 131-141).

Lindstorm, S.B. and Uesaka, T. (2007) Simulation of the motion of flexible fibers in viscous fluid flow, *Physics of Fluids,* 19, 113307.

Lindstrom, S.B. and Uesaka, T. (2008) Particle-level simulation of forming of the fiber network in papermaking. *Intern Journal of Eng. Science,* 46, 858-876.

Lohmander, S., & Rigdahl, M. (2000). Influence of a shape factor of pigment particles on the rheological properties of coating colors. *NORDIC PULP & PAPER RESEARCH JOURNAL*, *15*(3), 231-236.

Lyons, A., Iyer, R. and Bousfield, D. (2003). Particle motion modeling for particle size distributions in blade geometries. In *SPRING ADVANCCED COATING FUNDAMENTALS SYMPOSIUM.*

Metzner, A.B. (1985) Rheology of suspensions in polymeric liquids. Journal of Rheology, 29, 739-775.

Okomori, K., Yamaguchi, M., Suzuki, M. and Morii, H. (2002). Predicting high speed blade coating runnability. In *COATING CONFERENCE-TAPPI*. TAPPI PRESS

Olsson, F., & Isaksson, P. (1995). The influence of viscoelastic rheology on blade coating as revealed by numerical methods. *NORDIC PULP AND PAPER RESEARCH JOURNAL*, *10*, 234-244.

Pajari, H., Mansikka-ajo, J., Ketoja, J., & Bousfield, D. W. (2003). Blade coating with free jet applicator: modelling and experiments. In *8th Advanced Fundamentals Symposium, Chicago, IL, USA*.

Romagnoli, A., and Bousfield, D.W. (1999) Particle motion analysis of oblate spheroids in complex flow geometries. *Proceedings of the 1999 TAPPI Coating Conference,* TAPPI Press, Atlanta GA, pp 433-444.

Roper, J. A., & Attal, J. F. (1993). Evaluations of high-speed runnability using pilot coater data, rheological measurements, and computer modeling. In *COATING CONFERENCE-TAPPI* (pp. 107-107). TAPPI PRESS.

Russel, W.B., Savielle, D.A., and Schowalter, W.R. (1989) Colloidal Dispersions. Cambridge University Press, Cambridge.

Sand A., Nopola, T., Hjelt, T. and Toivakka, M. (2009) A particle motion model for the study of consolidation phenomena. *Computers and Chemical Engineering,* 33, 1227-1239.

Sand, A., Toivakka, M. and Hjelt, T. (2008a) Influences of drying strategy on coating layer structure formation. *Nordic Pulp and Paper Research Journal,* 23, 46-51.

Sand, A., Toivakka, M., and Hjelt, T. (2008) Investigation of filter cake stability using numerical simulation technique. *TAPPI Journal,* 7, 4-10.

Schmid, D.F., Switzer, L.H., and Klingenberg, D.J. (2000) Simulations of fiber flocculation: effect of fiber properties and interfiber friction. *Journal of Rheology,* 44, 781-809.

Sonn, J. S., & Bousfield, D. W. (2015). Modeling absorption and rheological changes as suspensions are applied to porous substrates. *Chemical Engineering Science*, *123*, 579-587.

Suontausta, O. T. (1993). Stalagmite formation in LWC-paper coating. In *COATING CONFERENCE-TAPPI* (pp. 97-97). TAPPI PRESS.

Teirfolk, J. E., & Laaja, V. (1996). An empirical study of blade coating at 2250 m/min. *Tappi journal*, *79*(2), 206-214.

Toivakka, M. O., & Eklund, D. E. (1996). Prediction of suspension rheology through particle motion simulation. *Tappi journal*, *79*(1), 211-222.

Toivakka, M., & Nyfors, K. (2001). Pore space characterization of coating layers. *Tappi journal*, *84*(3).

Toivakka, M.O, & Eklund, D.E. (1994). Particle movements during the coating process. *Nordic Pulp and Paper Research Journal (Sweden)*.

Tran, T. H., Coco, C. E., & Dill, D. R. (1993). Effect of CMC and Soy Polymer Binder Systems on High Speed Blade Runnability. In *COATING CONFERENCE-TAPPI* (pp. 51-51). TAPPI PRESS.

Vodnick, J. L., Clark, P. C., Takamura, K., & Branston, R. (1995). Weeping in Blade Coating, Part III: Effects Revealed by Flow Visualization. In *COATING CONFERENCE-TAPPI* (pp. 135-135). TAPPI PRESS.

Weeks, L., and Bousfield, D.W. (2015). The influence of pigment particle shape and blade geometry on particle alignment. *PaperCon Conference Proceedings,* TAPPI Press, Atlanta, GA.

Weeks, L., Bousfield D.W., & Lyons, A. (2016). The Influence of Pigment Concentration, Particle Size Distribution, and Aspect Ratio on Rheology. *PaperCon Conference Proceedings,* TAPPI Press, Atlanta, GA.

Weigl, J., & Grossmann, H. (1997). Factors impeding high-speed runnability of blade coaters. *Tappi journal*, *80*(11), 223-232.

Willenbacher, N., Hanciogullari, H., & Wagner, H. G. (1997). High shear rheology of paper coating colors–more than just viscosity. *Chemical engineering & technology*, *20*(8), 557-563.

Zhu, Y.D., Allen, G.C., Adams, J.M., Gittins, D.I., Hooper, J.J., and Skuse, D.R. (2013) Barrier Properties of latex/kaolin coatings. *Polymer Chemistry,* 4, 4386-4395.

APPENDIX A: THE INFLUENCE OF PARTICLE SHAPE AND BLADE GEOMETRY ON PARTICLE ALIGNMENT

Introduction

Coatings are applied to paper and paperboard grades to improve the appearance of the final product and to give high quality printing results. Some coatings are also used to generate a barrier layer to water, oxygen or grease in some packaging grades. Various pigments are used in these grades and are often mixed in different amounts. It is desirable to apply these coatings at high solids content to give quality improvements and reduction in drying costs. However, some coatings that contain high aspect ratio pigments are known to be difficult to apply at high solids and need to be applied at some lower solids level. In general, it is understood that the rotation of these high aspect ratio pigments causes them to take up more volume during shear than pigments with low aspect ratios, but this rotation is not well understood. In addition, the influence of coating additives and blade geometry on particle rotation is not well understood.

The rheology of suspensions has a long history and has been reviewed by Jeffery and Acrivos (1976), Metzner (1985), and Russel *et al.* (1989). While others such as Lohmander and Rigdahl (2000) and Ferguson (1991) have looked into the effect that shape factor has on the viscosity of these suspensions. The asymmetrical nature of high aspect ratio particles results in a lower maximum particle packing fraction than spherical particles (Barnes *et al.* 1989). As a result of the shape of these pigments, in conjunction with the poor packing, suspensions containing particles with high aspect ratios have a higher viscosity at the same volume concentration (Conceição *et al*., 2005).

The rheology of the coating plays a major role in the runnability of a blade coater. The size and shape of the particles affect the viscosity of concentrated suspensions arising from the

impediment of neighboring particles. Coatings have regions of shear thinning and thickening at different shear rates. The predisposition of the suspension to have rapid rise in viscosity could be contributing to the processing struggles with runnability. However, simply a high viscosity coating should not lead to coater operational problems. Something more complex must occur at the blade tip to cause operational problems.

The orientation of particles influences the quality of the final product. The vapor barrier property of kaolin is dependent on the volume fraction, shape, and the orientation of the particles in the coating (Zhu *et al.,* 2013). Disorganization of particles in the coating increases the microroughness of the surface and decreases the gloss of the coated paper (Gane and Coggan, 1987). Understanding the rotations and final orientation of particles in the coating will prove to be a valuable tool to improve the quality of the final product.

Particle motions simulation or "Stokesian dynamics" has been a valuable tool since introduced by Brady and Bossis (1985; 1988). These simulations track the motion of particles in the flow of a suspension, taking into account particle-particle interactions. The simulations have been shown to predict a number of issues such as the increase in viscosity with increasing solids (Durlofsky *et al.* 1987), the reduction of the viscosity of a mixture of large and small spheres (Brady and Bossis, 1985), and the increase of viscosity at high shear rates (Boersma *et al.,* 1995). Bilodeau and Bousfield (1998) and Barbesta *et al.* (2001) used these types of simulations to link the shear thinning rheology of coatings to the interparticle colloidal forces and structures that develop during shear flow. Lyons *et al.* (2003) looked at the motion of a large number of spherical particles in a blade coating geometry. The simulations explained the buildup of material in the stagnation zone near the blade heel and the size distribution of coating components leaving the blade. Bousfield *et al.* (1997) also showed the potential for particle size differences generated by the exit flow of a blade coater. Sand *et al.* (2008; 2008a; 2009)

extended these simulations to three dimensions to describe the consolidation of the coating layer into a structure and to predict the influence of drying rate and colloidal forces on the resulting packing of particles. All of these simulations have been carried out for spherical particles.

Simulations have been extended to non-spherical particles by a few groups. Lindström and Uesaka (2007; 2008) and Schmid *et al.* (2000) used these types of particle motion models to describe during papermaking. These simulations allowed for the fiber to bend or flex during the flow. Hase and Bousfield (1994) and Romagnoli and Bousfield (1999) focused on rigid oblate spheroids to model the motion of disk like particles in simple shear and coating flow fields: these later studies were limited to small regions under the blade due to limited computer resources. The work here extends this work to look at larger regions of flow and how blade angle and blade thickness affect the rotation of particles in the coating flow field.

All particles will rotate in a shear field. The period of rotation for any particle, including oblate and prolate spheroids, is given by Jeffrey (1922) as

$$T = \frac{2\pi(b^* + {}^1/_{b^*})}{\dot{\gamma}} \qquad \text{Eq. A.1}$$

where *T* is the time for full rotation of the particle, $b^*$is the aspect ratio of the spheroid, and $\dot{\gamma}$ is the shear rate. This well-known equation describes the rotation or Jeffery's orbits of a particle in shear and has been confirmed by experiments.

Spherical particles revolve about their axis very quickly. But due to their shape, no disruption of the flow field is caused. High aspect ratio pigments, such as kaolin, have longer periods of rotation. The disk shape requires more available free volume to complete their

rotation. This could cause disorientation of particles in the coating leading to processing difficulties and defects in the final coating.

While the trajectory of particles in a flow field is a routine calculation in commercial finite element codes, the rotation of these particles during flow is not part of the calculation. The goal of this work is to develop a model that predicts the orientation and rotation of single particles in blade coating geometry. This work focuses on the effect that rheology, aspect ratio of particles and the geometry of the blade coater has on the number of rotations a particle will undergo during coating. This is the starting point of more advanced work that will examine the effect that multiple particle size and shape have on the coating process.

Experimental Method

A low aspect ratio ground calcium carbonate particle (Hydrocarb 60, Omya) was compared to a high shape factor pigment (Barrisurf HX, Imerys). This barrier pigment has a shape factor of about 90 and contains a dispersant. Slurries of dry powdered pigment and water were mixed by hand vigorously until a homogenous solution was achieved. The exact mass fraction was determined by a dry weight method. The volume fraction of the slurries was calculated by the following equation, where ϕ is the volume fraction of the slurry, S is the weight fraction and ρ_ℓ and ρ_s are the densities of the liquid and solid phase, respectively. Since these pigment slurries were mixed by hand, some pigments may not be fully dispersed and actually be in the form of pigment clusters. This may have some impact on the effective volume fraction and the rheology of these solutions. However, these suspensions seemed to be quite stable with little settling over time. Similar results were observed between the hand mixed suspensions and a dispersion mixed for an hour with a high shear mixer for the high aspect ratio pigment.

$$\phi = \frac{S\rho_\ell}{S\rho_\ell + (1-S)\rho_s} \qquad \text{Eq. A.2}$$

All rheology experiments were conducted isothermally at 25°C on a controlled stress rheometer (CVO, Bohlin). A double gap concentric cylinder geometry was chosen for this study. This particular set up was used since the study included both dilute and concentrated suspensions.

Theoretical Model

A simple blade geometry is modeled using a finite element method using a commercial code (COMSOL Multiphysics). Figure A.1 shows the basic geometry. The blade is assumed to always be running parallel to the web because steel blades are known to wear in this manner. Each of the major operating condition variables could be altered to assess the effect on the velocity, pressure and shear rate profiles. The four key parameters controlling blade coater operations are the blade angle (θ), the blade thickness (δ), the distance between the blade and base sheet (h), and the speed of the paper web (U). The edges of the blade were given no slip boundary conditions. The paper web was set to a moving wall boundary condition with the velocity set to the desired web speed. Zero gauge pressure boundary conditions are set at the entrance and exit of the flow direction. The simulations were run for three rheologies. One was a Newtonian fluid with a viscosity of 1 Pas. The other two fit the experimental viscosity-shear rate behavior for the kaolin and calcium carbonate slurries, respectively. These fits were using the Carreau model and described later. Without the inclusion of a latex or binder into the slurries, hydrodynamics of the system will be a close but not exact representation of true paper coating. For the purposes here, the generated velocity profiles are a near enough approximation to provide the necessary information for the particle motion simulations.

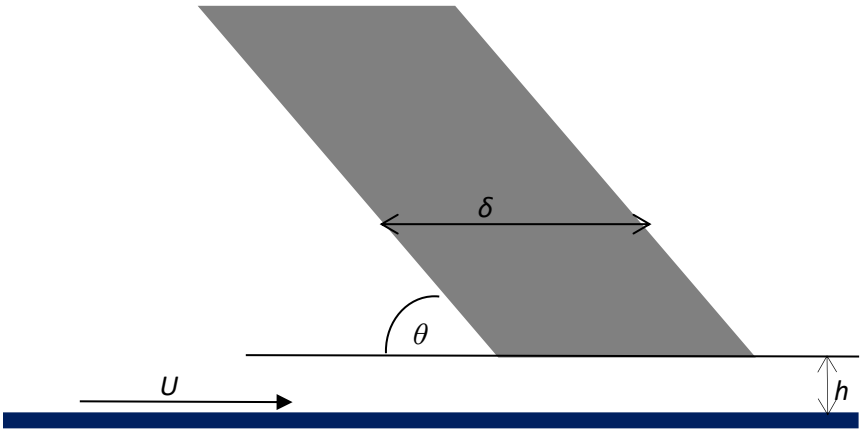

Figure A.1. Diagram of the blade coater geometry that was used in the fluid dynamics analysis.

The motion of the paper relative to the blade drags fluid into the blade-paper gap. Excess coating is rejected by the blade. Figure A.2 shows a sample result of the velocity distributions for two blade angles. Figure A.3a displays the pressure profile while Figure B illustrates the shear rate distribution at a 45° blade angle.

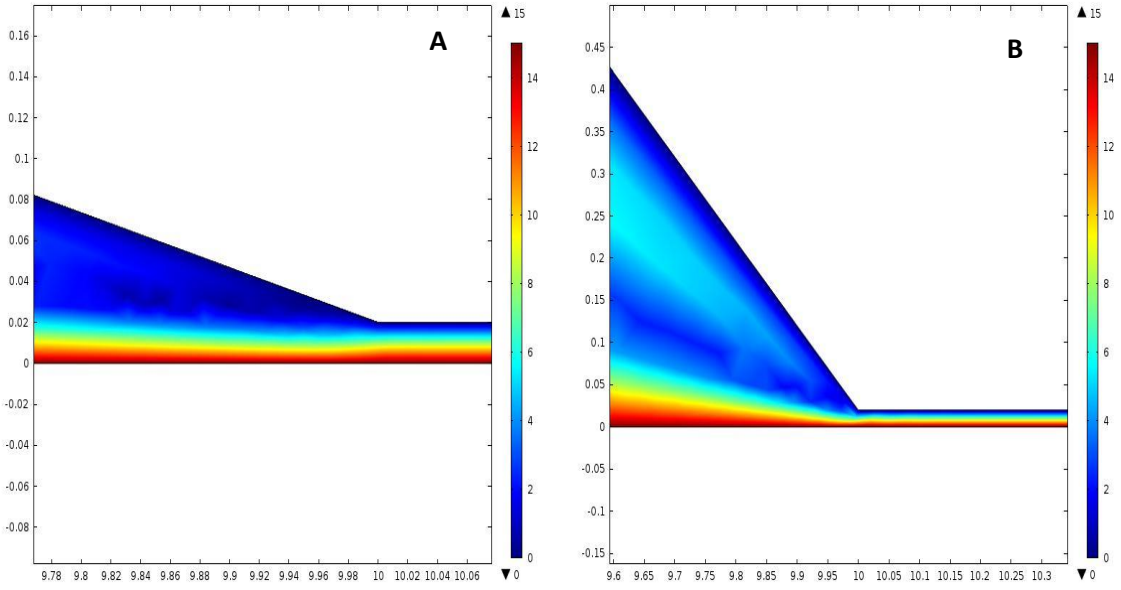

Figure A.2. Surface plot showing the velocity magnitude (m/s) of a fluid approaching the blade nip when the blade angle is at (A) 15° and (B) 45° using kaolin rheology.

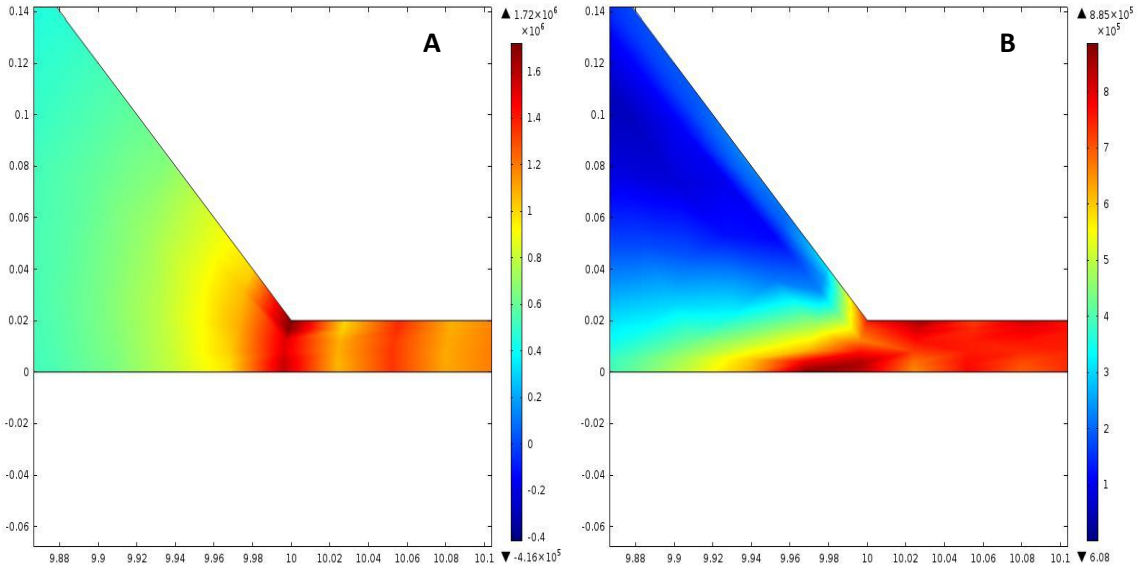

Figure A.3. Surface plots showing (A) the pressure (Pa) and (B) the shear rate (1/s) of a fluid approaching the blade nip when the blade angle is at 45° using kaolin rheology.

The motion of the particles is predicted using equations from Hsu and Ganatos (1989) for the force and torque on oblate and prolate spheroids. These same equations were reported by Hase and Bousfield (1994) and Romagnoli and Bousfield (1999) in earlier work. The key difference in this work is that a much larger travel path is described here, not just in the near region of the blade nip. This current work does not include particle-particle interactions or particle-boundary interactions but is concerned with how the blade geometry and the base rheology of the suspension influence the rotation of particles. These particle-particle interactions are important, but the work here targets the understanding of how single particles will move and rotate in a blade coater geometry.

The velocity field generated by the finite element code is interpolated to the current location of the particle to estimate the local fluid velocity as was done in Lyons *et al.* (2003). The code searches the velocity data field to find the closest three data points. These three points are weighted by their distance to estimate the *z* and *y* velocity at the present particle position. If the particle's current position is close to a particular data point from the finite element code, that

particle's *x* and *y* velocity will be heavily weighted. If the three points are almost equidistant to the particle's position, the *x* and *y* velocities will be averaged.

To estimate the shear rate at the particle's current position, the *x* velocity of a point higher than the particle is subtracted from the velocity of a point lower than the current position. Since almost all the shear is caused by relative velocity differences in the *y* direction, differences in the *y* velocities are neglected. There may be regions in the stagnation zone where this assumption is not valid, but that location of the flow field is not of high interested at present. The local shear rate is estimated as the difference of these *x* velocity values divided by the difference in the height or the positions of these velocity values.

The difference between the particle's *x* and *y* velocity and the interpolated velocity from the fluid flow field is used to calculate an *x* and *y* force on the particle using the drag coefficients of Hsu and Ganatos (1989). The torque on the particle is calculated in a similar manner. The torque coefficient depends on the orientation of the particle, as do the drag coefficients. When the particle is aligned with the shear field, the torque coefficient is small. When the particle is perpendicular, the coefficient is large, and rotation is rapid. Once the forces and torque are calculated for the particle, the updated velocity and angular velocity are calculated using a simple Euler numerical integration. The updated velocities and angular velocities are used to update the positions and rotation in a similar manner. Figure A.4 compares the rotation rate of two different aspect ratio particles in a steady shear field that is predicted with the program. Both undergo Jeffery's orbit, but the time scale is much different. For the higher aspect ratio particle, the particle spends much time aligned with the flow field, and when it rotates it rotates at a high rate of speed. The period of rotation is close to what is given in Eq. A.1: this validates that the torque coefficients are correct and that the integration method is accurate.

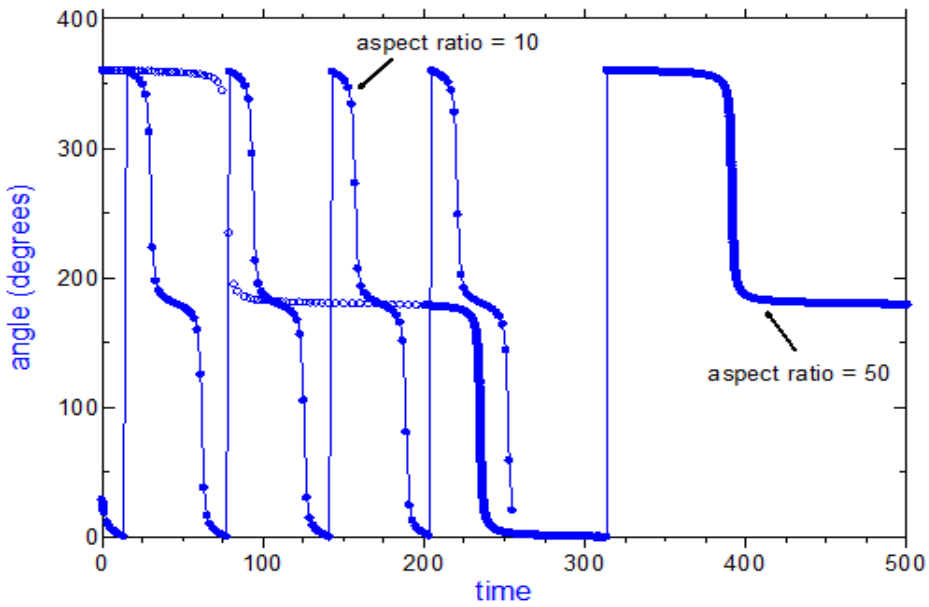

Figure A.4. Angle of unique axis relative to reference frame for two particles of aspect ratios 10 and 50 in steady shear with a shear rate of unity.

All calculations are carried out using dimensionless quantities to reduce the number of parameters that need to be studied. All velocities are normalized with the web velocity. All length scales are normalized with the small dimension of the particle. It is assumed that this length scale is 0.1 μm, similar to the dimensions of a kaolin pigment cross section. Time is made dimensionless with web velocity and this length scale.

This is a simple model that only consists of one single particle moving through the system. This straightforward model allows the examination of the rotation of a particle in a wide array for scenarios without consuming larger amounts of computer time. There are some limitations of this type of model. Interparticle interactions are not included. The hydrodynamic forces on a particle are of the same order of magnitude as particle-particle interactions in colloidal suspensions (Toivakka and Eklund, 1996). These colloidal forces will have an effect on the motion of a particle in a concentrated suspension. Stokesian dynamics have been successfully implemented to demonstrate particle motion for many various circumstances. It can be extrapolated into more complicated systems consisting of concentrated suspensions

containing multiple sizes on particles, which would be more consistent with a coating mixture containing pigment, binder and additives.

Results and Discussion

Figures A.5 and A.6 compare the viscosity shear rate relationship for the calcium carbonate and kaolin pigments. The concentrations are expressed in terms of volume fraction. For volume fractions of 0.4 and lower for calcium carbonate, the viscosity is fairly constant. There seems to be a shear thickening region at the higher shear rates, but this could be attributed to the development of Taylor vortices in the narrow gap of the concentric cylinders. For the kaolin suspension, the volume fraction should be less than 0.15 to obtain the Newtonian behavior. As the concentration increases towards the maximum flowing fraction, the viscosity increases three orders of magnitude. When the volume fraction of the calcium carbonate slurry is 0.60, it has the highest concentration that could be accurately run using this rheometer and geometry. For the kaolin suspension, the maximum concentration was only 0.35.

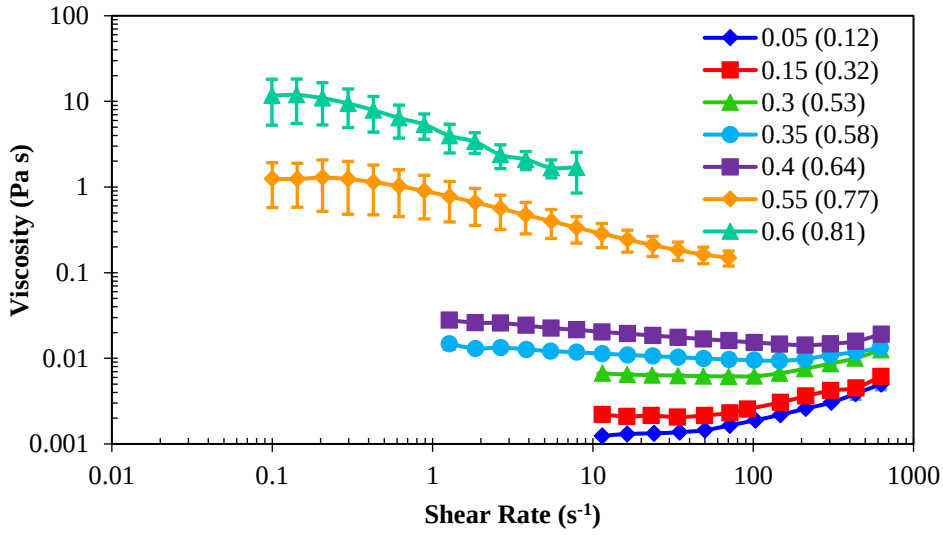

Figure A.5. Comparison of steady shear viscosity as a function of the shear rate for different volume fractions (weight fractions) of calcium carbonate slurries. Each set is an average of three runs with the error bars displaying the standard deviations

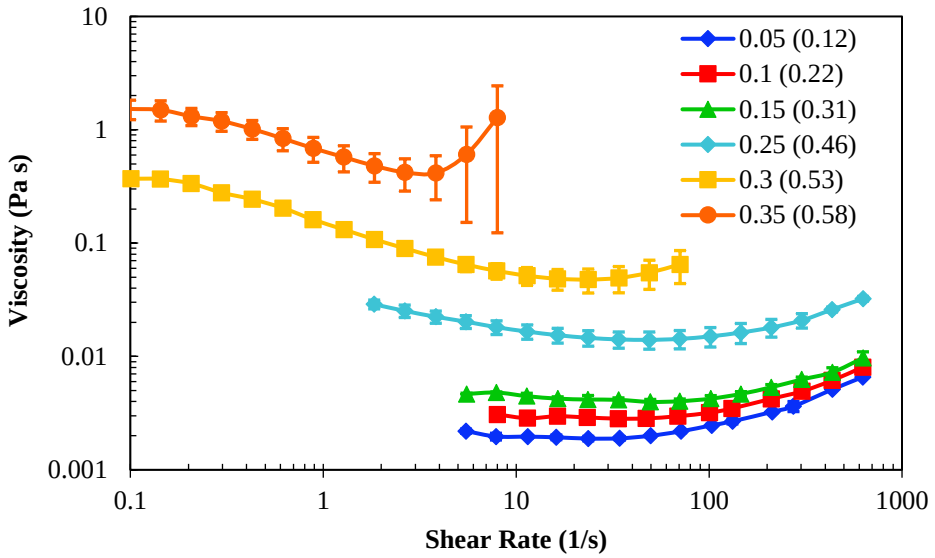

Figure A.6. Comparison of steady shear viscosity as a function of the shear rate for different volume fractions (weight fractions) of kaolin slurries. Each set is an average of three runs with the error bars displaying the standard deviations.

The kaolin suspension has similar behavior to the calcium carbonate, except the volume fraction is lower to obtain the similar result. For example, the calcium carbonate suspension at 0.4 volume fraction seems to give similar behavior as the kaolin at 0.25 volume fraction. The 0.55 volume fraction calcium carbonate has similar behavior to the 0.35 volume fraction kaolin. The ratio of these volume fractions in both these cases is 1.6.

When an oblate spheroid rotates in a steady shear field, for a short amount of time it takes up the volume of a sphere with a radius much larger than its true volume. Simplifying the geometry as a cylinder of thickness "a" and radius "b", the volume of the cylinder is $\pi a^2 b$. When this cylinder rotates, it would behave as a sphere of volume $4\pi b^3/3$. The ratio of these volumes is $4b^*/3$, where b^* is the aspect ratio or shape factor. For a shape factor of 80, this gives a volume ratio that is much larger than the value of 1.6 above. Using the example shown in Figure A., the particle with an aspect ratio of 50 is aligned with the sheet 91% of the time while the smaller aspect ratio is only parallel to the sheet 42% of the time. If this time fraction could be

combined with the factor of $4b^*/3$ to scale the volume fraction, then an improved understanding of the rheology of these systems could be generated.

The Carreau equation was used to describe the viscosity profile of calcium carbonate and kaolin. This equation quantifies the upper and lower Newtonian plateaus and the shear thinning region in the intermediate zone. Additional data points that would make the upper and lower plateaus more evident would be necessary to more accurately fit the data to the Carreau equation. This viscosity equation was chosen because it most truthfully described the actual behavior of the suspension better than a shear thinning power law model. The equation used in this study is shown in Eq. A.3. The parameters of this equation were determined by a least squares regression method. The calculated values are shown in Table A.1. The final equation for both suspensions was used in the fluid dynamics modeling of this study,

$$\frac{\eta - \eta_\infty}{\eta_o - \eta_\infty} = \frac{1}{(1 + (K_1\dot{\gamma})^2)^{\frac{m_1}{2}}} \qquad \text{Eq. A.3}$$

where η is the viscosity of the suspension, η_o and η_∞ are the asymptotic viscosity values at low and high shear rates, K_1 is a constant parameter with dimension of time, m_1 is dimensionless constant and $\dot{\gamma}$ is the shear rate.

Table A.1. Parameters of Carreau equation for calcium carbonate and kaolin

	Calcium Carbonate at 0.6 volume fraction	**Kaolin at 0.35 volume fraction**
Volume Fraction	0.6	0.35
$\boldsymbol{\eta_o}$ **(Pa s)**	11.7	1.5
$\boldsymbol{\eta_\infty}$ **(Pas s)**	1.68	0.42
$\boldsymbol{K_1}$	21.06	18.9
$\boldsymbol{m_1}$	0.303	0.354

All spheres and disks will follow the streamlines of the velocity field. What path the particle will move along is dependent on the initial starting position. If a particle begins near the paper web, then it will stay close to the web and move swiftly through the high shear rate zone. But when a particle is positioned too far from the paper web, it will be removed with the excess coating rejected at the blade nip. An example of four particle trajectories using different starting positions is shown in Figure A.7. Many other commercial codes will calculate the trajectories of particles with any system, but they do not consider the rotation of these particles within the same system.

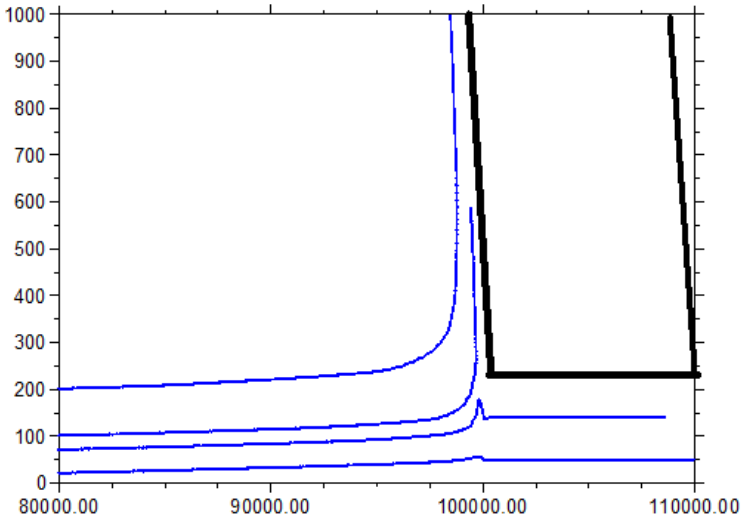

Figure A.7. Predicted particle trajectories from four starting positions nearing the blade nip for blade angle of 45°, Newtonian base velocities, and blade length of 1.0 mm. The length scale in the vertical direction is stretched such that results in the 45° angle appear to be much larger.

The number of times a particle flips is a function of the starting position and aspect ratio of the particle as shown in Figure A.8. As expected from Eq. A.1, the number of flips or rotations of low aspect ratio is large because the period of rotation is low. Particles that are near the web have a low number of flips because they are in the high shear zone a short amount of time compared to particles that start farther from the web and spend more time under the blade. Particles that start at a higher distance from the web are rejected by the blade. If the starting

angle or *x* location is moved, the particle may undergo one more or one less flip, but the trends should be the same.

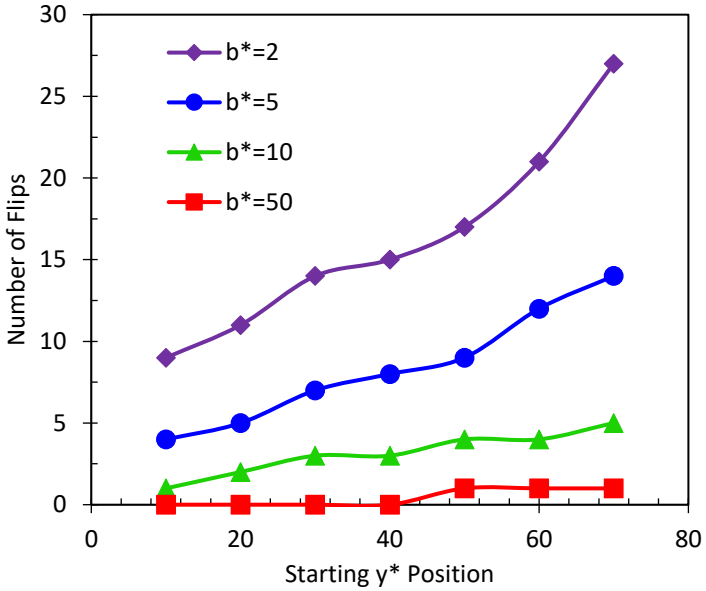

Figure A.8. The number of flips as a function of starting position from the web and the aspect ratio of the particle. Starting location is 20,000 dimensionless units from the blade heal. Starting angle is zero. The velocity field is for a Newtonian fluid with viscosity of 1 Pas and a blade angle of 45° and the blade paper gap of 20 µm.

Figure A.9 shows a typical result for the rotation of a particle with aspect ratio of 5 with a blade angle of 30°, and a starting position of 40 units from the web. The particle rotates counter clockwise that corresponds to an increasing angle. When the particle reaches the high shear rate region under the blade the rotation rate is high. The particle flips nine times in Figure A.9. As in simple shear calculations, the particle spends most of its time lined up with the flow direction.

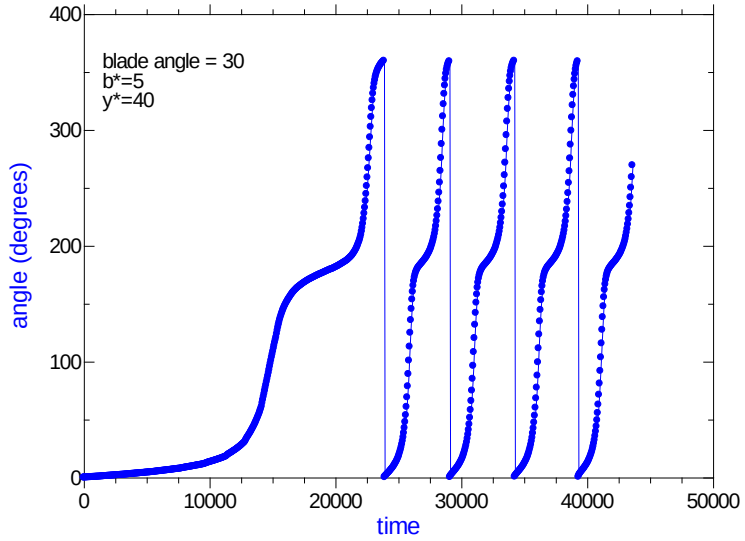

Figure A.9. Angle as a function of time for aspect ratio of 5, blade angle of 30° and the starting position from the web of 40 units.

The results for a higher starting position and blade angle are shown in Figure A.10. The larger number of rotations is caused by the trajectory of the particle that ends up closer to the blade surface and spends more time in the high shear rate zone. The larger blade angle reduces the amount of shear in front of the blade to a small extent and decreases the rotation.

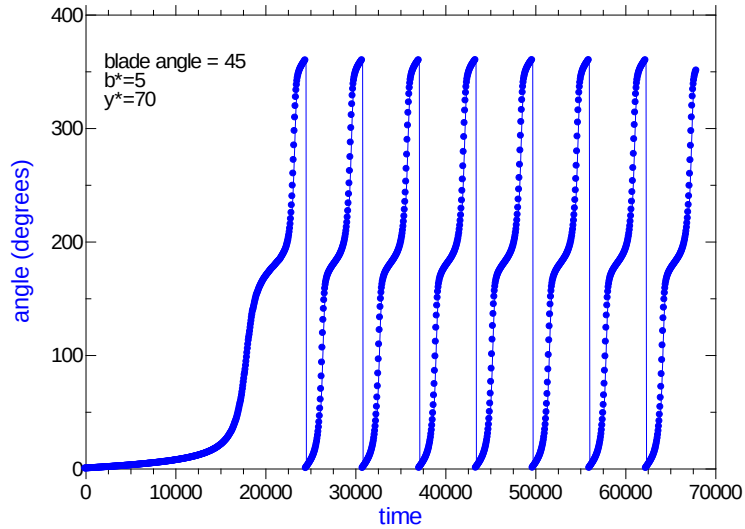

Figure A.10. Angle as function of time for an aspect ratio of b^*=5 and blade angle of 45° with starting position 70 units from the web.

When the velocity fields generated by using the shear thinning fluids as measured above are used, no differences are seen in the number of flips. This result is a surprise because shear thinning behavior can change the velocity field to a significant amount. However, since the high shear rate region is dominated by boundary driven flow, the shear rate profile in that region is the same. Therefore, the number of rotations is the same in these calculations. If the degree of shear thinning was increased to a significant amount, then some differences may be predicted.

The influence of blade angle is shown in Figure A.11 for two different aspect ratio particles. Again, higher aspect ratios cause the number of flips to decrease further. While there are some crossings of the points, in general, the low angle gives rise to more rotations. The effect is not large. The low angles generate more shear in front of the blade tip leading to more rotations before the particles enter the high shear rate region. These results indicate that high blade angles may lead to fewer rotations of the particles and a better flow under the blade tip.

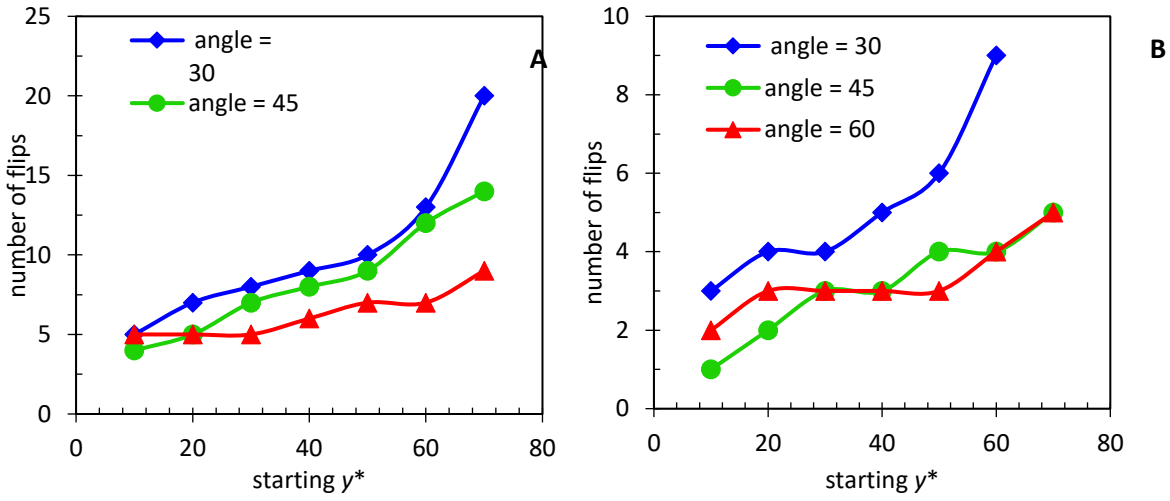

Figure A.11. Number of flips for different starting positions for three blade angles and a Newtonian base velocity field. Plot A is for b^* = 5 while plot B is when b^* = 10. The lines are present to help follow the trends.

Figure A.12 shows the effect of blade thickness on the number of rotations. As expected, the thicker the blade gives rise to more time in the high shear rate zone leading to

more rotations. A surprise is that going from 1 mm to 2 mm blade thickness did not increase the rotation to a large amount for the b^* = 5 case: doubling the blade thickness should double the time spent in the high shear zone, but this seems to hold in an approximate way.

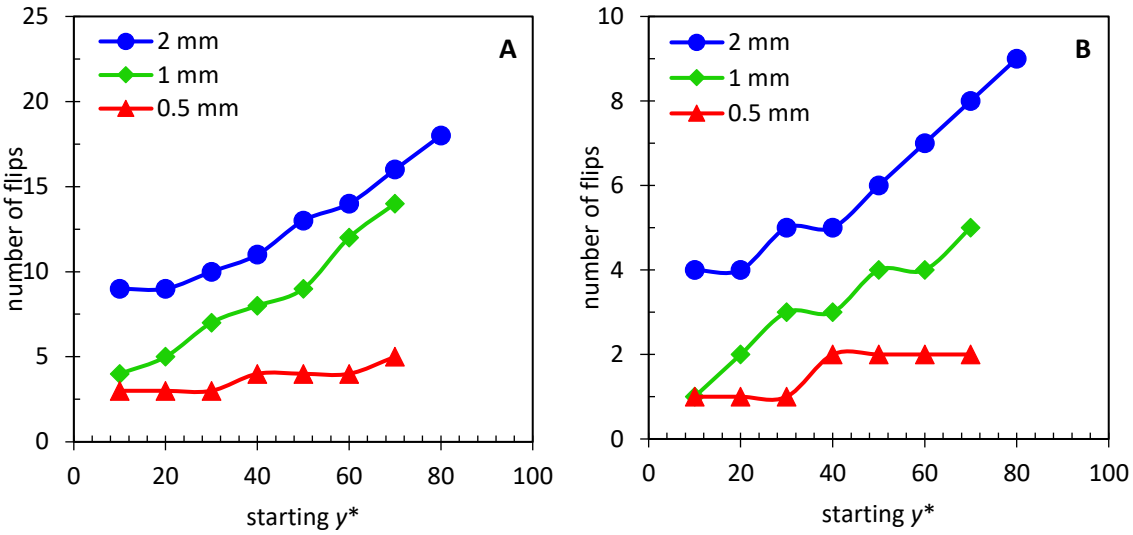

Figure A.12. Number of flips as a function of starting position for different blade thicknesses with the blade angle set at 45°. Plot A is for b^* = 5 and plot B is when b^* = 10.

Conclusions

Flow fields for blade coating geometry are used as an input to calculate particle trajectories and rotations. Velocity fields calculated from both Newtonian and shear thinning rheology predict the same number of rotations even though there are some small differences in the velocity fields. Subsequently, the geometry of the blade coater did have an effect on the number of rotations. High blade angles and thin blade thicknesses both decreased to the number of rotations a particle will complete. The aspect ratio of a particle also affected the amount of rotations. High aspect ratio particles may not be able to complete a full flip during the coating process. This could be attributed to the longer period of time required to complete the rotation.

APPENDIX B: BLADE ANGLE DETERMINATION ON BENCH TOP BLADE COATER

Proper alignment of the blade against the rubber backing roll on the bench top blade coater used in the runnability study discussed in Chapter 3 was necessary to ensure that blade effects were not the cause of the exhibited issues. Below in Figure B.1, is a side view of the blade housing; looking down the length of the blade. The blade angle was constant at 45° for all runnability trials. The angle was set at 45° from the tangent line where the blade makes contact with the roll. The red line is placed on top of the blade in the figure. The yellow line is the tangent line from the contact point between the backing roll and the blade. The green line is the normal line to the tangent.

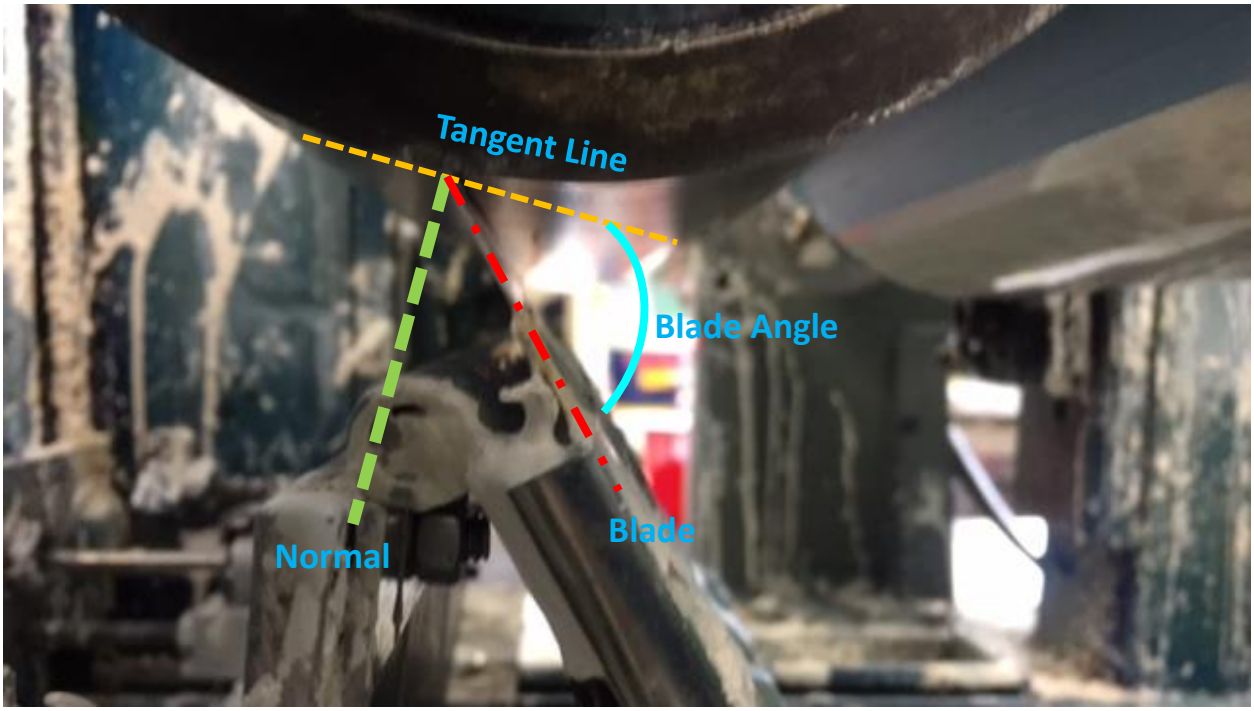

Figure B.1. Side photo of the blade on the bench top blade coater showing how the blade angle was determined

BIOGRAPHY OF THE AUTHOR

Lisa Weeks was born in New Symrna Beach, Florida on May 25, 1988. She was raised in Westfield, Massachusetts and graduated from Westfield High School in 2006. She attended Montana State University and graduated in 2011 with a Bachelor's Degree in Chemical Engineering. She also completed a Master of Science in Chemical Engineering in December of 2013 at Montana State University. She then entered the chemical engineering graduate program at the University of Maine in January 2014. After receiving her degree, Lisa will be joining the faculty in the Chemical and Biological Engineering department as a lecturer in Bioengineering. Lisa is a candidate for the Doctor of Philosophy in Chemical Engineering from the University of Maine in December 2017.